Wegener Center
SCIENTIFIC REPORT
107 | 2024

Atmospheric blocking – exploring its role in stratosphere-troposphere coupling and its influence on extreme weather events

Kamilya Yessimbet

December 2024

financially supported by

FWF Österreichischer Wissenschaftsfonds

Wegener Center

UNI GRAZ

Climate Change Graz
Field of Excellence
University of Graz

DOCTORAL PROGRAMME CLIMATE CHANGE

The Wegener Center for Climate and Global Change is an interdisciplinary, internationally recognized research and graduate education institute of the University of Graz that is pooling the University's expertise in Climate, Environmental and Global Change. It brings together research teams and scientists from fields such as geophysics and climate physics, meteorology, economics, geography, and social sciences. At the same time, close links are maintained and further developed with many national and international cooperation partners. The research interests range from monitoring, analysis, and modeling of climate and environmental change to the investigation of climate change impacts and the analysis of the human dimensions of these changes related to mitigation, adaptation, and loss & damage. More information at **wegcenter.uni-graz.at**.



Alfred Wegener (1880 – 1930), after whom the Wegener Center is named, was founding holder of the University of Graz Geophysics Chair (1924 – 1930). In his work in the fields of geophysics, meteorology, and climatology he was a brilliant scientist and scholar, thinking and acting in an interdisciplinary way, far ahead of his time with this style. The way of his ground-breaking research on continental drift is a shining role model. His sketch on the relations of continents based on traces of an ice age about 300 million years ago (left) as basis for the Wegener Center Logo is thus a continuous encouragement to explore equally innovative ways: paths emerge in that we walk them (motto of the Wegener Center).

The present report is the result of a PhD thesis work completed in December 2024. The work was funded by the Faculty of Environmental, Regional and Educational Sciences, University of Graz, and by the Austrian Science Fund (FWF) under research grant W 1256 (Doctoral Programme Climate Change – Uncertainties, Thresholds and Coping Strategies, https://dk-climate-change.uni-graz.at).

SR 107 | 2024 Atmospheric blocking – exploring its role in stratosphere-troposphere coupling and its influence on extreme weather events
ISBN 978-3-9508053-6-8 December 2024

Suggested citation:
Yessimbet, K. (2024), Atmospheric blocking – exploring its role in stratosphere-troposphere coupling and its influence on extreme weather events, Wegener Center Scientific Report 107-2024, Wegener Center Verlag, University of Graz, Austria, December 2024. ISBN 978-3-9505053-6-8

(c) 2024 Wegener Center Verlag, University of Graz, Austria
The usage of images, tables, or texts of this Scientific Report is permitted for non-commercial purposes if appropriate credit is given.
For any other purposes, please contact: wegcenter@uni-graz.at

Publishing institution:
Wegener Center for Climate and Global Change, University of Graz
Brandhofgasse 5, 8010 Graz, wegcenter.uni-graz.at

Contact: Andrea Steiner
andi.steiner@uni-graz.at

Kamilya YESSIMBET

Atmospheric blocking – exploring its role in stratosphere-troposphere coupling and its influence on extreme weather events

Doctoral thesis

submitted in fulfillment of the requirements for the

Doctor of Natural Sciences

in the Doctoral Program in Natural Sciences

at the University of Graz

Faculty of Environmental, Regional and Educational Sciences

Supervisor: Univ.-Prof. Dr. Andrea K. STEINER

Wegener Center for Climate and Global Change, University of Graz

2024

Co-supervisor
Univ.-Prof. Dr. Steffen Birk
University of Graz, Austria

External supervisor
Univ.-Prof. Dr. Theodore G. Shepherd
University of Reading, United Kingdom

Advisor
Ass.-Prof. PhD Albert Ossó
University of Graz, Austria

Abstract

Atmospheric blocking is a persistent, large-scale, quasi-stationary anticyclone that disrupts the westerly flow at midlatitudes, often leading to extreme weather. In the cold season, blocking influences stratospheric variability by modulating the upward propagation of planetary waves from the troposphere. This influence can contribute to the disruption of the stratospheric polar vortex (SPV) and lead to sudden stratospheric warming (SSW). An SSW event, in turn, can affect tropospheric circulation and favor blocking conditions. Both phenomena are associated with the occurrence of extreme weather, such as cold spells or heavy precipitation events. However, the details of their mechanisms and pathways of influence are not yet fully understood. This thesis aims to contribute to a better understanding of these processes by exploring the role of atmospheric blocking in the stratosphere-troposphere coupling and its influence on extreme weather events.

The first insight is provided by a case study of a record-breaking snowfall event in the northern Alps in 2019, associated with North Atlantic blocking, which was crucial for the advection of cold and moist air from the North Atlantic toward the Alps. The analysis shows the connection between blocking and specific SPV configuration during a major SSW event that occurred simultaneously and discusses their role in shaping this extreme snowfall and the implications for its prediction.

In the second part, the strength of the pathways of influence between European and West Pacific blocking and SPV variability is quantified using a causal inference-based framework and reanalysis data. Results show that both types of blocking affect the SPV primarily through upward wave activity fluxes, though this influence is not straightforward. In particular, for European blocking, the influence on the lower stratospheric wave activity flux is fully mediated by its effect on the upper tropospheric wave activity flux, while this is only partially the case for West Pacific blocking, suggesting that the mechanisms of their vertical influence differ. In addition, only two-thirds of the effect of upper tropospheric wave activity flux on SPV variability is mediated by lower stratospheric wave activity flux, while one-third occurs via a direct pathway. These findings clarify the pathways of influence between blocking and SPV variability.

Finally, an observational-based study of stratosphere-troposphere coupling and the influence of SSWs on blocking formation was conducted using Global Navigation Satellite System (GNSS) radio occultation (RO) measurements. GNSS RO data provide insight into the vertical structure of wave activity flux and its impact on the polar tropopause for different types of SSWs. In particular, reflecting SSW events connected to vortex displacement are observed to trigger downward propagation of wave activity that induces blocking over the North Pacific, while absorbing events connected to vortex split result in blocking over the North Atlantic and exhibit prolonged upward propagation of wave activity. Both types of SSWs lead to the enhancement of the polar tropopause inversion layer, with a stronger effect observed for absorbing events. The results highlight the differences in the magnitudes of downward impact on the troposphere and the resulting regional variations in blocking responses for different SSW types.

Zusammenfassung

Atmosphärisches Blocking ist eine persistente, großräumige, quasistationäre Antizyklone, die die Weströmung in mittleren Breiten unterbricht und häufig zu extremen Wetterlagen führt. In der kalten Jahreszeit beeinflusst Blocking die Variabilität der Stratosphäre, indem es die Ausbreitung planetarischer Wellen aus der Troposphäre nach oben moduliert. Dieser Einfluss kann zur Störung des stratosphärischen Polarwirbels (SPV) beitragen und zu einer plötzlichen Erwärmung der Stratosphäre (SSW) führen. Ein SSW-Ereignis wiederum kann die troposphärische Zirkulation beeinflussen und Blocking-Bedingungen begünstigen. Beide Phänomene werden mit dem Auftreten von Wetterextremen wie Kälteperioden oder Starkniederschlägen in Verbindung gebracht. Die Details ihrer Mechanismen und Einflusswege sind jedoch noch nicht vollständig geklärt. Diese Arbeit soll zu einem besseren Verständnis dieser Prozesse beitragen, indem sie die Rolle der atmosphärischen Blockierung in der Stratosphäre-Troposphäre-Kopplung und ihren Einfluss auf extreme Wetterereignisse untersucht.
Ein erster Einblick wird durch eine Fallstudie über ein Rekord-Schneefallereignis in den Nordalpen im Jahr 2019 gegeben, in Verbindung mit Blocking über dem Nordatlantik, das für die Advektion kalter und feuchter Luft aus dem Nordatlantik in Richtung der Alpen entscheidend war. Die Analyse zeigt den Zusammenhang zwischen dem Blocking und der spezifischen SPV-Konfiguration, während gleichzeitig ein großes SSW-Ereignisses stattfand, und erörtert ihre Rolle bei der Entstehung dieses extremen Schneefallereignisses und dessen Vorhersagbarkeit.
Im zweiten Teil wird die Stärke der Einflusswege zwischen Blocking über Europa und dem Westpazifik und der SPV-Variabilität mit Hilfe einer kausalen Inferenzmethode und Reanalysedaten quantifiziert. Die Ergebnisse zeigen, dass beide Arten von Blockings den SPV hauptsächlich durch aufwärts gerichtete Wellenaktivität beeinflussen, wobei dieser Einfluss nicht ganz eindeutig ist. Insbesondere wird der Einfluss von Blocking über Europa auf den Wellenaktivitätsfluss in die unteren Stratosphäre vollständig durch den Wellenaktivitätsfluss in der oberen Troposphäre vermittelt. Bei Blocking über dem Westpazifik passiert dies nur teilweise, was auf unterschiedliche Mechanismen hindeutet. Darüber hinaus werden nur zwei Drittel der Auswirkungen der Wellenaktivität in der oberen Troposphäre auf die Variabilität der SPV über die Wellenaktivität in der unteren Stratosphäre vermittelt, während ein Drittel über einen direkten Weg erfolgt. Diese Ergebnisse verdeutlichen die Einflusswege zwischen Blocking und SPV-Variabilität.

Schließlich wurde eine auf Beobachtungen basierende Studie der Stratosphären-Troposphären-Kopplung und des Einflusses von SSWs auf die Blockbildung unter Verwendung von Global Navigation Satellite System (GNSS) Radio-Okkultationsmessungen (RO) durchgeführt. Die GNSS-RO-Daten geben Aufschluss über die vertikale Struktur des Wellenaktivitätsflusses und seine Auswirkungen auf die polare Tropopause für verschiedene Arten von SSWs. Insbesondere wird beobachtet, dass reflektierende SSW-Ereignisse, die mit einer Verschiebung des polaren Vortex einhergehen, eine abwärts gerichtete Ausbreitung der Wellenaktivität auslösen, die zu einem Blocking über dem Nordpazifik führt, während absorbierende Ereignisse, die mit einer Aufspaltung des polaren Vortex einhergehen, zu einem Blocking über dem Nordatlantik führen und eine länger andauernde, aufwärts gerichtete Ausbreitung der Wellenaktivität aufweisen. Beide Arten von SSWs führen zu einer Verstärkung der polaren Tropopausen-Inversionsschicht, wobei bei absorbierenden Ereignissen ein stärkerer Effekt beobachtet wird. Die Ergebnisse verdeutlichen die unterschiedlichen Auswirkungen von verschiedenen SSW-Typen auf die Troposphäre und damit regional unterschiedliche Blockings.

Acknowledgements

First of all, I would like to sincerely thank my supervisor, Prof. Andrea Steiner, for allowing me to pursue my PhD and explore the field of climate science. Her patience, support, and guidance have been invaluable, providing help and freedom in dealing with various challenges, as well as all her efforts, ideas, feedback, and, just as importantly, the life lessons she has taught me.

I dedicate my work to my mother *Лилия* and grandmother *Саравила* for their love, inspiration, patience, support and the countless sacrifices they have made since the day I was born. I also dedicate it to my husband, Tomislav, whom I thank for being my life role model and for his kindness, support, and love.

I thank Prof. Albert Ossó for supervising and teaching me and for the ideas, discussions, collaborative work, input, and feedback on papers. I thank Professor Ted Shepherd for hosting me at the University of Reading, for his collaboration and teaching me not only about science but also showing me, along with members of his research group, how kindness can play a role in academia, especially in creating an inclusive environment for young scientists. I thank Florian Ladstädter for the friendly and interesting discussions and our work together. I also thank people from the Wegener center, particularly Josef, Armin, Marc, and Lena, for the help with work-related questions, IT, and admin support, and Hallgeir and Clara for help and discussions beyond work. I thank Mastawesha for the best friendly advice during my PhD.

I thank my friends, particularly Zulfiya, Kumush, Akmaral, and Aisulu, for their support and connection. I thank my doctor, Arijana T., for her critical help. I thank Seung, Rutger, and Laura S. for the talks and joyful cat-filled experience.

I would like to thank the members of the Doctoral Programme Climate Change (DKCC), faculty, administration, and fellow students for the training and for teaching me about the interdisciplinary aspects of climate change, as well as for all their efforts in making the programme run. I especially thank Regina. My PhD was funded by the Austrian Science Fund (FWF) under research grant W1256 (Doctoral Programme Climate Change – Uncertainties, Thresholds and Coping Strategies) and the University of Graz.

The PhD time, which coincided with my personal maturation away from my home in Shymkent and many difficulties and obstacles faced during this period, had a profound impact on me. Although my work is modest, for me, it represents the completion of a meaningful and transformative journey. One of the lessons I've learned is how profoundly people contribute to one another, from the very first words we learn to the tools and ideas we share. It feels like a shared consciousness, where each person is not simply on their own but part of a collective stream of thought and knowledge. For that matter, the number of people and things to acknowledge and thank is enormous, from my school teachers, A. Irina Nikolayevna and C. Tatyana Konstantinovna, to tools such as Python, Linux, and Grammarly.

Finally, I thank the reviewers of my PhD thesis: Prof. Andrea Steiner, Prof. Ulrich Foelsche (Institute of Physics, University of Graz), and Prof. Ted G. Shepherd (University of Reading). I also thank Andrea and Albert for their helpful feedback during the thesis writing.

Contents

Preface **1**

Part I. Synopsis

1. Introduction **5**
2. Weather and Climate in the Extratropics **7**
2.1. Climate Change and Extreme Events 7
2.2. Extratropical circulation 9
2.3. Research Questions 11
3. Data Sets **13**
3.1 Reanalysis, forecast and model data 13
3.2 Meteorological station snow data 13
3.3 Satellite-based GNSS Radio Occultation 14
4. Theoretical Framework and Methods **17**
4.1. Atmospheric blocking and Sudden Stratospheric Warmings: Theories, Definition and Frequency 17
4.1.1. Atmospheric blocking 17
4.1.2. Sudden Stratospheric Warmings 20
4.2. Stratosphere-troposphere coupling: Blocking-SSW linkage 23
4.2.1. Upward influence 23
4.2.2. Downward influence 25
4.2.3. Influence of SSWs on the polar tropopause 28
4.2.4. Wave-reflection mechanism 30
4.2.5. Wave activity diagnostics 31
4.3. Links to extreme weather 34
5. Summary and Conclusions **37**
5.1. Addressing the Research Questions 37
5.2 Conclusions 39

Part II. Papers Published

Paper I. Heavy Alpine snowfall in January 2019 connected to atmospheric blocking 43
Paper II. Pathways of influence between Northern Hemisphere blocking and stratospheric polar vortex variability 55
Paper III. Observational perspective on sudden stratospheric warmings and blocking from Eliassen–Palm fluxes 67
List of Acronyms **97**
List of Figures **99**
Bibliography **101**

Preface

This thesis is based on the following peer-reviewed publications:

Yessimbet, K., Ossó, A., Kaltenberger, R., Magnusson, L., and Steiner, A.K. (2021). Heavy Alpine snowfall in January 2019 connected to atmospheric blocking. Weather, https://doi.org/10.1002/wea.4020

Contributions: Y.K. contributed to the conceptualization and methodology of the study, collected and analyzed the data, wrote software for data analysis, plotted figures and wrote the original manuscript. O.A. contributed to the conceptualization and methodology of the study, and manuscript writing, review and editing. K.R. contributed to data curation, visualization, and manuscript writing and review. M.L. contributed with data visualization and manuscript review. A.K.S. contributed to the conceptualization and methodology of the study, funding acquisition, resources, supervision, manuscript writing, review and editing.

Yessimbet, K., Shepherd, T. G., Ossó, A. C., and Steiner, A. K. (2022). Pathways of influence between Northern Hemisphere blocking and stratospheric polar vortex variability. Geophysical Research Letters, 49, e2022GL100895, https://doi.org/10.1029/2022GL100895

Contributions: Y.K. contributed to the conceptualization and methodology of the study, collected and analyzed the data, wrote software for data analysis, plotted all the figures and wrote the original manuscript. T.G.S. contributed to the conceptualization and methodology of the study, manuscript writing, review and editing. O.A. contributed with supervision, manuscript writing, review and editing. A.K.S. contributed with funding acquisition, resources, supervision and manuscript writing, review and editing.

Yessimbet, K., Steiner, A. K., Ladstädter, F., and Ossó, A. (2024). Observational perspective on sudden stratospheric warmings and blocking from Eliassen–Palm fluxes, Atmos. Chem. Phys., 24, 10893–10919, https://doi.org/10.5194/acp-24-10893-2024

Contributions: Y.K. contributed to the conceptualization and methodology of the study, collected and analyzed the data, wrote software, utilized existing software, and performed computations, plotted all the figures and wrote the original manuscript. A.K.S. provided the initial design for this study. F.L. provided the gridded RO dataset. All authors contributed to the design of the study and figures, the discussion of the results, and the revision of the text. A.K.S., F.L., and A.O. provided guidance and advice on all aspects of the study

Part I. Synopsis

1. Introduction

At the beginning of January 2019, Graz, Austria, experienced light snowfall. Simultaneously, the northern Alps experienced heavy snowfall, breaking 100-year records at some weather stations. This event was linked to a large-scale atmospheric pattern involving blocking over the North Atlantic – a persistent quasi-stationary anticyclone over the North Atlantic region – that elongated the jet stream in the meridional direction for about two weeks, which facilitated the transport of moist air masses from higher latitudes to the Alps, resulting in the extreme precipitation.

At the same time, an equally remarkable event occurred in the stratosphere over the Arctic: a sudden stratospheric warming (SSW) characterized by abrupt adiabatic heating due to the weakening of the stratospheric polar vortex and the subsidence of air masses over the Arctic. The development was such that the daughter vortices of the disrupted and split polar vortex aligned with low-pressure systems upstream and downstream of the blocking ridge, highlighting potential stratosphere-troposphere interactions. Understanding the mechanisms behind such events remains an active area of research in climate science.

It is known that blocking can lead to different extreme events depending on the season and region. In summer, blocking often leads to heatwaves and prolonged droughts over Eurasia and North America. In contrast, in the cold season, blocking is often associated with cold waves. Blocking can also lead to extreme precipitation events by modulating the jet stream and storm tracks.

Currently, there is no unified dynamical description of atmospheric blocking. Furthermore, blocking can interact with other atmospheric phenomena, such as SSWs, the mechanisms of which are also not fully understood.

This lack of comprehensive understanding hinders accurate predictions in weather and climate models. This thesis focuses on some aspects of blocking formation, its connection with the stratospheric circulation, and its impact on surface weather.

2. Weather and Climate in the Extratropics

This chapter discusses selected aspects of extratropical weather and climate. The first glimpse on the research subject is given through the context of climate change, and its influence on extreme events. Then, the chapter narrows down to discuss atmospheric processes that underlie wintertime extreme weather events, particularly emphasizing atmospheric blocking and its interaction with the stratospheric polar vortex, which is central to this thesis.

2.1. Climate Change and Extreme Events

Climate fluctuations have been observed throughout the history of the Earth, as evidenced by paleoclimatic data (IPCC, 2021). Current climate change, also known as global warming, refers specifically to the increase in global mean surface air temperature that began after the industrial revolution and has since intensified at rates not seen in millennia. According to the large body of accepted scientific evidence summarized, e.g., in IPCC (2021), global warming is primarily driven by increasing concentrations of anthropogenic greenhouse gases in the atmosphere. Besides temperature increases, climate change is manifested in other components of the Earth's climate system, such as the reduction of Arctic Sea ice, the retreat of mountain glaciers worldwide, or rising sea levels (IPCC, 2021).

The response of the climate system to direct thermodynamic forcing is well understood. For instance, an increase in upper ocean heat content, a reduction of the sea ice extent, and sea level rise can all be directly linked to an increase in global mean surface air temperature. Changes in these quantities are robust in both observations and models (IPCC, 2021). However, the response of dynamic processes such as atmospheric circulation remains uncertain (Shepherd, 2014; IPCC, 2021). This is due to several key factors, including different levels of understanding of their underlying mechanisms and the different nature of their responses to climate change (Shepherd, 2014; 2016). Thermodynamic processes exhibit a more direct and approximately linear response to climate forcing. In contrast, dynamic processes are more complex and multiscale and exhibit a higher degree of chaos. Small signal-to-noise ratios in the response of dynamic quantities to climate forcing and incomplete understanding of the underlying mechanisms are associated with greater uncertainty in their predictions (Shepherd, 2014).

The differences in how climate processes respond to global warming are particularly relevant when considering weather extremes, which are characterized by significant deviations of hydrometeorological parameters from their average values for a particular region or season in terms of magnitude, intensity, or timing of occurrence (WMO, 2024).

Some examples of extreme weather events at midlatitudes are extreme temperature events (heatwaves and cold waves), severe storms, and associated phenomena such as extreme wind, tornadoes, hail, and extreme precipitation. These events vary on a temporal and spatial scale. Thus, some events, such as squalls, are ultra-short-lived (lasting a few minutes) and influenced by mesoscale convective processes at a spatial scale up to a few hundred kilometers. Other events, such as heatwaves, can persist for a few weeks, often driven by large-scale processes extending over thousands of kilometers.

Extreme weather events are commonly assessed using statistical indices. A simple example is indices based on absolute or relative (e.g., 10th/90th percentile) thresholds of meteorological values below/above which events are considered extreme. When these events are analyzed statistically it usually is assumed that they are governed by the same physics as ordinary events, differing primarily in the amplification of characteristics that are less pronounced under typical conditions. In this context, weather extremes are considered to belong to the same distribution function as ordinary events, with extremes defined by the tails of these distributions. The more extreme and rare the event, the further it lies in the tail.

In this respect, a very rare extreme weather event can be linked to Nassim Taleb's concept of "black swans" (Taleb, 2007). A black swan can be described as a highly rare and unpredictable event that can have a significant impact on a society or system. Such events can be considered outliers in the distribution function or random events, making them difficult to explain or predict using traditional models or theories. Taleb (2007) suggests that "although randomness is an inherent property in theory, in practice randomness is incomplete information". One potential example of a black swan event could be the very unusual February 2021 cold wave in the Texas region of the USA. The cold wave, snowfall, and ice accumulation led to a humanitarian and energy crisis because the subtropical region was unprepared for such an event. This event was linked to the polar vortex disruption that involved planetary wave reflection, the mechanisms of which are still not fully understood (Cohen et al., 2021).

Understanding the underlying mechanisms is, therefore, essential when it comes to the effects of climate change on weather extremes, which are shaped by both thermodynamic and dynamic factors to varying degrees. For example, predictions of changes in temperature extremes (both hot and cold) are robust because of the strong thermodynamic component. Many regions of the world have reliably recorded significant increases in hot temperature extreme events (e.g., Dong et al., 2018; IPCC, 2021; Engdaw et al., 2023). Future projections show with high confidence that hot extremes will become more frequent and intense while cold extremes are expected to decrease (IPCC, 2021). However, because of changes in circulation, there is still the possibility of increased cold weather extremes in warmer climates. For instance, regions like Central Asia have shown an increase in low-temperature extremes since 1990, arguably attributed to circulation changes responsible for cold air transport from the Arctic (Horton et al., 2015). In midlatitudes, cold waves are often associated with circulation anomalies such as blocking and the polar vortex (Woollings et al., 2018; Kretschmer et al., 2018). For instance, Messori et al. (2022) demonstrated that stratospheric variability coupled with North Pacific blocking is linked to cold temperature extremes in North America. Similarly, Pfahl (2014) found that European cold temperature extremes are frequently driven by blocking over the North Atlantic region.

Regarding extreme precipitation, a warmer atmosphere is expected to have a higher saturation vapor pressure, indicating a potentially higher water vapor content in the air (according to the Clausius-Clapeyron equation). As a result, the intensity of extreme precipitation events is likely to increase globally (O'Gorman, 2015). However, the projections of regional extreme precipitation are associated with high uncertainties due to the local effects of topography and multiscale dynamic atmospheric processes.

Other hydrological extremes such as droughts and floods are also subject to the complex impacts of climate change, including changes in atmospheric circulation, rising air temperature, precipitation patterns, changes in snow cover and glacier melt, depletion of soil moisture with

a range of implications for agriculture, water supply, and ecosystems. In some arid regions, such as Central Asia, the frequency of droughts will likely increase due to the combined effects mentioned above (IPCC, 2021). In contrast, in other regions, such as the monsoon region in South Asia, the likelihood of flooding will increase (IPCC, 2021). It is also likely that other types of floods, such as river overflows due to extreme precipitation events, will increase in the future (e.g., in Europe), as will flash floods in mountainous areas due to overloaded river systems or glacier outbursts (e.g., in the Tien Shan mountains in Central Asia) (IPCC, 2021; Saidaliyeva et al., 2024). However, predicting floods in a changing climate remains uncertain (IPCC, 2021).

Overall, global warming affects all components of the Earth's climate system and will have mostly negative consequences for humanity. A better understanding of the physical mechanisms of extreme events could allow scientists to develop better models. Incorporating factors that influence the occurrence and development of extreme events into weather and climate models will help to improve prediction and develop strategies for risk adaptation and mitigation (IPCC, 2013; 2022).

2.2. Extratropical circulation

The extratropical circulation consists of two main streams of fast-moving air around the pole in the upper troposphere and stratosphere (Figure 1). These “two rings” are the troposheric jet stream and the SPV, also known as the polar vortex, both driven by the equator-to-pole temperature gradients and the Coriolis effect due to the planet's rotation.

Among the main elements of the tropospheric circulation shaping the weather in the extratropics are blocking and storm tracks. The jet stream modulates the distribution of weather systems. Blocking, in turn, disrupts the normally eastward progression of weather systems, can change the direction of the jet stream and lead to prolonged periods of stagnant weather conditions (Kautz et al., 2022).

Another major ingredient of the extratropical circulation is the planetary Rossby waves, large-scale atmospheric oscillations embedded in the jet stream that give it the pronounced meandering aspect. Rossby waves are caused by uneven heating, topography, and the Earth's rotation. Rossby waves transport momentum and heat across the hemisphere and vertically. Their wavelengths typically range from several thousand kilometers to tens of thousands of kilometers (Andrews et al., 1987).

During the cold season, which lasts roughly from November to March in the Northern Hemisphere, the circulation becomes more dynamic due to increased equator-to-pole temperature gradients. Planetary waves intensify, leading to more pronounced high- and low-pressure systems. As a result, blocking can form in the amplified stationary ridge of the planetary wave pattern (Legras and Ghil,1985; Suitters et al., 2023). An illustrative case of a North Atlantic blocking embedded in the amplified jet stream meander that occurred in January 2019 is shown in Figure 2.

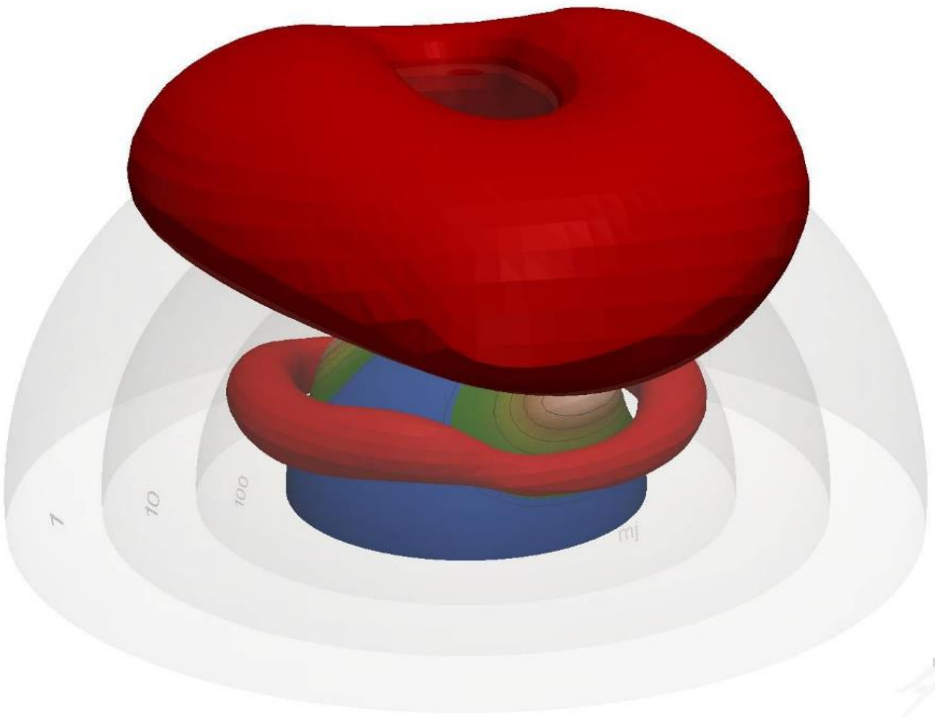


Figure 1. The 3D illustration of the jet stream and polar vortex structure in a simple climate model in the presence of wave-two topography. The three grey domes represent atmospheric height levels at 100 hPa, 10 hPa, and 1 hPa, respectively. Reprinted from https://www.martin jucker.com/viz/ (accessed on 20.10.2024).

As Rossby waves propagate from the troposphere into the stratosphere, they transfer momentum and exert a drag on the polar vortex, weakening it. In extreme cases, these disturbances to the polar vortex can lead to SSWs characterized by rapid adiabatic heating of the stratosphere. In this context, atmospheric blocking, as a circulation anomaly, is considered one of the anomalous tropospheric wave activity forcings that influence the polar vortex and contribute to the development of SSWs. At the same time, changes in the stratospheric circulation in the aftermath of SSW events can have a downward effect on the jet stream and play a role in the formation of blocking. For instance, the blocking situation depicted in Figure 2, reportedly a large-scale driver of extreme snowfall in Europe, was simultaneously associated with the 2019 SSW event (Yessimbet et al., 2022a).

SSW events are also frequently associated with extreme cold spells in Europe. A prime example is the 2018 SSW event, which was linked to a blocking over Scandinavia that was responsible for the extreme cold spell in Northwestern Europe, commonly referred to as the "Beast from the East" (Greening and Hodgson, 2018). Some SSWs have also been connected to North Pacific blocking, which is associated with wave reflection from the stratosphere to the troposphere (Kodera et al., 2016). In turn, the occurrence of North Pacific blocking is often linked to cold waves over North America (Messori et al., 2022).

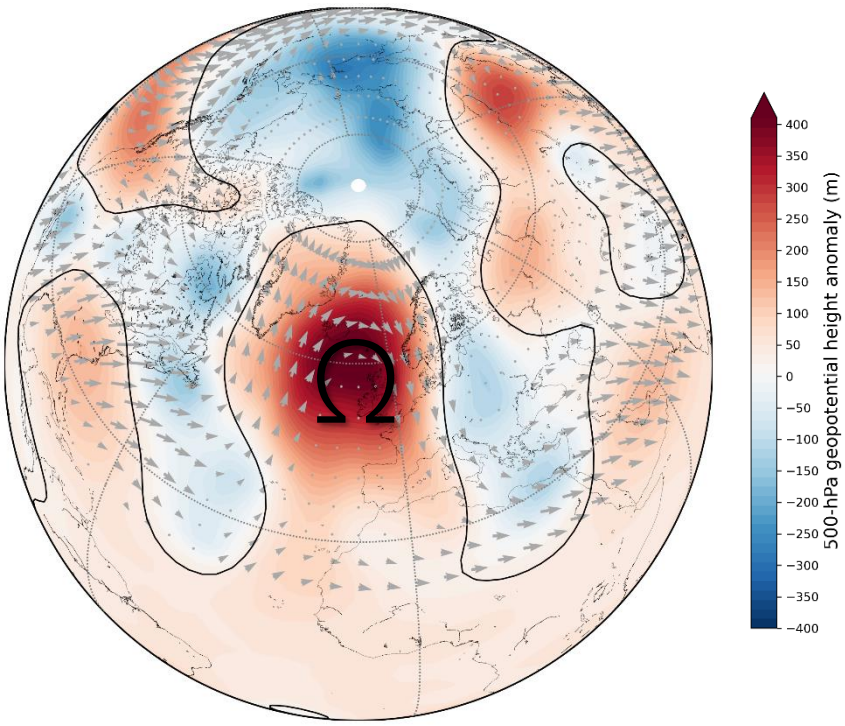


Figure 2. North Atlantic blocking is shown as an anomaly in geopotential height at 500 hPa (shading) with the jet stream (wind at 250 hPa) represented by vectors for 2 January 2019, based on ERA5 reanalysis data. The omega symbol marks the position of the omega-shaped blocking pattern (see Yessimbet et al., 2022a; Fig. 4d).

In summary, blocking and SSWs are the key large-scale flow phenomena critical in shaping weather in the cold season. The details of these mechanisms are still not fully understood. It is thus important that research aims for improved understanding of these processes for enhancing predictability as well as disaster risk assessment.

2.3. Research Questions

In this context, this thesis aims to understand better the specific mechanisms involved in atmospheric blocking, stratosphere-troposphere coupling, and their links to extreme weather. The thesis addresses the following research questions:

1. How does atmospheric blocking and its interaction with stratospheric dynamics affect cold season surface weather?

2. What are the causal links between atmospheric blocking, SPV variability, and SSWs?

3. How do observational data, particularly GNSS radio occultation data, elucidate the stratosphere-troposphere coupling, particularly the dynamical links between SSWs and atmospheric blocking events?

3. Data Sets

3.1 Reanalysis, forecast and model data

Reanalysis data are the long-term datasets that assimilate different historical observations (e.g., satellite observations, balloon soundings, station data) into a fixed version of a numerical weather prediction model. In other words, they are a blend of models and observations to produce globally complete "maps without gaps" (Hersbach et al., 2020).

This thesis uses the European Centre for Medium-Range Weather Forecasts (ECMWF) fifth-generation reanalysis ERA5 (Bell et al., 2021; Hersbach et al., 2020). First, these data were used to analyze synoptic conditions of the European winter of 2018/2019 that led to heavy Alpine snowfall in January 2019 connected with atmospheric blocking (Yessimbet et al., 2022a). Then, the data were used in the causal inference-based study of the pathways of influence between Northern Hemisphere blocking and SPV variability (Yessimbet et al., 2022b). The data were utilized daily from November to March for the period 1950–2019 and utilized at a horizontal grid resolution of 2.5° × 2.5°.

The prediction of the snowfall event described in Yessimbet et al. (2022a) was based on short- and medium-range forecasts from the ECMWF high-resolution forecast (HRES) and ensemble forecast (ENS) provided four times a day, and extended range forecast provided twice per week (ECMWF, 2021). The forecasts were based on the ECMWF Integrated Forecasting System (IFS) cycle 46r1.

Among the other model data sets used by Yessimbet et al. (2022a) are data from SNOWGRID, an operational snow cover model of the Austrian weather service ZAMG (Zentralanstalt für Meteorologie und Geodynamik, now Geosphere). SNOWGRID is driven with gridded meteorological data from ZAMG's nowcasting system INCA (Integrated Nowcasting through Comprehensive Analysis) (Olefs et al., 2013). The model is based on a radiation model and simulates the temporal development of snow height and snow water equivalent for Austria in 15-minute time steps.

3.2 Meteorological station snow data

Snow cover data from selected meteorological stations, provided by ZAMG (Schöner et al., 2019), were utilized in Yessimbet et al. (2022a) to examine extreme snowfall events in January 2019. Four meteorological stations located in the northern Alpine region and representative of both the western and eastern sections of the Austrian Alps were selected for this study. The stations are situated in the following areas: Seefeld, Tyrol (1182 m above mean sea level, 47°32′N, 11°17′E); Hochfilzen, Tyrol (962 m, 47°46′N, 12°61′E); Abtenau, Salzburg (709 m, 47°58′N, 13°34′E); and Bad Aussee, Styria (667 m, 47°61′N, 13°78′E).

3.3 Satellite-based GNSS Radio Occultation

The Global Navigation Satellite System (GNSS) radio occultation (RO) is a remote sensing method used to study planetary atmospheres. This method is based on detecting radio signals transmitted by GNSS satellites refracted by the Earth's atmosphere as they propagate through it to satellites in Low Earth Orbit (LEO). The schematic setup of this process is shown in Figure 3. An occultation event occurs when a GNSS satellite sets (or rises from) behind the horizon as seen from a LEO satellite. A GNSS receiver records the signals in an oblique vertical scan of the atmosphere due to the relative motion of the satellites, resulting in an RO measurement profile (e.g., Steiner et al., 2011; Scherllin-Pirscher et al., 2021).

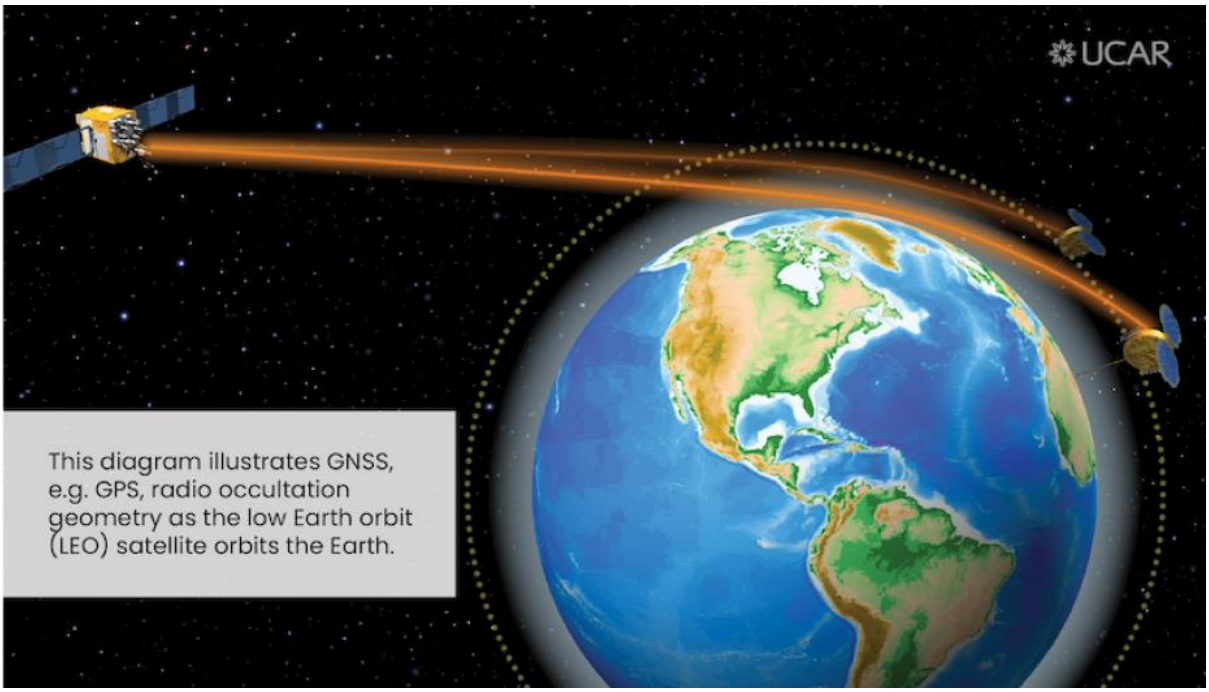


Figure 3. Schematic illustration of the GNSS RO method. Reprinted from https://www.cosmic.ucar.edu/what-we-do/gnss-radio-occultation (accessed on 22.10.2024).

When the radio RO signals are detected, the measured phase changes are converted into bending angle and refractivity profiles using the Abel transform. Refractivity profiles are then used to retrieve pressure and temperature under the assumption of a dry atmosphere. These retrievals are called “dry atmospheric profiles”. In the presence of moisture, background information (e.g., weather forecast data from ECMWF) is used to retrieve pressure, temperature, and humidity. Moist air conditions prevail in the lower and middle troposphere, especially in tropical regions. Due to the reliance on background data, the derived RO temperature data exhibit uncertainties in the lowermost humid regions of the troposphere and at higher altitudes (above about 30 km). For a detailed overview of the retrieval process and related structural uncertainties, refer to Steiner et al. (2020). In the upper troposphere and lower stratosphere (UTLS), RO measurements maintain high quality with minimal structural uncertainty, as highlighted by Scherllin-Pirscher et al. (2017; 2021) and Steiner et al. (2020).

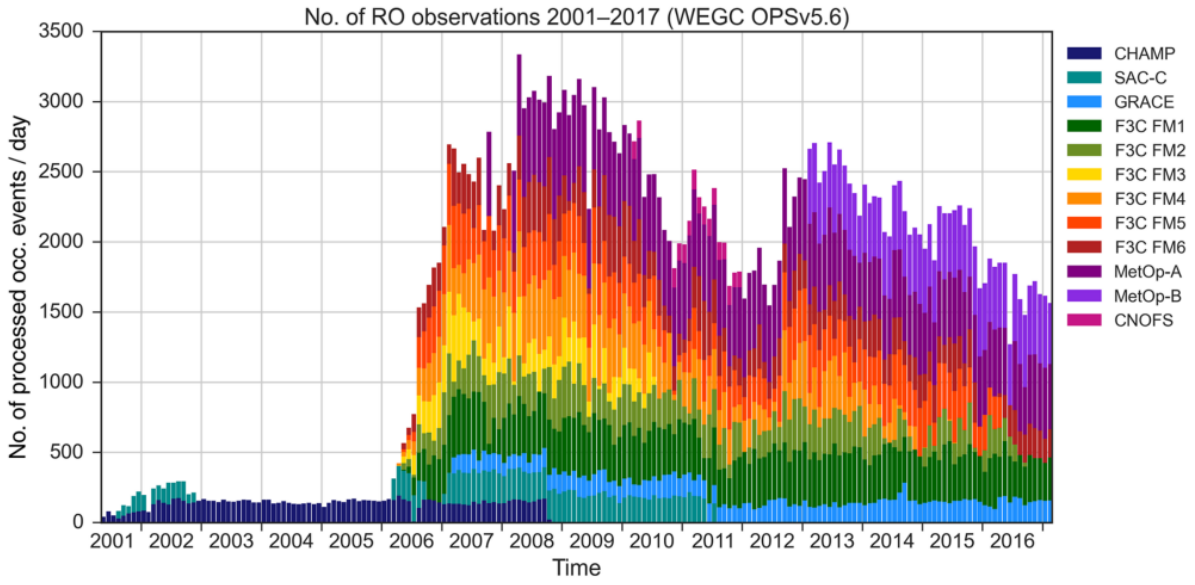


Figure 4. Daily number of RO profiles for different satellites (different colors) as a function of time from 2001 to 2017. Reprinted from Angerer et al. (2017).

This thesis uses geopotential height and physical temperature profiles as a function of pressure processed at the Wegener Center for Climate and Global Change (WEGC) using Occultation Processing System (OPS) version 5.6 (Angerer et al., 2017; Steiner et al., 2020) with phase delay data from the University Corporation for Atmospheric Research (UCAR)/Constellation Observing System for Meteorology, Ionosphere, and Climate (COSMIC) Data Analysis and Archive Center (CDAAC). These GNSS RO measurements were collected by various satellite missions, including Challenging Minisatellite Payload (CHAMP; Wickert et al., 2001), Scientific Application Satellite-C (SAC-C; Hajj et al., 2004), Gravity Recovery and Climate Experiment (GRACE; Beyerle et al., 2005; Wickert et al., 2005), Meteorological Operational Satellite (MetOp; Luntama et al., 2008), and Formosa Satellite mission #3/Constellation Observing System for Meteorology, Ionosphere, and Climate (Formosat-3/COSMIC; Anthes et al., 2011).

GNSS RO measurements from 2006 to 2019 were employed, a period during which data from multiple RO missions were available. The number of daily RO profiles from different missions fluctuated over the period from 2006 to 2019, with the highest number of profiles from 2007 to 2010 (>2500 profiles per day) and a decrease in the number of profiles (from more than 2500 to less than 2000 profiles) from 2012 onwards (Figure 4) due to the exceeding of the lifetime of some of the RO missions (Angerer et al., 2017).

Specifically, the RO profiles were interpolated onto a vertical grid consisting of 147 pressure levels from 1000 to 10 hPa (equidistant in altitude space at 200 m up to 20 km and 500 m above that). Horizontally, a spatial and temporal weighting methodology is applied to generate 2.5° × 2.5° gridded bins from the profile data. This involves applying Gaussian weighting according to the latitude-longitude distances of each profile in relation to the bin center, taking all profiles within 600 km from the center into account. An additional temporal Gaussian weighting of +/- 2 days around the given day is also applied. Thus, in the range of vertical pressure levels from 10 to 850 hPa, there are fewer than 10 missing grid points in the daily gridded fields, with the

number increasing towards the surface. Bilinear interpolation is used to fill any remaining missing grid points. This gridding strategy was determined to be optimal for resolving large-scale atmospheric phenomena such as blocking events and planetary waves while minimizing the number of missing grid points. Several other gridding strategies were tested, including 5° × 5° binning and RO profiles sampled within 300 km and 600 km radii using different spatial weighting methods.

4. Theoretical Framework and Methods

This chapter describes relevant aspects of atmospheric processes and some methods used to study them.

4.1. Atmospheric blocking and Sudden Stratospheric Warmings: Theories, Definition and Frequency

4.1.1. Atmospheric blocking

Atmospheric blocking – a quasi-stationary high-pressure system or, in other words, a quasi-stationary anticyclone (see Section 2.2) – is vertically traceable throughout the troposphere and lower stratosphere and horizontally disrupts the usual zonal propagation of Rossby waves with high- and low-pressure systems and climatological zonal flow, deflecting it in the meridional direction. On a temporal scale, the blocking can last from a few days to a few weeks; on a spatial scale, it can extend over thousands of kilometers.

To date, there is still no unified theory of blocking mechanisms (i.e., onset, maintenance, and decay), although research has been ongoing since the last century (Rex, 1950; Woollings et al., 2018; Suitters et al., 2023). Theories of the blocking formation mechanisms can be divided into two main types: based on low- and high-frequency dynamics (Nakamura et al., 1997). Low-frequency theories generally relate to the role of planetary wave dynamics. Some of these theories emphasize the role of topography and temperature contrasts between ocean and land, planetary wave resonance, and constructive interference of atmospheric waves at different scales. High-frequency theories can be called localized theories because they emphasize the role of synoptic atmospheric processes, such as the role of the cyclone in initiating blocking.

In addition to considering the scale factor of blocking mechanisms, other important theories such as the selective absorption mechanism (Yamazaki and Itoh, 2009), “traffic jam” theory (Nakamura and Huang, 2018), and those emphasizing the role of upstream cyclones (e.g., Nakamura and Wallace, 1990) and moist dynamics and latent heating (e.g., Steinfeld and Pfahl, 2019) in the formation and maintenance of blocking can be highlighted.

The existence of different blocking theories is rooted in the large variability of blocking, e.g., in terms of geographical distribution, type of pressure configuration (i.e., omega/dipole), intensity, spatial extent, and diversity of synoptic conditions. For instance, Figure 5 shows some examples of different synoptic patterns that are referred to as blocking. However, there is no uniform method to identify all synoptic blocking patterns. This is also reflected in the existence of different definitions and detection methods applied to gridded data sets (Barriopedro et al., 2010; Woollings et al., 2018).

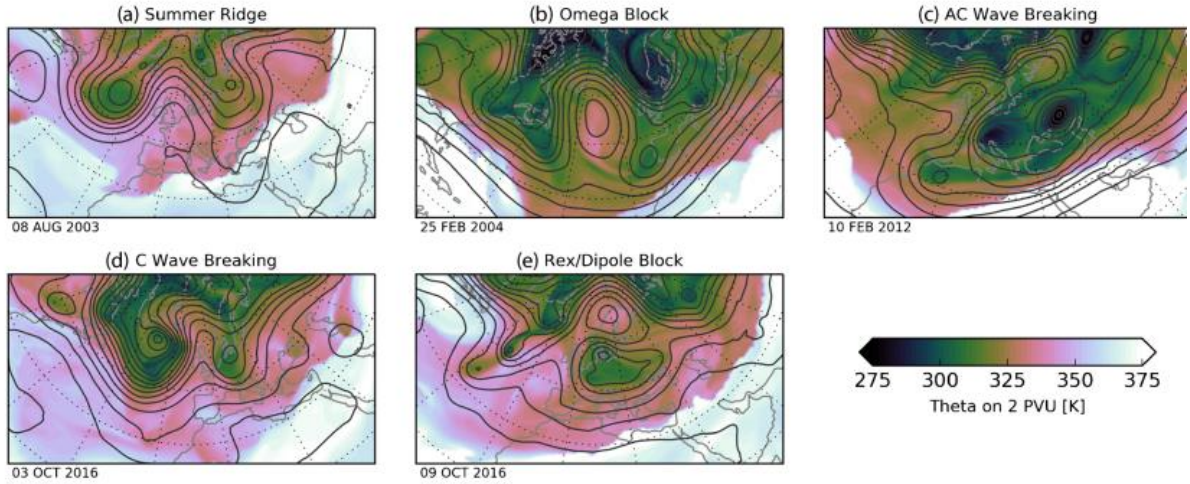


Figure 5. Variety of circulation patterns associated with atmospheric blocking in the North Atlantic. Potential temperature θ (shading, in K) on the dynamical tropopause and 500-hPa geopotential height (black contours, every 60 m) for different dates indicated at the bottom of each panel. The abbreviations AC and C stand for anticyclonic and cyclonic, respectively. Figure reprinted from Woollings et al. (2018).

Typically, blocking is defined using the so-called blocking indices, which specify local and instantaneous blocking conditions on a grid field, taking into account additional criteria to define basic blocking characteristics such as minimum spatial extent, quasi-stationarity and stability (typically 4 or 5 days). To derive these indices, different meteorological parameters (often geopotential height or potential vorticity) are applied at different vertical levels (e.g., in the mid-troposphere at 500 hPa or at dynamical tropopause levels) to datasets with different spatial and temporal resolution (Tibaldi and Monteni, 1990; Barriopedro et al., 2010; Barnes et al., 2012; Small et al., 2014; Woollings et al., 2018).

In this thesis, a standard algorithm is used to calculate blocking indices following Brunner and Steiner (2017) and Brunner (2018). The three-step blocking detection algorithm is based on the reversal of 500-hPa geopotential height gradients. First, the geopotential height gradients are calculated over a latitude width of $\Delta\phi$=15° for each latitude between 75°S and 75°N:

$$\Delta Z_N(\lambda,\phi) = \frac{Z(\lambda,\phi+\Delta\phi) - Z(\lambda,\phi)}{\Delta\phi} \tag{1}$$

$$\Delta Z_S(\lambda,\phi) = \frac{Z(\lambda,\phi-\Delta\phi) - Z(\lambda,\phi)}{\Delta\phi}$$

$$\Delta Z_E(\lambda,\phi) = \begin{cases} Z_S(\lambda,\phi-\Delta\phi) & if\ \phi > 15\,°N \\ Z_N(\lambda,\phi+\Delta\phi) & if\ \phi < 15\,°S \\ 0 & else, \end{cases}$$

where ΔZ_N, ΔZ_S and ΔZ_E are the northward, southward and equatorward gradients, respectively. Based on this, the first index, called Instantaneous blocking (IB) is defined for a

certain grid point and a certain day if the three gradients simultaneously fulfill the following criteria:

$$\Delta Z_N(\lambda', \phi') = \begin{cases} < -10\ m\ /\ (°\text{lat}) & if\ \phi' \geq 0° \\ < 0\ m\ /\ (°\text{lat}) & else \end{cases} \quad (2)$$

$$\Delta Z_S(\lambda', \phi') = \begin{cases} < 0\ m\ /\ (°\text{lat}) & if\ \phi' \geq 0° \\ < -10\ m\ /\ (°\text{lat}) & else \end{cases}$$

$$\Delta Z_E(\lambda', \phi') \quad > 5\ m\ /\ (°\text{lat})$$

Next, the scale criterion is applied so that only extended events are detected. Extended IB is defined if IB is found continuously over at least 15° of longitude. Finally, the criterion of persistence and stationarity is applied to define the blocking index. According to this, extended IB has to be found on each of the neighboring ±2 days within a box of 10° in longitude ($\lambda' \pm 5°$) and 5° in latitude ($\phi' \pm 2.5°$) at a given grid point at longitude λ' and latitude ϕ' .

Although different definitions and blocking detection methods result in some discrepancies in identifying blocking climatologies and trends, numerous studies agree on common climatological patterns of blocking in terms of the general geographical and seasonal characteristics of blocking (e.g., Woollings et al., 2018; Lupo, 2021).

Figure 6 shows the climatology of the Northern and Southern Hemisphere blocking frequency for the winter and summer seasons, based on the index described in Eq. 1 and Eq. 2. Boreal winter blocking occurs most often over oceans east of warm ocean currents (in the North Pacific and Euro-Atlantic region) and over continents in summer. This supports the theory of the importance of ocean-land temperature gradients, according to which the temperature contrasts between the cold land and warmer oceans in winter, and, vice versa, warm land and cooler oceans in summer create favorable conditions for blocking formation. In favor of the same theory is also the fact that blocking occurs much more frequently in the Northern Hemisphere than in the Southern Hemisphere, where there are fewer regions of ocean-land temperature gradients and fewer mountain ranges.

The thesis focuses on blocking in the two ocean basins, the North-Atlantic/Euro-Atlantic and the North Pacific regions, where blocking is most frequent in the cold season. The formation of these blocking events is influenced by various factors and processes (e.g., Suitters et al., 2023). This work explores the role of large-scale dynamic processes linking blocking and SSW events. These mechanisms will be discussed in more detail in the following sections.

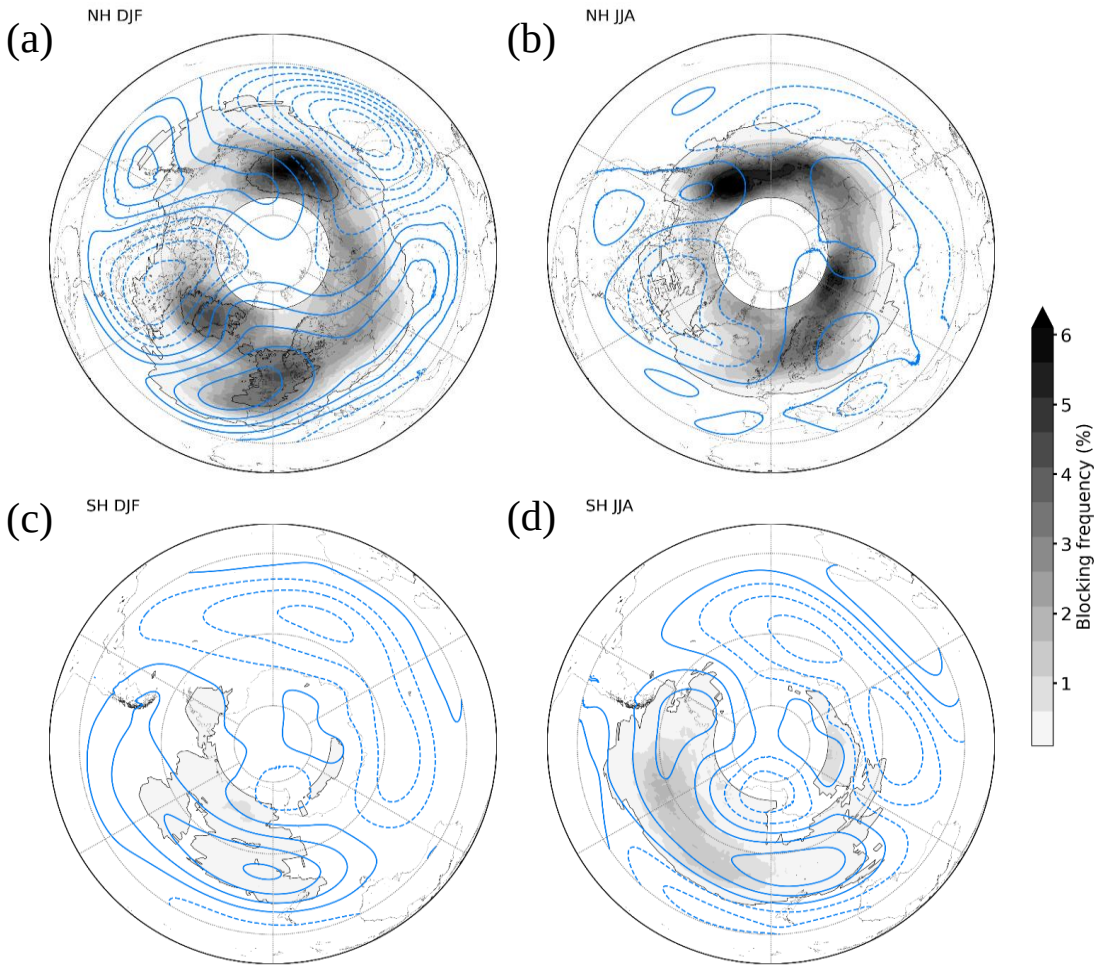


Figure 6. Climatological blocking frequency (shading) expressed as the percentage of blocked days per grid point for (a) the Northern Hemisphere for DJF (December, January, February) and (b) JJA (June, July, August) seasons, (c) the Southern Hemisphere for DJF and (d) JJA seasons based on the ERA5 reanalysis dataset for the period 1950 to 2010. Contours indicate the zonally asymmetric component of the 500-hPa geopotential height climatology.

4.1.2. Sudden Stratospheric Warmings

The SPV is one of the main elements of winter atmospheric circulation, characterized by large-scale cyclonic flow and strong westerly winds driven by the equator-to-pole temperature gradients and the Coriolis effect (see Section 2.2). The polar vortex is present in both the Northern and Southern Hemispheres. However, the northern vortex is much weaker and more variable than the southern vortex.

The SPV is centered around the pole, well-defined horizontally near 60° latitude, and extends vertically from approximately the lower stratosphere throughout the stratosphere to the mesosphere. The SPV is often defined as zonal-mean zonal wind at 60° of latitude and 10 hPa. Extreme cases of polar vortex variability are usually referred to as abrupt weakening or collapse of the stratospheric zonal winds, which can even lead to a change in flow direction. This weakening of the stratospheric flow causes air masses to descend from higher to lower altitudes within the stratosphere. As these air masses descend, they undergo adiabatic

compression, resulting in rapid stratospheric heating. These events are called sudden stratospheric warmings (SSWs).

This thesis applies the commonly used WMO (World Meteorological Organization) definition of SSWs (WMO, 1978):

"*A major SSW event is defined when the zonal-mean zonal wind at 10 hPa and 60°N becomes easterly. The first day on which it occurs is referred to as the central date of an SSW. The additional criterion of a minimum interval of 20 days between SSW events is used to separate individual instances of polar vortex disruption*".

These 20 days correspond to the approximate timescale of thermal damping of the vortex at 10 hPa (Charlton and Polvani, 2007; Butler et al., 2017). A total of 44 major SSWs in the ERA5 reanalysis dataset were reported from 1950 to 2010 by Yessimbet et al. (2022b) following the WMO definition.

It should be noted that different authors interpret this definition slightly differently, e.g., by introducing additional criteria for defining SSWs, such as temperature gradients (e.g., Limpasuvan et al., 2004; Dörnbrack et al., 2012). Furthermore, a distinction can be made between major and minor SSWs. Minor SSWs are characterized by the weakening of the westerly winds, which do not reverse, and adiabatic heating in the stratosphere, which is weaker than observed during major SSW events. Additionally, there is also the concept of a final SSW, which refers to the seasonal weakening of the SPV in spring or early summer.

Major SSW events occur relatively rarely, one or two times per season. The frequency of such events is higher in the Northern Hemisphere than in the Southern Hemisphere. Only one major SSW was recorded in the Southern Hemisphere – in 2002 (Roscoe et al., 2005). This difference can be attributed to the variability of the polar vortices between the hemispheres, with the polar vortex being more robust in the Southern Hemisphere due to the distribution of land masses.

There are two classifications for SSWs. Depending on the geometry of the SPV, the first classification subdivides SSWs into displacement and split events. In the case of displacement, the polar vortex shifts away from the pole, while in the case of split, the polar vortex breaks up into daughter vortices (Butler et al., 2017). Figure 7 shows the configuration of the two vortex event types before and after the split and displacement occurrence.

The second classification, introduced by Kodera et al. (2016), divides SSWs into reflecting and absorbing events based on the evolution of the vertical propagation of planetary wave flux between the troposphere and stratosphere during the SSW recovery phase (when the SPV recovers and re-establishes its typical eastward flow). Absorbing SSWs are characterized by the upward propagation of wave activity or the absorption of waves by the stratosphere, while reflecting SSWs are characterized by the downward propagation of wave activity or the reflection of planetary waves from the stratosphere back into the troposphere during this phase. In contrast to absorbing SSWs, the reflecting events are characterized by a quick termination of a warming episode, resulting in a shorter duration of zonal mean flow reversal. Figure 8 summarizes the differences between absorbing and reflecting events in terms of the evolution of wave activity flux (indicated as vertical component of Eliassen-Palm flux averaged over 45-75°) and SPV strength.

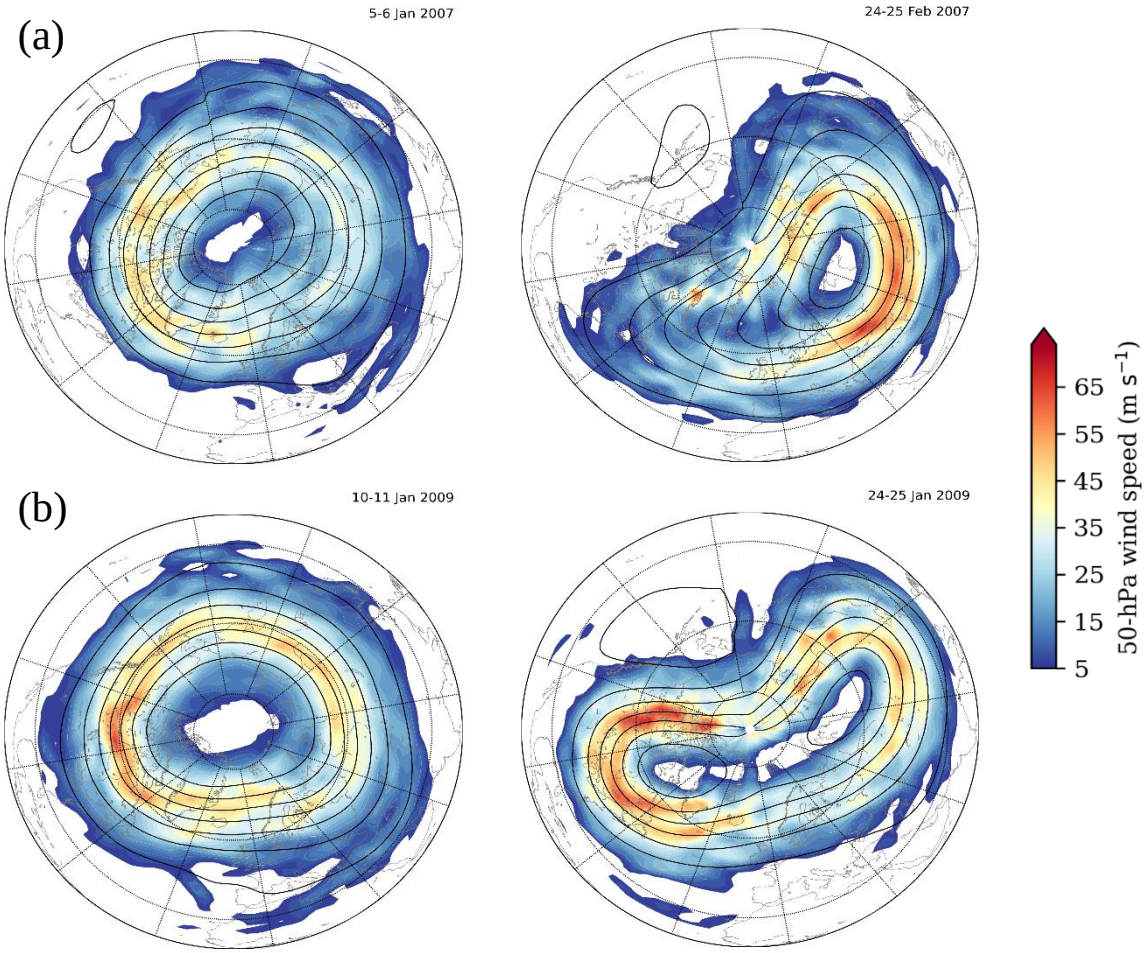


Figure 7. The SPV configuration is shown for the two types of SSWs: (a) a displacement event in 2007 and (b) a split in 2009, highlighting the stages before and during the events (left and right columns). Based on GNSS RO, the shading indicates the wind speed at 50 hPa and the contours the geopotential height at 50 hPa.

While the split/displacement classification focuses on the mature phase of SSW development, the absorbing/reflecting classification pertains to the recovery phase of SSWs, placing greater emphasis on their effects on the troposphere. To date, no direct statistical comparison was undertaken to connect these two SSW classifications.

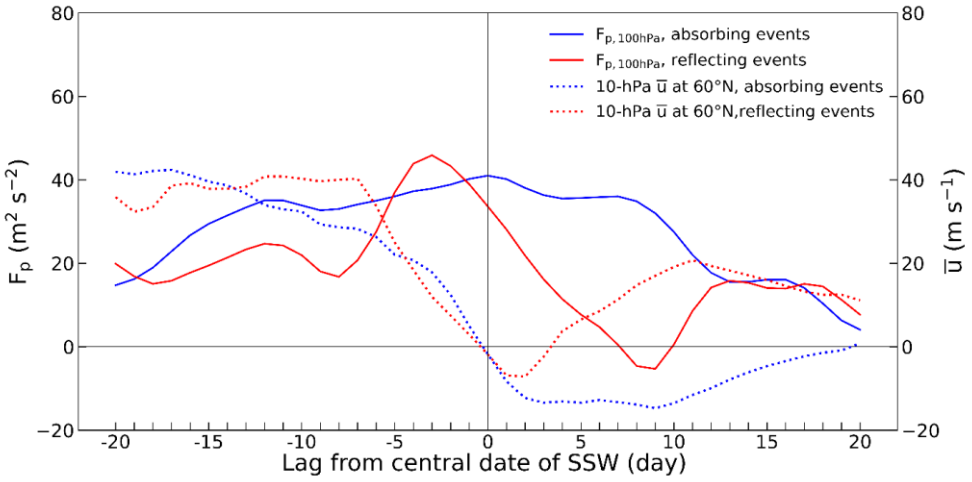


Figure 8. Composite mean of the evolution of SPV strength, indicated as zonal-mean zonal wind at 10 hPa and 60°N (dotted lines), and wave activity, indicated as vertical component of Eliassen Palm flux averaged over 45–75°N (solid lines), for absorbing SSWs (blue lines) and reflecting SSWs (red lines) based on GNSS RO observations.

4.2. Stratosphere-troposphere coupling: Blocking-SSW linkage

It is well established that the troposphere dynamically influences the stratosphere through the vertical propagation of quasi-stationary planetary waves (Matsuno, 1970). In this regard, it can be assumed that the coupling between the stratosphere and troposphere can occur in both upward and downward directions. This section discusses both aspects of this interaction, particularly in the context of the relationship between atmospheric blocking and SSWs, which represent some of the most prominent manifestations of stratosphere-troposphere coupling.

4.2.1. Upward influence

The upward influence can be considered in the context of SSW initiation. Although there is no scientific consensus on the exact mechanisms that trigger SSW initiation, it is known that they are closely related to the absorption of stratospheric wave activity. Since these waves primarily originate in the troposphere, the vertical transfer of angular momentum by planetary waves from the troposphere to the stratosphere is the key process involved in the weakening of the polar vortex, as the waves exert a torque, or a wave drag, on the mean flow. Figure 9 illustrates the evolution of the polar vortex under the influence of the upward wave activity flux. The momentum and energy exchange between waves and the zonal flow is termed the wave-mean-flow interaction.

It is also a matter of debate as to the extent to which the upward propagation of tropospheric waves affects the stratosphere. A central question in this context is whether a minimum threshold or an anomalous level of wave activity is necessary to trigger an SSW event (Matsuno, 1970; Baldwin et al., 2021). Based on a conceptual model, Holton and Mass (1976) suggested that only a minimum amount of wave energy is required to disrupt the polar vortex. In this regard, other idealized GCM (General Circulation Model)-based studies addressed the

role of planetary-scale zonal asymmetries, caused by variations in topography and ocean-land temperature contrasts, in increasing the frequency of SSWs (Gerber and Polvani, 2009; Taguchi and Yoden, 2002; Garfinkel et al., 2020).

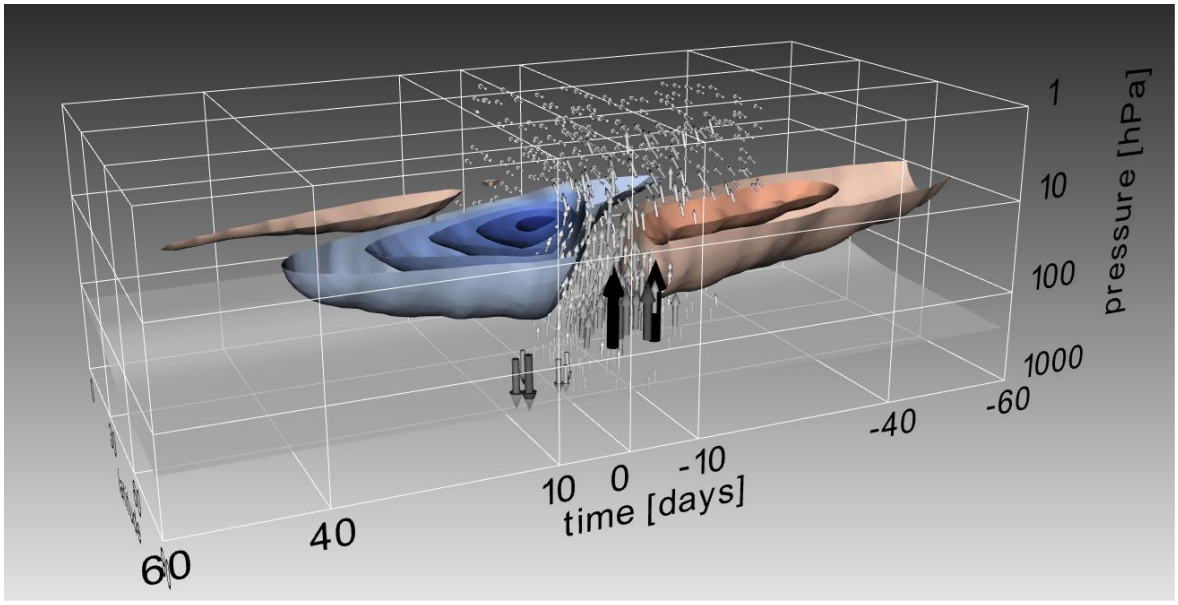


Figure 9. 3D view of the SPV evolution during an SSW event shown as the zonal mean evolution of anomalous zonal wind (isosurfaces/contours) and anomalous Eliassen-Palm flux (arrows) as a function of latitude, time, and pressure. Reprinted from Jucker (2016).

In terms of anomalous wave activity forcing, blocking events are often thought to be responsible for anomalously strong bursts of tropospheric wave activity that subsequently propagate into the stratosphere. Blocking events often precede SSWs, and many studies focused on their role in the occurrence of SSWs (e.g., Martius et al., 2009).

The vertical influence of blocking on the polar vortex is thought to vary by geographic region through constructive and destructive interference between climatological stationary waves and anomalous waves generated by blocking (e.g., Attard & Lang, 2019). Figure 6a shows that blocking frequency maxima over Europe and the Euro-Atlantic region coincide with positive anomalies of the zonal asymmetric component of the 500-hPa geopotential height climatology. This implies that blocking can increase the amplitude of stationary waves through constructive interference, leading to enhanced wave activity, which may contribute to polar vortex warming and increased SSW probability (Attard & Lang, 2019). Similarly, blocking frequency maxima over the western Pacific, coincident with the negative anomaly tends to suppress upward wave propagation through destructive interference with the stationary wave. Although the extent to which blocking can influence the occurrence of an SSW is still a subject of research, it is clear that blocking influences the variability of the polar vortex and SSW development.

Blocking extends vertically into the upper troposphere and tropopause and the effect on the stratosphere can be viewed as an anomalous signal of upward wave activity, propagating from around 200-300 hPa to 100 hPa, which corresponds to the bottom level of the polar vortex.

In this context, using a causal inference-based framework, Yessimbet et al. (2022b) quantified the strength of the pathways of influence between blocking and SPV variability through the upper tropospheric (at 300hPa) and lower stratospheric (at 100hPa) wave activity fluxes. While they confirmed that the influence of blocking on the SPV is entirely mediated by the upward wave activity fluxes, this causal pathway was not entirely straightforward. In particular, they found that, unlike the vortex-weakening effect of European blocking, the vortex-strengthening influence of West Pacific blocking on lower stratospheric wave activity fluxes is only partially mediated by wave activity fluxes in the upper troposphere, which may indicate that the mechanisms of vertical influence differ for European and West Pacific blocking. In addition, they found that neither upper tropospheric nor lower stratospheric wave activity fluxes alone can fully explain this pathway of influence. Two-thirds of the effect of upper tropospheric wave activity flux on the SPV variability is mediated by lower stratospheric wave activity flux, while one-third directly influences the SPV.

Some authors consider the initial SPV strength and size to be important in controlling the upward propagating wave activity that forces SSW initiation (e.g., Albers and Birner, 2014; Jucker and Reichler, 2018). Beyond this, other authors, e.g., Sjoberg and Birner (2012), address the role of duration of wave activity entering the stratosphere, suggesting that more prolonged pulses of wave activity driving the SPV are more critical for the formation and evolution of SSW than stronger but shorter pulses. This was also addressed by the observations-based study of Yessimbet et al. (2024).

It should also be noted that some studies suggest SSW initiation is not always preceded by upward propagating tropospheric wave activity fluxes, indicating the possible involvement of other mechanisms, such as nonlinear stratospheric wave resonance (e.g., Matthewman and Esler, 2011). However, this issue is not addressed in this thesis.

4.2.2. Downward influence

Regarding the downward influence, there is also no scientific consensus on the precise mechanisms or the extent to which stratospheric circulation affects the troposphere. The evidence suggests that SSWs can influence the troposphere through the deformation of the tropopause height affecting the tropospheric jet stream, storm tracks, the formation of blocking events and surface pressure systems, which, in turn, influence surface weather.

SSWs are typically accompanied by anomalies in temperature and geopotential height fields that extend from the stratosphere into the troposphere, resembling downward propagation. However, Baldwin and Dunkerton (2001) suggest that the observed downward propagation of anomalies does not imply that the anomalies in the lower atmosphere originate from the upper layers. It is rather a manifestation of a downward phase propagation of the zonal mean zonal wind anomalies as a result of vertical angular momentum transport driven by upward propagating waves. In other words, the flow in the stratosphere is modified by waves from the troposphere, altering atmospheric conditions that affect the wave propagation in a way that way-mean flow anomalies are drawn poleward and downward.

This vertical coupling between polar vortex variability and tropospheric pressure fields is usually described by “annular modes”, which are hemispheric-scale patterns of atmospheric pressure anomalies of one sign over the polar caps and of the opposite sign at midlatitudes. The Northern Annular Mode (NAM) index describes the variability in atmospheric pressure at different atmospheric pressure levels between the polar region and the midlatitudes around

45°N. The NAM index reflects the integrated wave activity influence of the troposphere on the stratosphere over 1 or 2 months (Polvani and Waugh, 2004). In this respect, the downward influence via the NAM index can be considered "zonal mean" influence, manifested in coherent "downward propagating" zonal mean anomalies. Karpechko et al. (2017) use the metric based on the negative NAM index at 1000 hPa to predict the downward influence of the SSWs and its influence on surface weather.

The negative phase of the NAM index, indicating a weakened polar vortex (high pressure over the poles, low pressure at mid-latitudes), often follows the SSWs (Baldwin et al., 2021). Figure 10 shows the difference between weak vortex events, followed by a negative NAM index, and strong vortex events, followed by a positive NAM index.

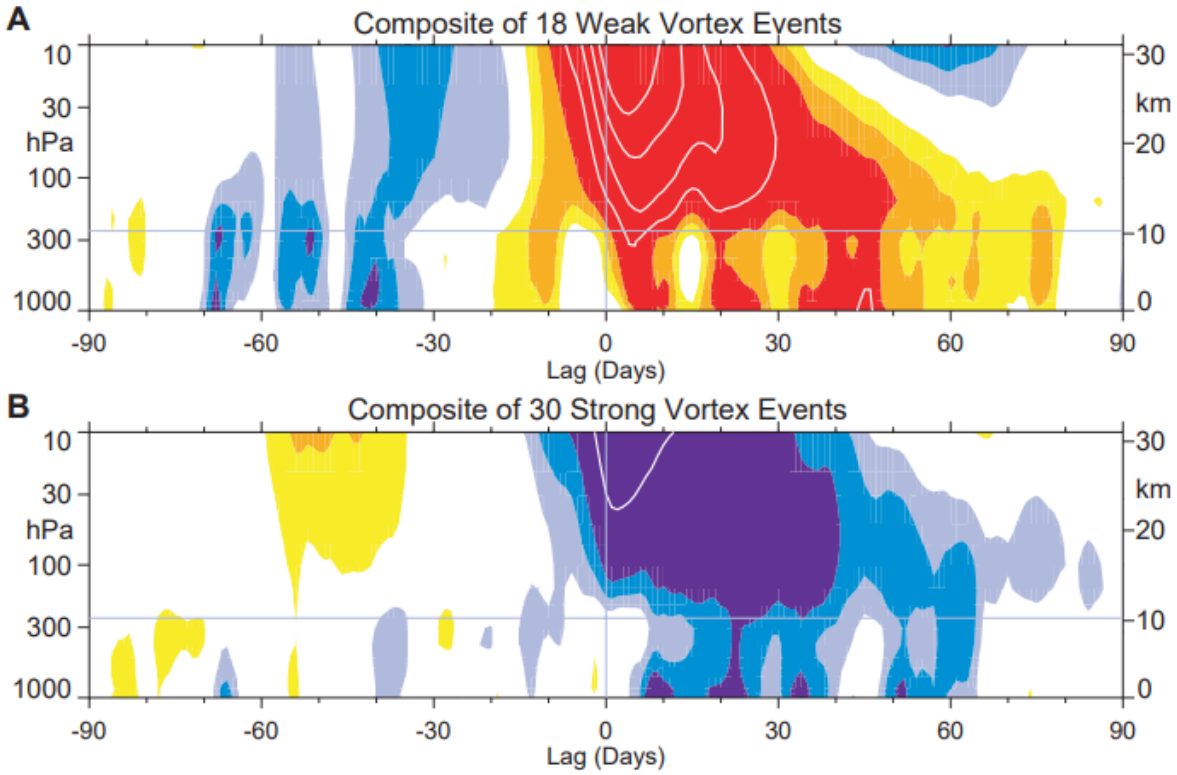


Figure 10. Composites of time-height development of the northern annular mode for (a) 18 weak vortex events and (b) 30 strong vortex events. The events are determined by the dates on which the 10-hPa annular mode values cross –3.0 and +1.5, respectively. The indices are nondimensional; the contour interval for the color shading is 0.25, and 0.5 for the white contours. Values between -0.25 and 0.25 are unshaded. The horizontal lines near 10 km/300 hPa indicate the approximate boundary between the troposphere and the stratosphere. Reprinted from Baldwin and Dunkerton (2001).

While it is often discussed that major SSWs are typically followed by a coherent coupling of the negative NAM signal in both the stratosphere and troposphere, only two-thirds of SSWs have been associated with a negative NAM in both models and observations (Karpechko et al., 2017; Afargan-Gerstman and Domeisen, 2020). Figure 11 shows an example of the NAM index evolution during the winter of 1998-1999, when two SSWs occurred. It can be observed that the negative NAM index during the first event does not extend into the troposphere, which,

according to Karpechko et al. (2017), is a non-downward propagating SSW event. On the contrary, the second SSW event exhibits downward propagation.

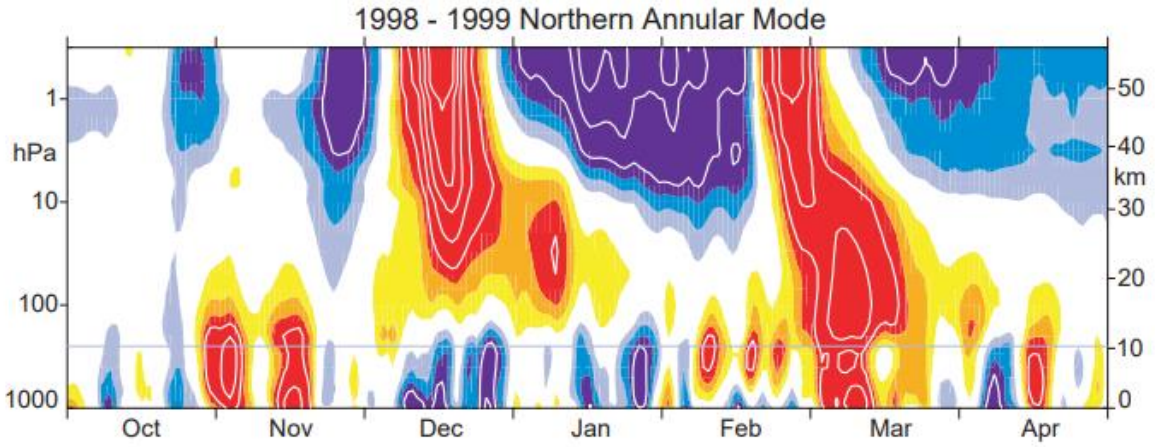


Figure 11. Time-height development of the NAM during the winter of 1998 –1999. The indices have daily resolution and are nondimensional. Blue corresponds to positive values (strong polar vortex), and red corresponds to negative values (weak polar vortex). The contour interval is 0.5, with values between -0.5 and 0.5 unshaded. The thin horizontal line indicates the approximate boundary between the troposphere and the stratosphere. Reprinted from Baldwin and Dunkerton (2001).

This highlights the relevance of the strength of annular responses in the tropospheric circulation and the magnitude of the downward influence associated with SSWs, which is manifested, for example, in tropopause height variability, downward propagation of easterly winds, and temperature anomalies, implying different tropospheric responses. To date, few studies have linked the strength of annular responses to different types of SSWs. One example is the study of Mitchell et al. (2013), who claimed that displacement SSW events are associated with a weaker downward influence and a negative NAM phase that does not exhibit significant downward propagation. In contrast, split events demonstrate a stronger stratosphere-troposphere coupling (Mitchell et al., 2013). For instance, SSW 1998 in Figure 11 has been classified as a displacement (Kodera et al., 2016), while SSW 1999 has been classified as a split event (Martineau et al., 2018). As for the second SSW classification, Kodera et al. (2016) suggest that, unlike reflecting SSWs, absorbing events have a stronger annular response in the tropospheric fields (Kodera et al., 2016). They consistently describe the 1998 SSW event as reflecting and the 1999 event as absorbing.

The regional manifestation of the NAM index is the North Atlantic Oscillation (NAO) index, is frequently used to describe specific tropospheric responses. Specifically, the NAO is defined as "*a north-south dipole in sea level pressure characterized by simultaneous out-of-phase pressure and height anomalies between temperate and high latitudes over the Atlantic sector, and therefore corresponds to changes in the westerlies across the North Atlantic into Europe.*" (IPCC, 2007). The negative phase of NAO is characterized by higher-than-normal pressure over Iceland and lower-than-normal pressure over the Azores. Woollings et al. (2010) suggested that the negative NAO regime is strongly correlated with atmospheric blocking over Greenland (e.g., Woollings et al., 2010). Athanasiadis et al. (2020) also showed that the high frequency of wintertime blocking in the North Atlantic, particularly at high latitudes, is strongly

linked to the negative NAO regime. Conversely, the absence of blocking in this region is associated with a positive NAO regime.

In this context, Yessimbet et al. (2024), using GNSS RO observations, showed that the major split SSW events over the last decade, also classified as absorbing, triggered a tropospheric response, resembling a negative NAO pattern, and induced blocking in the Euro-Atlantic region. In contrast, the reflecting events, also classified as displacement SSW events, induced a different tropospheric response, characterized by North Pacific blocking and a positive NAO regime in the North Atlantic. To illustrate this, Figure 12 presents geopotential height configuration during the split SSW event in winter 2009/2010 that was marked by a strongly negative NAO phase and a prominent blocking extending across the Euro-Atlantic region from Greenland to Scandinavia, and a displacement SSW event in winter 2007/2008, which featured North Pacific blocking.

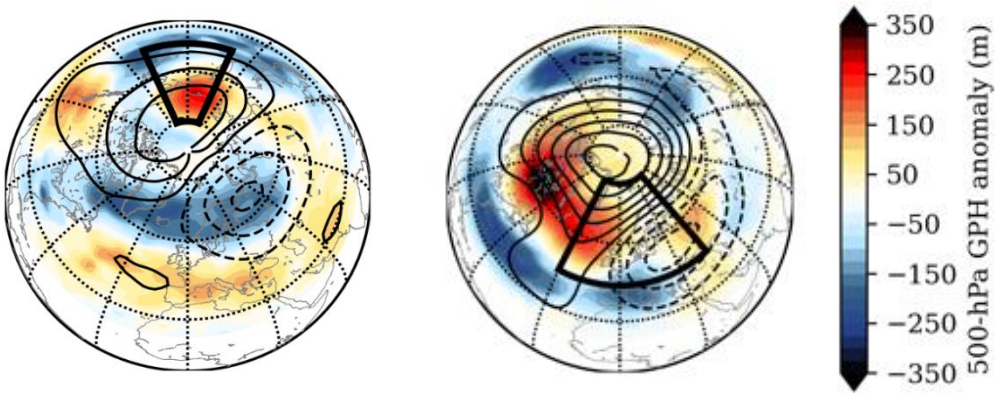


Figure 12. Geopotential height anomalies at 500-hPa (shading) and 50-hPa (contours) depicting the negative NAO pattern during the SSW event in winter 2009-2010 (right) and the solid box indicating the Euro-Atlantic blocking; and a positive NAO pattern during the displacement SSW event in winter 2007-2008 (left) with the solid box indicating the North Pacific blocking.

In other words, unlike reflecting SSWs, absorbing SSWs exhibit a stronger annular mode response in the tropospheric circulation, characterized by more prolonged and pronounced downward-propagating thermal and zonal-mean zonal wind anomalies associated with a weakened polar vortex (Kodera et al., 2016; Yessimbet et al., 2024). This suggests that the magnitude of the downward impact can be considered a potential factor to assess whether displacement and split SSW events trigger different tropospheric responses and whether this classification is connected to the absorbing/reflecting SSW categories.

4.2.3. Influence of SSWs on the polar tropopause

To further explore how SSW events differ in the magnitude of their downward impact and associated tropospheric responses, the influence of SSWs on the polar tropopause was assessed in Yessimbet et al. (2024). Figure 13 presents the evolution of static stability anomalies, which characterize the strength of the tropopause inversion layer (TIL), during eight major SSWs, based on GNSS RO observations. It can be observed that strengthening of the TIL, indicated

by enhancement of the static stability anomaly near the tropopause, occurs during the events. The absorbing and split events from 2009 to 2019 induced a more pronounced TIL strengthening than the reflecting and displacement SSWs in 2007 and 2008. These results are consistent with Wang et al. (2023), who, also using GNSS RO data, documented a decrease in tropopause height during major SSWs that was larger for 2009, 2010, and 2013 SSW events and considerably smaller for 2007 and 2008 events. The study by Wargan and Coy (2016), based on reanalyses, supports these results, showing both TIL enhancement and a simultaneous decrease in polar tropopause height during the major SSWs in 2004, 2006, 2009, 2010, and 2013. Their findings also indicate that the magnitudes of the TIL strength qualitatively correspond to the intensity of the SSWs.

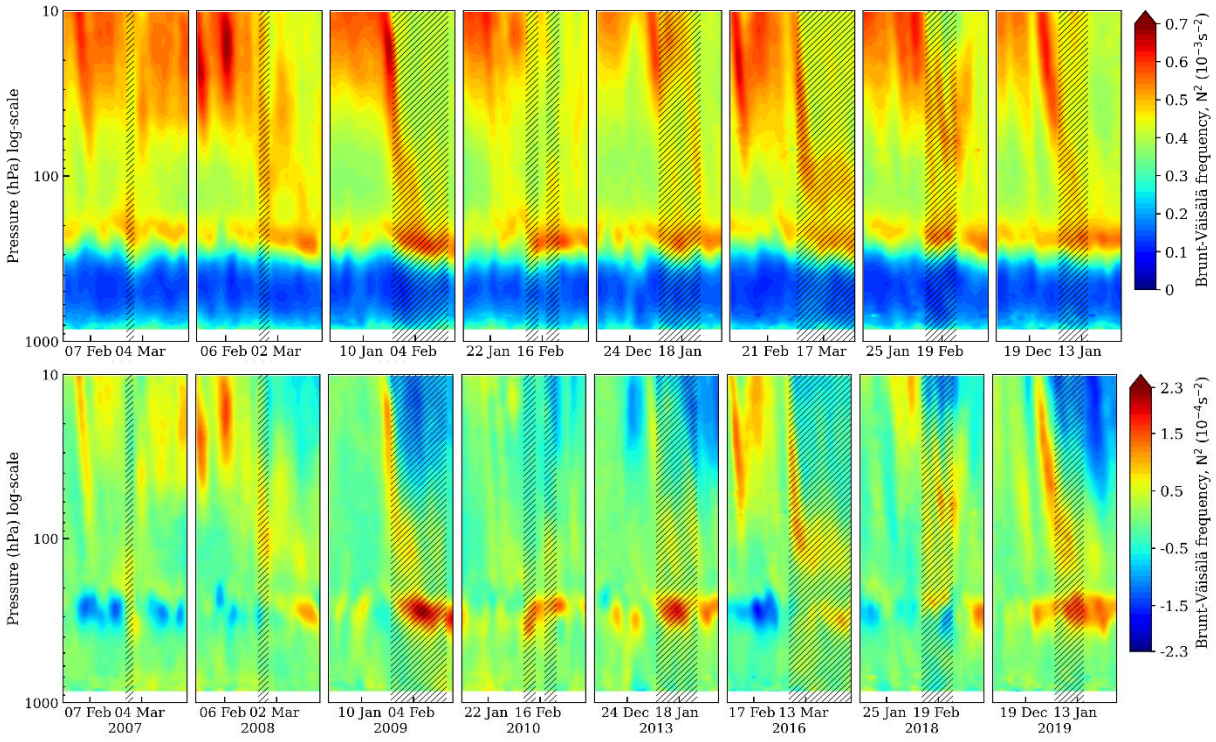


Figure 13. Brunt-Väisälä frequency computed from GNSS RO averaged over 75-90° N within a time frame of +/- 30 days relative to the onset of the SSW events from 2007 to 2019. The upper panel shows the absolute values, and the lower panel shows the anomalies. Hatched regions indicate dates when the zonal-mean zonal wind at 60° N and 10 hPa is negative (Yessimbet et al., 2024).

The possible mechanism describing the relation between surface pressure changes manifested in the NAO index, the strength of the polar vortex, and how they impact the height of the polar tropopause is illustrated schematically in Figure 14. When the NAO index is positive, implying lower surface pressure over Iceland, upward-propagating planetary waves refract from the polar region, thereby strengthening the polar vortex. The stronger polar vortex is associated with a positive PV anomaly that results in the rising of the tropopause over the North Pole. Conversely, when the NAO index is negative, implying higher surface pressure over Iceland, the upward-propagating planetary waves refract towards the pole and weaken the polar vortex. This results in a decrease in the polar tropopause height.

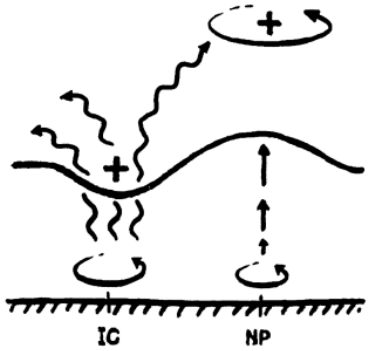


Figure 14. Schematic illustration summarizing the interactions between the strength of the NAO, the height of the tropopause, and the strength of the SPV. Reprinted from Ambaum and Hoskins (2002).

4.2.4. Wave-reflection mechanism

Another perspective on downward influence is the wave-reflection mechanism, in which waves bounce back or reflect when they encounter certain atmospheric conditions. Some authors (Chen and Robinson, 1992; Weinberger et al., 2021; Boljka and Birner, 2022) consider that the tropopause, particularly the vertical buoyancy frequency gradient around the tropopause, is an important control on the upward propagation of wave activity into the stratosphere, i.e., the tropopause acts as a valve. These studies also address the importance of stratospheric wind shear control. Thus, a reflective condition can be created around the tropopause or in the stratosphere that prevents the upward propagation of wave activity or reflects it back into the troposphere. The reflected wave activity interferes with the tropospheric wave field and influences the circulation. The wave reflection mechanism is another facet of the wave-mean-flow interaction and has been documented in several studies (Hines, 1974; Geller and Alpert, 1980; Perlwitz and Harnik, 2004, Kodera et al., 2008; 2013).

When wave reflection occurs during SSWs, such SSWs are called “reflecting SSWs” (see Section 4.1.2). As described by Kodera et al. (2008; 2016), wave reflection during such events occurs because a negative vertical wind shear forms in the stratosphere. This wind shear is characterized by weaker, easterly winds in the upper stratosphere and stronger, westerly winds in the lower stratosphere. As a result, wave packets experience a transition from lower regions where westerly winds support their upward propagation to easterly winds that oppose it. This creates an effective barrier, causing some of the wave activity to be reflected downward. A characteristic of reflecting SSW events is that the recovery of the polar vortex is rapid, which can be both a result of and a contributing factor to the generation of negative wind shear.

It has been suggested that downward propagation of wave activity can amplify tropospheric waves and enhance the meandering of zonal flows, creating favorable conditions for blocking. Specifically, as discussed by Kodera et al. (2013, 2016), wave packets that propagate upward from the Eurasian sector are reflected downward over the North American-North Atlantic sector following an SSW, inducing a trough over eastern Canada and a ridge over the North Pacific in the upper troposphere. This pattern favors the development of a North Pacific blocking, which is then maintained through interactions with transient synoptic eddies.

In this regard, Yessimbet et al. (2024) highlighted the role of downward wave reflection over the North American continent in forming the North Pacific blocking due to reflecting SSWs. Other studies also linked wave reflection mechanisms to North Pacific blocking (e.g., Messori et al., 2022).

4.2.5. Wave activity diagnostics

The following section presents the specific formulae utilized in the calculations of planetary wave activity in this thesis, particularly used in Yessimbet et al. (2024). As all the formulae are generally accepted, their detailed derivation is not provided. Detailed derivations of these equations can be found in Eliassen and Palm (1960), Edmon et al. (1980), Plumb (1985), and Andrews et al. (1987).

Since the large-scale circulation in the extratropical region is away from the Earth's equator and approaches a state of geostrophic balance – where the Coriolis force and the pressure gradient force are in equilibrium – this thesis uses the quasi-geostrophic (QG) framework. This framework simplifies the governing equations and is commonly used to analyze the extratropical circulation.

To analyze wave activity flux, the Eliassen-Palm (EP) theory is used, providing a zonally averaged framework for studying the vertical transfer of momentum by upward-propagating planetary waves and their associated meridional heat transport. The QG form of the EP flux for the real atmosphere in spherical coordinates is defined as follows:

$$\mathbf{F} = \begin{pmatrix} F_\phi \\ F_p \end{pmatrix} = a\cos\phi \begin{pmatrix} -\overline{u'v'} \\ f\dfrac{\overline{v'\theta'}}{\dfrac{\partial\overline{\theta}}{\partial p}} \end{pmatrix} \tag{3}$$

where F_ϕ and F_p are the meridional and vertical components of the EP flux, a denotes the equatorial radius of the Earth, p denotes log-pressure, ϕ is the latitude, and θ is potential temperature, and $\cos\phi$ is a geometric term. The Coriolis parameter $f = 2\Omega\sin\phi$, where Ω is the Earth's angular velocity, u and v are the geostrophic meridional and zonal winds. The overlines denote zonal averages, and primes are deviations from zonal averages. The geostrophic meridional u and zonal v winds are defined as follows (Holton and Hakim, 2012):

$$u = -\frac{1}{fa}\frac{\partial\Phi}{\partial\phi} \tag{4.1}$$

$$v = \frac{1}{fa\cos\phi}\frac{\partial\Phi}{\partial\lambda} \tag{4.2}$$

with $\Phi = Z\,g$, where g is standard gravity at mean sea level (9.80665 m/s^2).

In the QG framework, the vertical component of the EP flux is approximately proportional to zonal mean eddy heat flux, $\overline{v'T'}$:

$$-F_p = -\frac{\overline{v'\theta'}}{\frac{\partial \bar{\theta}}{\partial p}} \propto \overline{v'T'}. \quad (5)$$

Therefore, $\overline{v'T'}$ is used as a proxy for the vertical propagation of wave activity. Evaluated at 100 hPa, which corresponds to the bottom of the polar vortex, it estimates the wave activity flux entering the stratosphere (Yessimbet et al., 2022b).

The EP flux divergence is defined as follows:

$$\nabla \cdot \mathbf{F} = \frac{1}{a\cos\phi}\left(\frac{\partial F_\phi}{\partial \phi} + \frac{\partial F_p}{\partial p}\right). \quad (6)$$

The EP flux divergence represents the net effect of eddies on the zonal mean flow. For a steady flow, the total EP flux is conserved, i.e., $\nabla \cdot \mathbf{F} = 0$. In the regions where the EP flux converges, i.e., $\nabla \cdot \mathbf{F} < 0$, eddies transfer negative momentum to the zonal mean flow, exerting a wave drag and causing a deceleration of the flow. Conversely, when divergence is positive, i.e., $\nabla \cdot \mathbf{F} > 0$, eddies carry negative momentum away from the region, leading to an acceleration of the zonal flow.

This can be observed in the wintertime climatology of the EP flux and its divergence for the Northern Hemisphere (Figure 15). The dominant pattern of the EP flux divergence is the strong divergence near the surface in the midlatitudes and large convergence zone above it. The midlatitude near-surface troposphere is a source for the Rossby planetary waves, which is associated with baroclinic instability and is associated with acceleration of the zonal flow. It can be observed that the waves propagate upwards, and the EP flux is almost vertical in the lower troposphere. Part of the flux converges in the upper troposphere decelerating the flow, but most of it continues to propagate upward. In the stratosphere the flux is deflected meridionally, towards subpolar, but mostly towards subtropical regions, where it reaches the critical layer and converges decelerating the flow in these regions.

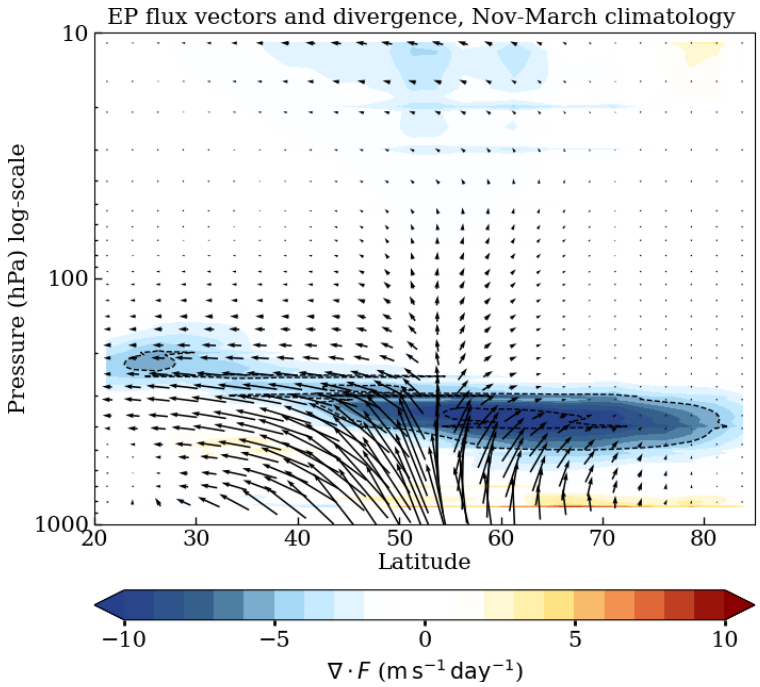


Figure 15. Climatological QG Eliassen–Palm flux vectors and divergence (shading) for November to March from 2006 to 2019 based on GNSS RO data.

Plumb flux is a diagnostic tool for the analysis of wave activity propagation in the atmosphere on a three-dimensional plane (Plumb, 1985). Plumb flux helps to identify regions of wave reflections or wave activity sources by showing changes in the transport and distribution of potential vorticity due to planetary waves. The expression for Plumb flux, denoted as $\boldsymbol{F_s}$:

$$\mathbf{F_s} = \begin{pmatrix} F_x \\ F_y \\ F_z \end{pmatrix} = p\cos\phi \begin{pmatrix} \frac{1}{2a^2\cos^2\phi}\left[\left(\frac{\partial\psi'}{\partial\lambda}\right)^2 - \psi'\frac{\partial^2\psi'}{\partial\lambda^2}\right] \\ \frac{1}{2a^2\cos\phi}\left(\frac{\partial\psi'}{\partial\lambda}\frac{\partial\psi'}{\partial\phi} - \psi'\frac{\partial^2\psi'}{\partial\lambda\partial\phi}\right) \\ \frac{2\Omega^2\sin^2\phi}{N^2 a\cos\phi}\left(\frac{\partial\psi'}{\partial\lambda}\frac{\partial\psi'}{\partial z} - \psi'\frac{\partial^2\psi'}{\partial\lambda\partial z}\right) \end{pmatrix} \quad (7)$$

where F_x and F_y and F_z are the zonal, meridional and vertical components of Plumb flux, the stream function $\psi = \frac{\Phi}{2\Omega sin\phi}$ and N^2 is Brunt-Väisälä frequency, defined as follows:

$$N^2 = -\frac{pg^2\frac{\partial\theta}{\partial p}}{RT\theta} \quad (8)$$

4.3. Links to extreme weather

A characteristic of blocking is that it is associated with stationary and persistent large-scale circulation anomalies. Blocking can modulate westerly flow, the location of cyclones and hence storm tracks, and affect moisture and temperature advection.

Figure 16 shows an example of an omega-shaped blocking situation over the Euro-Atlantic region and the associated potential extreme weather events. Extreme cold temperature anomalies are usually observed at the southeastern flank of the blocking system. The frequency of these anomalies in Europe increases when blocking occurs over Greenland, especially in central Europe when blocking is present over the North Atlantic and Scandinavia (Sillmann et al., 2011; Brunner et al., 2018; Kautz et al., 2022). Statistically, up to 70% of winter cold spells in central Europe are linked to a blocking system between 60° W and 30° E (Brunner et al., 2018). European cold spells associated with North Atlantic blocking have been connected to the negative NAO phase, which is also linked to SSW events (refer to Section 4.2).

Similarly, the advection of cold air from higher latitudes downstream of the blocking has been linked to cold spells over North America, particularly with North Pacific blocking and the wave reflection mechanism responsible for this phenomenon (Matthias and Kretschmer, 2019; see Section 4.2).

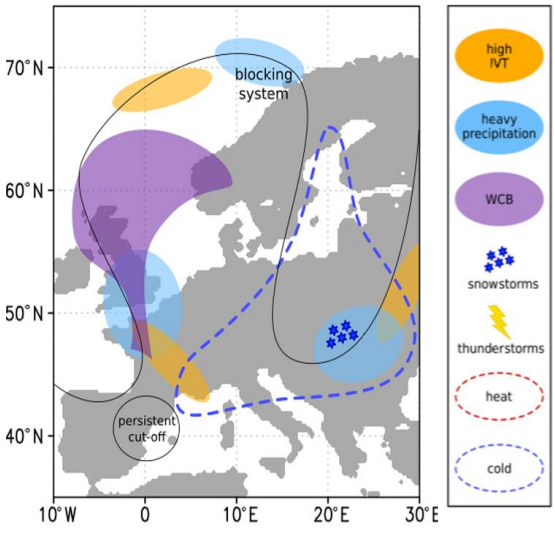


Figure 16. Schematic illustration of a blocking system (black line, indicating a geopotential height or PV contour) and associated surface extremes during the cold season (October–March). Blue stars show areas where snowstorms are observed (eastern flank of the block). Areas with heavy precipitation are marked in light blue (poleward edge of the ridge and at both flanks). Areas with high integrated water vapor transport are illustrated in orange. Area with cold temperature extreme is marked with blue dashed line. Reprinted from Kautz et al. (2022).

Heavy precipitation and snowstorms can be observed in the eastern trough of the blocking. This is mainly due to the advection of cold temperatures and moist air from higher latitudes and from the ocean by the meridional flow due to the blocking configuration. In this context, Yessimbet et al. (2022a) analyzed and described an extreme snowfall case in 2019 in Austria that resulted from such a situation.

It is important to differentiate between extreme seasonal snowfalls and short-term snowfalls associated with blocking. An unusually high frequency of blocking during the winter can result in significant snow accumulation, potentially leading to avalanches and spring flooding (Pinto, 2007; Stucki et al., 2012; Kautz et al., 2022). In this respect, snow accumulation in Eurasia and North America has been linked to blocking frequency over the Atlantic (Garcia-Herrera and Barriopedro, 2006). Additionally, significant snow accumulations in central Europe during the winter of 2005-2006 have been partially attributed to blocking (Pinto et al., 2007). Similarly, seasonal snow cover in Switzerland is closely associated with Scandinavian blocking (Scherer and Appenzeller, 2006). Cold-season blocking can also play a pivotal role in flood events. For instance, a flood event in October 2011 in Switzerland was driven by an atmospheric river modulated by a blocking over the Atlantic (Piaget et al., 2015).

The mechanisms driving extreme events are multifaceted. While blocking events play a significant role in the occurrence of extremes, many other factors – both regional and remote – also contribute to their development.

5. Summary and Conclusions

This thesis investigates the mechanisms of atmospheric blocking, its dynamic interplay with stratospheric processes – particularly SSWs – and its role in extreme weather events, such as the extreme snowfall in January 2019 in the Austrian Alps.

5.1. Addressing the Research Questions

Here, the answers to the research questions formulated in Section 2.3 are addressed and summarized.

1. How does atmospheric blocking and its interaction with stratospheric dynamics affect cold season surface weather?

This research question was investigated in Paper I (Yessimbet et al., 2022a), which was based on a case study of an extreme weather event: the record snowfall in the northern Alps in January 2019.

This study identified mechanisms by which atmospheric blocking influenced the occurrence of this extreme snowfall event. In particular, it was analyzed and described how atmospheric blocking modulates the jet stream by deviating it from its typical latitudinal trajectory, resulting in the jet stream slowing down or elongating in a meridional orientation, which facilitated the transport of moist air masses in the lower atmosphere from north to south.

The connection between this extreme event and the concurrent processes in the stratosphere, specifically SSW and polar vortex split, was also identified. In particular, the results showed that the daughter vortices resulted from the vortex split were barotropically aligned with the omega-block ridge-trough configuration, indicating the connection between stratospheric and tropospheric processes.

Thus, the importance of considering the zonal asymmetry of the polar vortex for the development of surface weather, rather than its zonal mean influence on the tropospheric circulation (which is usually used to determine the likelihood of the downward impact of the SSW), was emphasized. More generally, the importance of considering the stratosphere-troposphere coupling and the need for a better understanding of it to improve the prediction of these extreme events in climate and weather models has been highlighted by Yessimbet et al. (2022a).

2. What are the causal links between atmospheric blocking, SPV variability, and SSWs?

This question was investigated in Paper II (Yessimbet et al., 2022b) using a causal inference-based analysis method applied to the blocking index, upper tropospheric heat flux, lower stratospheric heat flux, and SPV index.

The findings of Yessimbet et al. (2022b) confirm that the influence of atmospheric blocking on the SPV is entirely mediated by upward wave activity fluxes, consistent with classical views.

The pathways of influence have been found to differ between blocking events in Europe and the West Pacific. Specifically, the results indicate that European blocking has a weakening effect on the polar vortex, with its effect on lower stratospheric wave activity fluxes being fully mediated by upper tropospheric wave activity fluxes. In contrast, West Pacific blocking leads to a strengthening of the polar vortex, but its effect on lower stratospheric wave activity fluxes is only partially mediated by upper tropospheric wave activity fluxes. This implies that the mechanisms governing the vertical influence of West Pacific blocking may differ from those of European blocking.

The study also finds that only two-thirds of the influence of upper tropospheric wave activity fluxes on SPV variability is mediated via lower stratospheric wave activity fluxes. This indicates that some other factors or pathways contribute to SPV variability. The results also show that SSWs are not entirely explainable in terms of upward wave activity fluxes.

Overall, Yessimbet et al. (2022b) clarified the causal links between atmospheric blocking and polar vortex variability.

3. How do observational data, particularly GNSS radio occultation data, elucidate the stratosphere-troposphere coupling, particularly the dynamical links between SSWs and atmospheric blocking events

Paper III (Yessimbet et al., 2024) provides a detailed description of the main dynamic and synoptic evolution of major SSW events from 2007 to 2019, based solely on GNSS RO observations. These major SSW events were categorized into displacement/split events and reflecting/absorbing events – whereas classification is typically conducted using a single method.

Yessimbet et al. (2024) identified distinct patterns in the influence of reflecting and absorbing sudden stratospheric warming (SSW) events on stratosphere-troposphere coupling. Their findings indicate that reflecting events involve stratospheric wave reflection characterized by downward wave propagation during the recovery phase, which induces blocking over the North Pacific, supporting previous studies. In contrast, absorbing events are associated with prolonged wave absorption, evident as continuous upward wave activity propagation from the troposphere into the stratosphere and are linked to blocking over the Euro-Atlantic region.

The study also demonstrated that enhanced tropospheric wave activity typically precedes SSWs events by a few days. In seven of the eight SSW events analyzed, the increase in stratospheric wave activity was preceded by a rise in tropospheric wave activity for several days, with the exception of the 2007 event. In that case, stratospheric amplification occurred without the short-term tropospheric precursors observed in the other events. However, the findings revealed that an anomalous tropospheric precursor contributed to preconditioning the polar vortex 20 days prior to the SSW in 2007. Although this tropospheric precursor was not immediate, it established the conditions necessary for the subsequent enhancement in the stratosphere. It is important to note that the peak of wave activity amplification exhibited distinct temporal characteristics for reflecting and absorbing SSW events. Specifically, the

amplification peak for reflecting SSWs was shorter in duration compared to that for absorbing events.

Moreover, Yessimbet et al. (2024) demonstrated how different SSW events affect the polar tropopause. Specifically, the enhancement of the polar tropopause inversion layer (TIL) following absorbing SSWs was found to be stronger than that associated with reflecting SSWs.

Finally, the results emphasized that GNSS radio occultation (RO) data are effective in capturing the key dynamic features of SSWs and stratosphere-troposphere interactions. This data captures profiles of temperature, geopotential height, wind, and wave-activity flux. Additionally, the findings indicate that the geostrophic approximation of wind and wave activity profiles effectively resolves these dynamic interactions.

In conclusion, this research improves the observational evidence on stratosphere-troposphere coupling and SSWs, showing their dynamic and synoptic description, providing their classification and interaction with blocking events and demonstrating the effectiveness of GNSS RO data in studying these phenomena.

5.2 Conclusions

To date, there is no scientific consensus on the detailed dynamic mechanisms describing the various types of blocking and SSW events, as well as their coupling between the stratosphere and troposphere. This lack of a complete understanding of their dynamics is one of the major limitations in accurately predicting these phenomena within weather and climate models. Therefore, one of the primary objectives of this thesis was to enhance our understanding of the mechanisms governing the interactions between these atmospheric processes, with the potential to improve forecasts of related extreme events.

This thesis primarily relies on reanalysis and observational data, employing a case study approach (as demonstrated in Papers I and III) alongside statistical methods, particularly causal network analysis (as demonstrated in Paper II). The latter study has helped to clarify the pathways of influence between Northen Hemisphere blocking and SPV variability. Furthermore, to the best of my knowledge, Paper III is the first study of atmospheric dynamics, particularly the stratosphere-troposphere coupling and the link between blocking and SSWs, based entirely on GNSS RO data. This work has also demonstrated the effectiveness of GNSS RO measurements in analyzing atmospheric dynamics, providing valuable observational insights.

In terms of future work, the results of Paper II suggest that the wave reflection mechanism should be considered in the causal network of stratosphere-troposphere coupling to enhance understanding of North Pacific blocking mechanisms. Additionally, Paper III concludes that the utilization of GNSS RO, especially exploiting its high vertical resolution, has the potential to further illuminate the relationship between tropopause structure and wave activity propagation.

Part II. Published Papers

Paper I. Heavy Alpine snowfall in January 2019 connected to atmospheric blocking

Kamilya Yessimbet[1,2] , Albert Ossó[1] , Rainer Kaltenberger[3] , Linus Magnusson[4] and Andrea K. Steiner[1,2,5]

[1]Wegener Center for Climate and Global Change, University of Graz, Graz, Austria
[2]FWF-DK Climate Change, University of Graz, Graz, Austria
[3]Zentralanstalt für Meteorologie und Geodynamik (ZAMG), Vienna, Austria
[4] European Centre for Medium-Range Weather Forecasts, Reading, UK
[5]Institute for Geophysics, Astrophysics, and Meteorology, Institute of Physics, University of Graz, Graz, Austria

Weather, 77: 7-15.
doi: doi.org/10.1002/wea.4020

© 2021 The Authors. Weather published by John Wiley & Sons Ltd on behalf of the Royal Meteorological Society. This is an open access article under the terms of the Creative Commons Attribution License.

Heavy Alpine snowfall in January 2019 connected to atmospheric blocking

Kamilya Yessimbet[1,2], Albert Ossó[1], Rainer Kaltenberger[3], Linus Magnusson[4] and Andrea K. Steiner[1,2,5]

[1]*Wegener Center for Climate and Global Change, University of Graz, Graz, Austria*
[2]*FWF-DK Climate Change, University of Graz, Graz, Austria*
[3]*Zentralanstalt für Meteorologie und Geodynamik (ZAMG), Vienna, Austria*
[4]*European Centre for Medium-Range Weather Forecasts, Reading, UK*
[5]*Institute for Geophysics, Astrophysics, and Meteorology, Institute of Physics, University of Graz, Graz, Austria*

Introduction

Atmospheric blocking often triggers anomalous weather patterns in the mid-latitudes. Blocking is characterised by a quasi-stationary high-pressure system and reversal of the westerly flow near its southern edge, which can persist for several weeks and lead to extreme weather events (Rex, 1950; Tibaldi and Molteni, 1990; Pelly and Hoskins, 2003). In summer, atmospheric blocking over Europe is associated with heatwaves, while in winter, it is linked to cold weather extremes associated with the equatorward advection of cold air masses from the polar region (Tyrlis and Hoskins, 2008; Sillmann *et al*., 2011). Regions on the edge of the block can also be affected by hydrological extremes due to the deflection of the storm track or moisture advection downstream of the blocking high (Barnes *et al*., 2013; Sousa *et al*., 2017).

European weather and climate are strongly affected by the Euro-Atlantic blocking regimes, which modulate tropospheric moisture transport (Pasquier *et al*., 2019). The topography of the Alpine mountain range, located in Central Europe, acts as a barrier for meridional moisture fluxes by inducing precipitation via orographic lifting. Two distinct precipitation patterns are observed depending on the moisture sources (Sodemann and Zubler, 2009). In winter, the northern Alpine slope and Central Europe are affected mainly by moisture advected from the North Atlantic. In contrast, precipitation at the southern Alpine slope is associated with moisture transport from the Mediterranean. Typically, a northwesterly flow resulting from a blocking ridge over the eastern North Atlantic produces heavy snowfalls in the Alps (Burroughs, 2000).

Previous studies have highlighted the important role of troposphere–stratosphere interactions for winter surface weather (Thompson and Wallace, 1998; Baldwin and Dunkerton, 2001; Karpechko *et al*., 2018). Several other studies linked winter tropospheric blocking to polar stratospheric variability, suggesting that blocking may alter the vertical propagation of planetary waves and trigger sudden stratospheric warmings (SSWs) (Martius *et al*., 2009). SSWs are dramatic events characterised by a breakdown of the westerly stratospheric circulation and a reversal to easterlies, with associated rapid warming of the polar stratosphere. Martius *et al*. (2009) reported that SSWs are often preceded by tropospheric blocking and that its location over the Atlantic or Pacific can affect the type of SSW, involving either vortex displacement or vortex splitting. Blocking can also follow an SSW, such as blocking over Greenland during a negative phase of the North Atlantic Oscillation (e.g. Domeisen *et al*., 2020). A two-way connection of these phenomena is possible: the stratospheric circulation perturbed by an SSW, itself initially forced by blocking, can further influence the persistence of that blocking (Woollings and Hoskins, 2008). Both phenomena are associated with cold air outbreaks in Eurasia (Kolstad *et al*., 2010; King *et al*., 2019).

In January 2019, the Northern Hemisphere extratropics featured two remarkable atmospheric phenomena: a major SSW (2 January) and persistent North Atlantic blocking. At the same time, a persistent northwesterly to northerly flow set in over the Alpine region, and significant snow accumulation took place in the Northern Alps. The January snowfall amount broke the 100-year snow records at some sta-

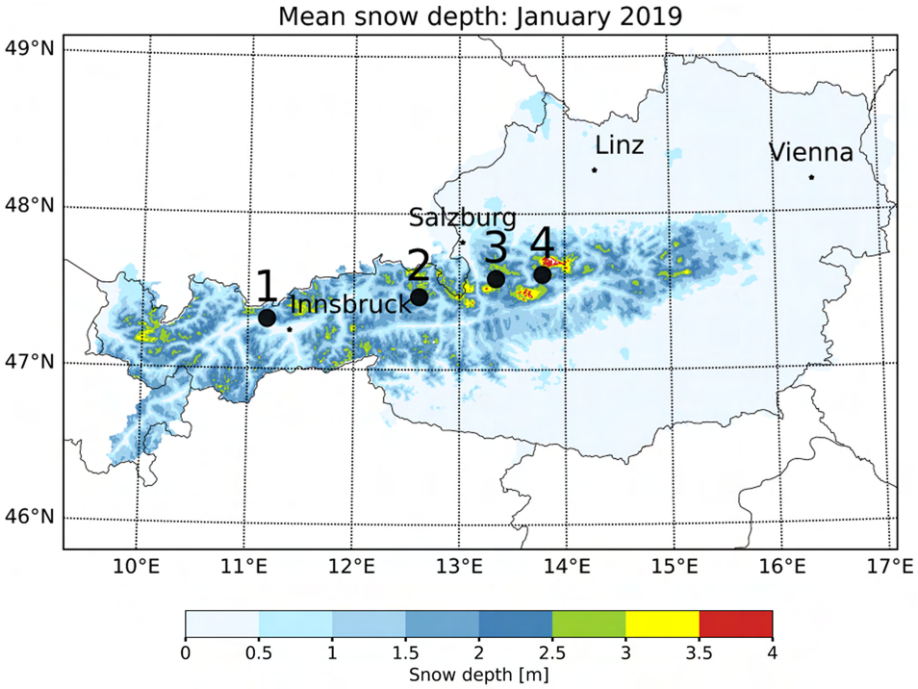


Figure 1. Mean snow depth for January 2019 in the Austrian Alpine region based on SNOWGRID data. Indicated are four selected stations: 1, Seefeld in Tyrol; 2, Hochfilzen in Tyrol; 3, Abtenau in Salzburg; and 4, Bad Aussee in Styria.

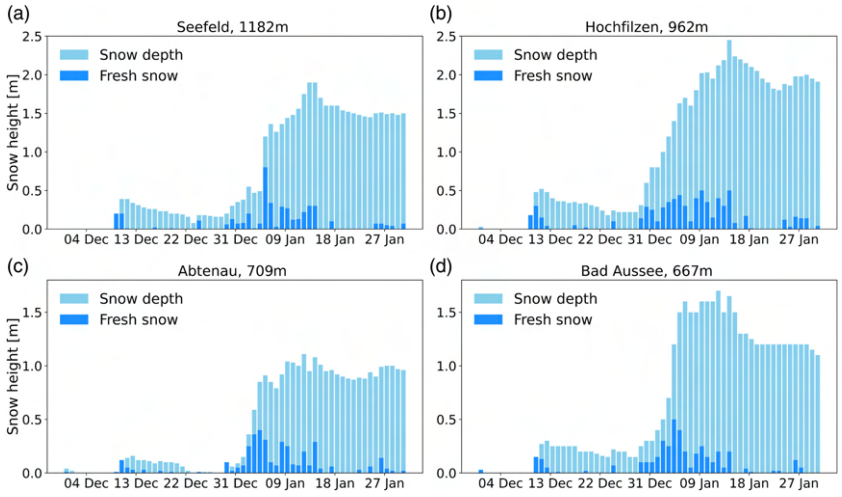


Figure 2. Daily fresh snow (dark blue) and snow depths (light blue) at the stations (a) Seefeld, (b) Hochfilzen, (c) Abtenau and (d) Bad Aussee showing the development of heavy snowfall for December 2018 to January 2019.

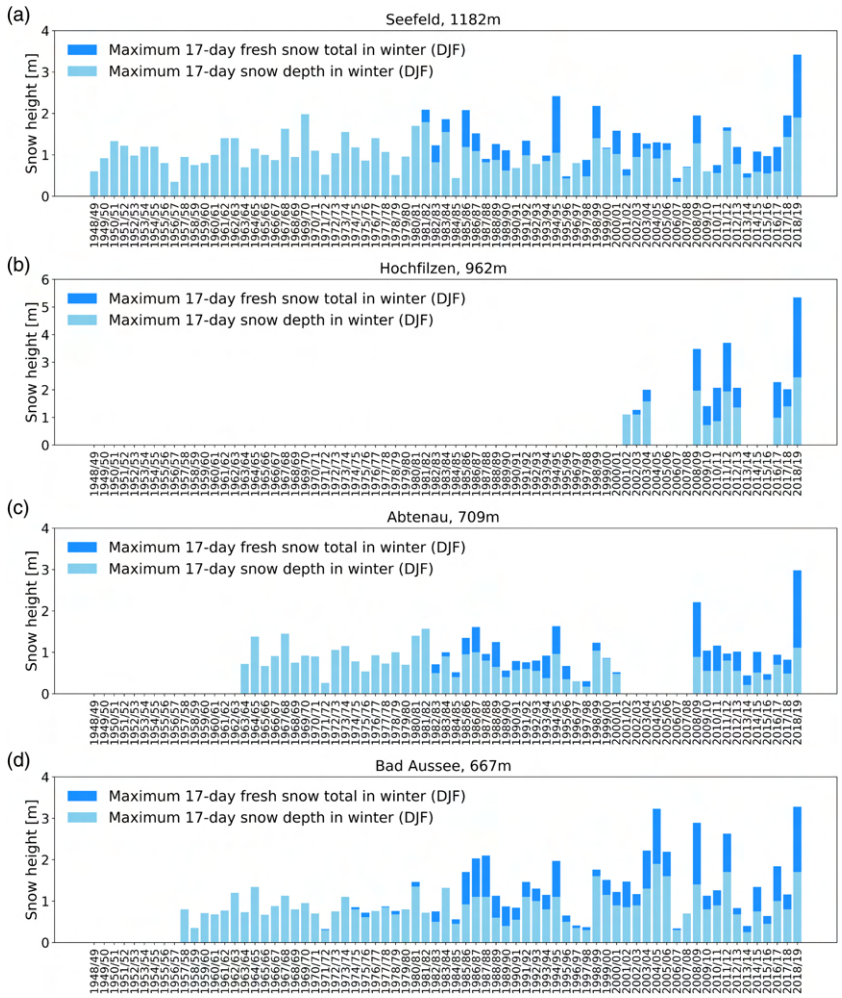


Figure 3. Measurement series of maximum 17-day snow depths (light blue) and maximum 17-day fresh snow totals (dark blue) in December-January-February (DJF) at the stations (a) Seefeld available since 1948 and 1981, (b) Hochfilzen since 2001, (c) Abtenau since 1963 and 1981 and (d) Bad Aussee since 1957 and 1971, respectively.

tions (Radlherr *et al*., 2019). Zentralanstalt für Meteorologie und Geodynamik (ZAMG) – the national meteorological service of Austria – issued the highest alert (red level) for fresh snow three times in a row (4–6 January, 8–10 January, 13–15 January).

Such extreme snowfall is a natural hazard that often causes direct and indirect damages, with severe socio-economic consequences posing risks to human lives, transport and infrastructure. An improved understanding of the event's evolution and underlying processes responsible for the extreme precipitation is crucial for both enhancing its predictability and disaster risk assessment.

In this paper, we investigate the synoptic conditions that prevailed during European winter (December–January) 2018/2019 and how they led to the episode of extreme snow accumulation across the Northern Alpine region during January 2019.

Data

Data from ERA5 (Hersbach *et al*., 2020), the fifth-generation reanalysis of the European Centre for Medium-Range Weather Forecasts (ECMWF), are used as a basis for this study. In the impact analysis, we use station data and snow cover model data provided by ZAMG. The spatial distribution of accumulated snow is estimated using the snow cover model SNOWGRID, which is driven with gridded meteorological data from ZAMG's nowcasting system INCA (Integrated Nowcasting through Comprehensive Analysis) (Olefs *et al*., 2013). The model is based on a radiation model and simulates the temporal development of snow height and snow water equivalent for Austria in 15-min time steps.

In addition, we use snow measurements from selected meteorological stations provided by ZAMG (Schöner *et al*., 2019) to highlight the extreme snowfall in January 2019. Four stations located in the northern part of the Alpine range and representative of the western and eastern regions of the Austrian Alps are selected in our study. The selected stations are: Seefeld, Tyrol (1182m above mean sea level (amsl), 47°32′N, 11°17′E); Hochfilzen, Tyrol (962m amsl, 47°46′N, 12°61′E); Abtenau, Salzburg (709m amsl, 47°58′N, 13°34′E) and Bad Aussee, Styria (667m amsl, 47°61′N, 13°78′E).

For discussion of the prediction of the event, we use short- and medium-range forecasts from the ECMWF high-resolution forecast (HRES) and ensemble forecast (ENS) provided four times a day, and extended-range forecast provided twice per week (ECMWF, 2021). The forecasts were based on the ECMWF Integrated Forecasting System (IFS) cycle 46r1.

Methods

In this study, we focus on the Euro-Atlantic region (45–72°5′N, 30°W–45°E), which covers the area of the North Atlantic blocking and the affected part over Europe. We calculate daily anomalies of geopotential height (GPH) and temperature with respect to the climatological daily-mean from 1981 to 2010. To identify blocking, we compute blocking indices based on 500hPa GPH gradients. We follow the three-step algorithm described by Brunner and Steiner (2017)

14778696, 2022, 1, Downloaded from https://rmets.onlinelibrary.wiley.com/doi/10.1002/wea.4020 by CochraneAustria, Wiley Online Library on [28/10/2024]. See the Terms and Conditions (https://onlinelibrary.wiley.com/terms-and-conditions) on Wiley Online Library for rules of use; OA articles are governed by the applicable Creative Commons License

14778696, 2022, 1, Downloaded from https://rmets.onlinelibrary.wiley.com/doi/10.1002/wea.4020 by CochraneAustria, Wiley Online Library on [28/10/2024]. See the Terms and Conditions (https://onlinelibrary.wiley.com/terms-and-conditions) on Wiley Online Library for rules of use; OA articles are governed by the applicable Creative Commons License

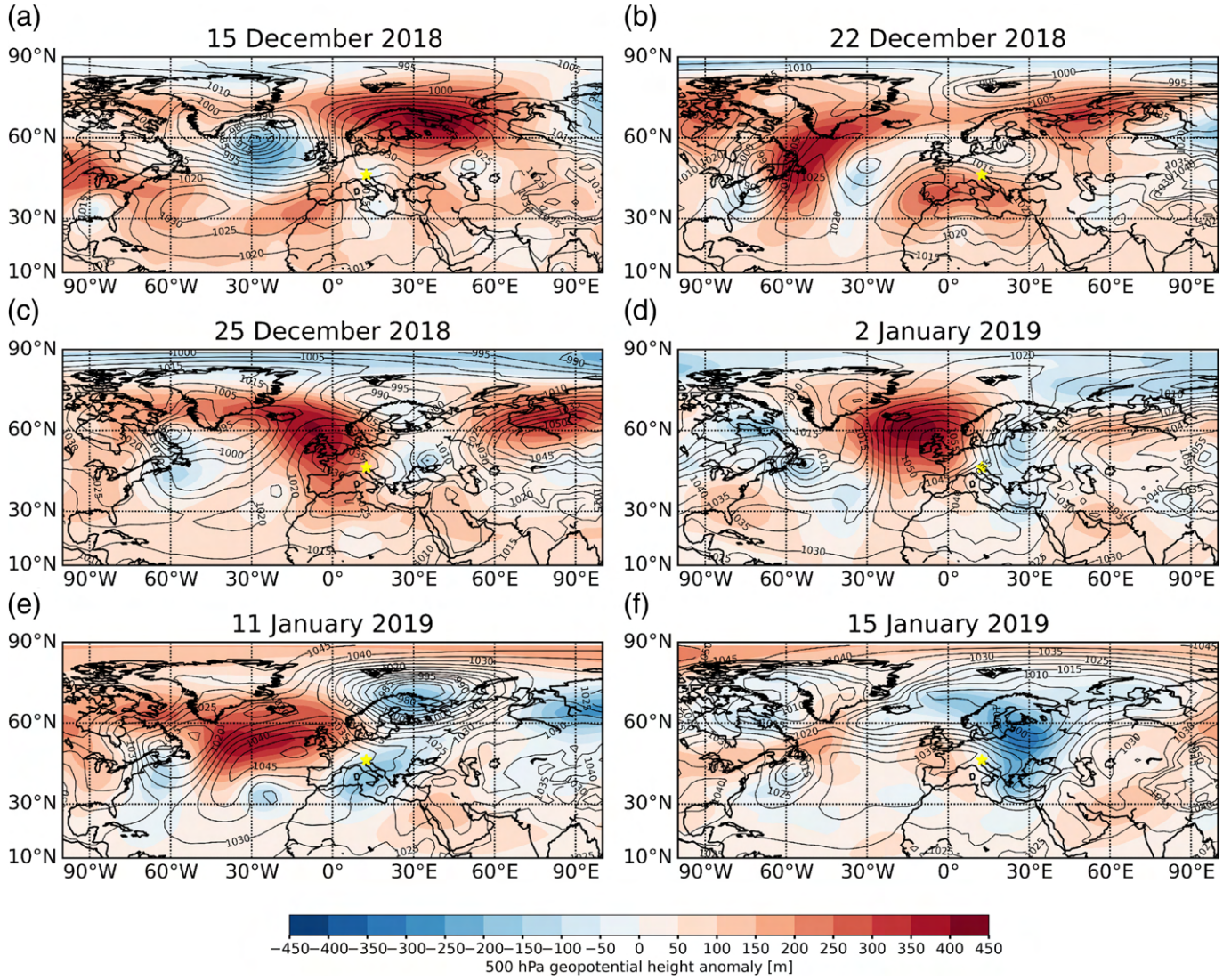


Figure 4. Evolution of GPH anomalies at 500hPa (shading) and mean sea-level pressure (black contours) for (a–f) 15 December to 15 January 2019 based on ERA5.

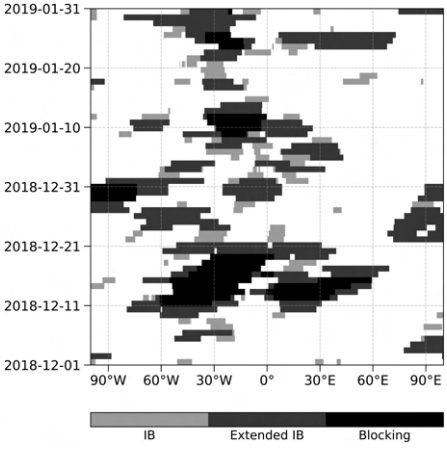


Figure 5. Hovmöller diagram of the blocking evolution for December 2018 to January 2019. Light grey contours correspond to IB, dark grey to extended IB, and black contours to blocking.

and Brunner (2018). At the first step, the algorithm identifies instantaneous blocking (IB) if the meridional 500hPa GPH gradient is reversed within the region from 35 to 80°N. Then, extended IB events are selected if the meridional GPH gradient reversal spans at least 15° in longitude, i.e. only large systems are considered. Finally, blocking is identified when extended IB occurs within a region of 10° in longitude and 5° in latitude for at least five consecutive days, defined as blocking (B). This approach identifies persistent and stationary upper-level high-pressure systems.

Heavy snowfall events in the Austrian Alps

From 30 December 2018 to 15 January 2019, a sequence of heavy snowfall events affected the entire Austrian side of the northern Alps. Highest-level avalanche warnings were issued in Salzburg, Styria (e.g. LWD Steiermark, 2020), Upper Austria and Lower Austria, and in some parts of Tyrol and Vorarlberg (Radlherr *et al*., 2019). Infrastructure and traffic were significantly affected. As the event evolved, many roads were blocked and 86 500 people were left without a transport connection. Although the entire Austrian Alpine region (46–49°N, 9–17°E) was affected by the snowfall, the amounts of snow were different from region to region. Radlherr *et al*. (2019) explained the complexity of the situation as a result of several frontal systems from the north leading to varying snowfall levels during the 17 day episode resulting in high snow loads and related impacts. Figure 1 shows the affected region with the four selected stations (Seefeld, Hochfilzen, Abtenau and Bad Aussee) marked on the map. In January 2019, the mean snow depth in the Austrian Alps ranged from 1m to more than 4m. Three peaks of fresh snow measurements (4–6 January, 8–10 January, 13–15 January) were recorded during the 17 day snowfall event (Figure 2).

In some regions, the amount of fresh snow was unusually large, e.g. 3.71m of accumulated snow over 17 days at Seefeld, which statistically occurs only every 50 or 100 years (Radlherr *et al*., 2019). The largest reported accumulation of fresh snow over this period was 5.21m at Hochfilzen.

RIGHTSLINK

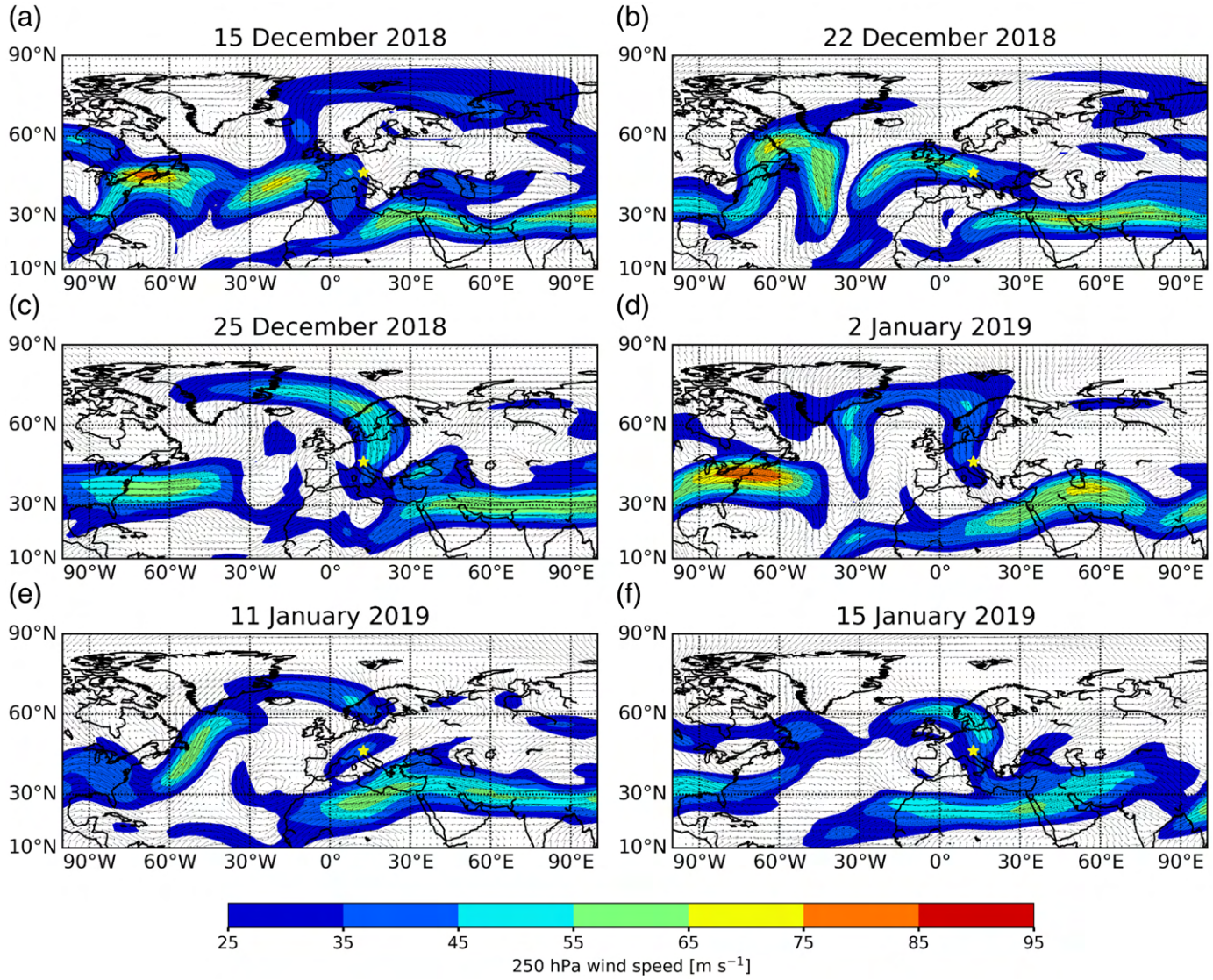


Figure 6. 250hPa wind speed (shading) and wind direction (arrows) for (a–f) 15 December 2018 to 15 January 2019.

To provide a historical perspective, we show long-term snow measurement series for the four selected stations (Figure 3). Analysis of maximum 17-day snowfall periods for each winter reveals that the 2018/2019 event was exceptionally large with record amounts of fresh snow accumulation in Seefeld, Hochfilzen, Abtenau and Bad Aussee, where fresh snow measurements are available since 1981, 2001, 1981 and 1971, respectively. The measurements of maximum snow depth at Seefeld (available since 1948), Hochfilzen (since 2001), Abtenau (since 1963) and Bad Aussee (since 1957) (Figure 3) are the highest or second highest on record.

Synoptic evolution

From early December, synoptic conditions in the Euro-Atlantic region were characterised by persistent blocking centred over Eurasia, extending over Scandinavia and the North Atlantic. Figure 4 shows the evolution of the 500hPa GPH anomalies and mean sea-level pressure from 15 December 2018 to 15 January 2019. An upper-level ridge associated with blocking over Scandinavia and the North Atlantic persisted from 10 to 21 December 2018 (Figure 4a). On 25 December, a ridge emerged over the eastern North Atlantic and northwestern Europe with the maximum GPH anomaly centred at 60°N and 10°W (Figure 4c). After that, the ridge evolved into an omega-shaped blocking high with low-pressure systems upstream and downstream of the blocking ridge over eastern Canada and Scandinavia, respectively (Figures 4c–e). The slightly retrograding omega block over the North Atlantic remained well established for the next 3 weeks until its dissipation on 15 January (Figure 4f). The near-surface circulation pattern resembled the mid-tropospheric ridge-trough configuration (Figures 4a–f). On 2 January, the two low-pressure systems associated with the upper-level troughs to the west and east of the blocking ridge deepened and increased their spatial extent (Figure 4d). In the region to the east of the blocking high, the amplifying trough reached southern Europe.

The temporal evolution of blocking in December 2018 and January 2019 is illustrated in a Hovmöller diagram (Figure 5) indicating IB (light grey) and extended IB (grey) and final persistent blocking (black) (as defined in Methods). During this period, there were mainly three blocking processes consistent with the evolution of the 500hPa GPH anomalies shown in Figure 4. The first two blocking patterns occurred in December 2018 (from 10 to 17 December between 0°E and 60°E and from 10 to 22 December between 60°W and 0°W) and correspond to the upper-level ridge over Scandinavia and the North Atlantic shown in Figure 4. The third block emerged during the first two weeks of January 2019 and extended over the eastern North Atlantic and western Europe (centred between 30°W and 0°W).

Figure 6 shows the evolution of the 250hPa wind, which is the approximate altitude of the jet stream core. Figures 4 and 6 show that the jet stream configuration

14778696, 2022, 1, Downloaded from https://rmets.onlinelibrary.wiley.com/doi/10.1002/wea.4020 by CochraneAustria, Wiley Online Library on [28/10/2024]. See the Terms and Conditions (https://onlinelibrary.wiley.com/terms-and-conditions) on Wiley Online Library for rules of use; OA articles are governed by the applicable Creative Commons License

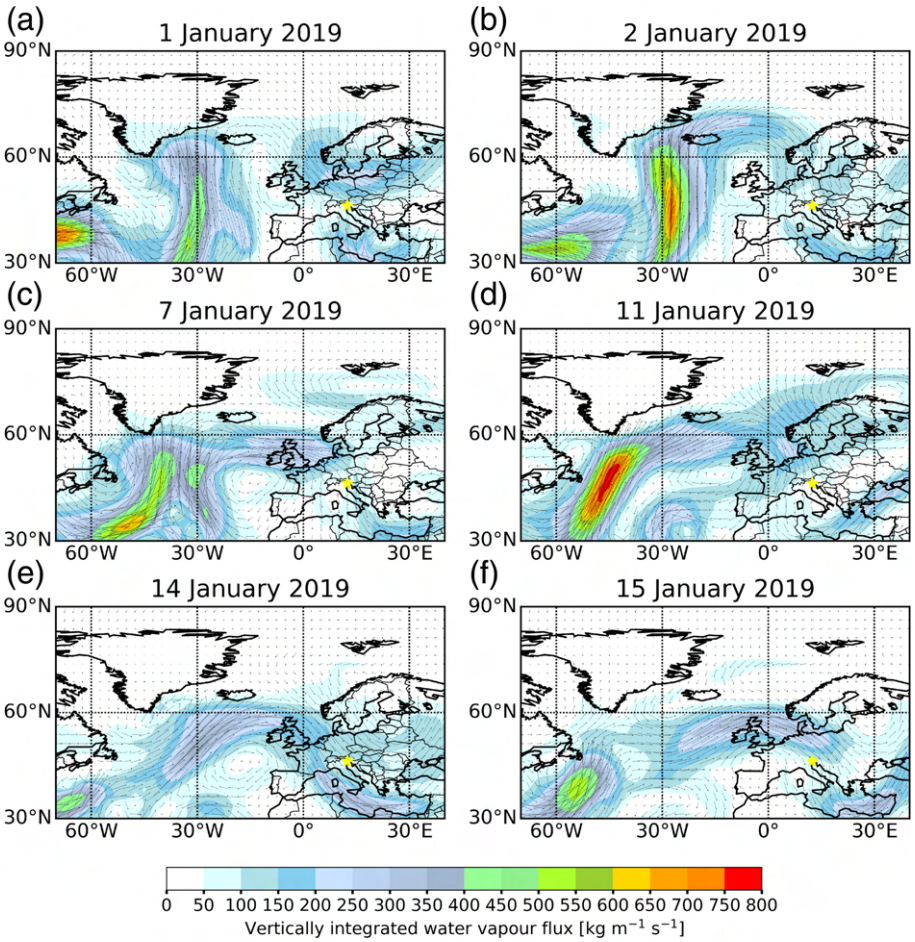


Figure 7. Vertically integrated water vapour flux magnitude (shading) and direction (arrows) for (a–f) 1 to 15 January 2019.

is aligned with the high-pressure system over the North Atlantic and evolves within the zone of strong GPH gradients. The jet stream was initially split into northern and southern branches by the anticyclonic flow associated with blocking over Scandinavia, as indicated in Figure 6(a). Then, the configuration changed (Figure 6b), and the jet stream displaced poleward over the eastern North Atlantic, forming a ridge (Figures 6(c–f)).

Figures 4(c) and 6(c) show that the tropospheric flow configuration established a northerly wind regime over Central Europe on 25 December. The occurrence of heavy snowfall during this period suggests the availability of above-normal amounts of moisture. To understand why the snowfall was so extensive, we analyse horizontal water vapour transport represented as vertically integrated water vapour flux in Figure 7. During the 17-day snowfall event, a relatively large amount of moisture (100–300kgm^{-1}s^{-1}) was transported from the North Atlantic towards the Alps. Also, Sodemann and Zubler (2009) and Froidevaux and Martius (2016) found the Atlantic source dominant for the moisture delivery to the Alps in the winter season. Figures 6 and 7 suggest that the jet stream position and intensity modulated the water vapour flux. Thus, the blocking played a central role in the advection of cold and moist air from the North Atlantic to the Alps, setting the stage for the heavy snowfall event.

Connection to the stratosphere

In January 2019, a major SSW occurred in the Arctic stratosphere (Rao *et al*., 2020). To characterise the SSW, we analyse the temporal evolution of the 10hPa zonal-mean zonal wind (U) at 60°N and the 10hPa meridional zonal-mean temperature difference (ΔT) between 60°N and 85°N for December 2018 to January 2019 (Figure 8a). There was a significant deceleration of U from 22 December and finally a wind reversal (from 30 to −10ms^{-1}) on 2 January. This process was accompanied by a rapid increase in stratospheric temperature starting on 25 December and lasting during January (Figure 8b). The easterly regime persisted for 21 days until 23 January 2019. This is classified as a major SSW (see, e.g. Charlton and Polvani, 2007; Butler *et al*., 2017).

The January 2019 SSW was of a mixed type, i.e. the polar vortex was first displaced, and then it split. Figures 9(a–c) show the polar vortex evolution from 25 December to 15 January. The vortex displaced in the last week of December and split into two vortices on 2 January, with one lobe residing over eastern Canada and another over Eurasia. The vortex split co-occurred with the North Atlantic blocking (Figure 4) and coincided with a peak of upward propagating eddy heat flux from the troposphere to the stratosphere (Rao *et al*., 2019; Butler *et al*., 2020; Lee and Butler, 2020), suggesting that the blocking pattern may have helped split the vortex. This association is further supported by the analysis of the evolution of GPH anomalies for a vertical cross-section of the North-Atlantic blocking region (50–60°N and 30°W–0°W) in Figure 10(a), which shows coherent GPH anomalies throughout the entire atmospheric column from 25 December to 12 January. This suggests a dynamic coupling between the troposphere and the stratosphere.

Figure 10(b) gives a more detailed insight by resolving the longitudinal structure of the GPH anomalies for 4 January. It illustrates coupling in the region of the block (30°W–10°E) and on the western (50–80°W) and eastern (10–60°E) side of the block, where the vortex lobes resided. Additionally, Figure 10(b) reveals the almost barotropic structure of the block from the troposphere to the stratosphere over the North Atlantic region.

The event was classified as non-downward propagating (i.e. with less probable tropospheric impact) (Rao *et al*., 2020). This is true in the zonal-mean sense (Figure 10c). However, it is plausible that once split, the 'daughter' vortices could have enhanced the tropospheric troughs on either side of the blocking for a few days from 2–6 January when coupling was observed.

Our analysis is consistent with Martius *et al*. (2009), which revealed a strong link between tropospheric blocking and major SSWs since the stratospheric flow can be disturbed by vertically propagating Rossby waves emitted from the blocking regions.

Prediction of the event

On 27 December, the ECMWF ensemble forecast (ENS) predicted a low-pressure anomaly centred over the North Atlantic for the week of 7–13 January (day 12 to 18 in the forecast, Figure 11). The forecast from 31 December had changed to an anticyclonic anomaly over the same area and a cyclonic anomaly over northeastern Europe, bringing cold air towards Austria. This change agrees with the increased signal for precipitation over Austria for 4–6 January that appeared in the forecasts from 28–30 December (Figure 12). This setup left Central Europe and the Alpine region exposed to a northwesterly to northerly flow, part of a meandering frontal zone (Figures 4d,e). It separated maritime sub-

14778696, 2022, 1, Downloaded from https://rmets.onlinelibrary.wiley.com/doi/10.1002/wea.4020 by CochraneAustria, Wiley Online Library on [28/10/2024]. See the Terms and Conditions (https://onlinelibrary.wiley.com/terms-and-conditions) on Wiley Online Library for rules of use; OA articles are governed by the applicable Creative Commons License

tropical air mass in the west from maritime polar air mass in the east, setting the stage for the 17-day extreme snowfall event (30 December 2018 to 15 January 2019) in the Northern Alps (see the section Synoptic evolution).

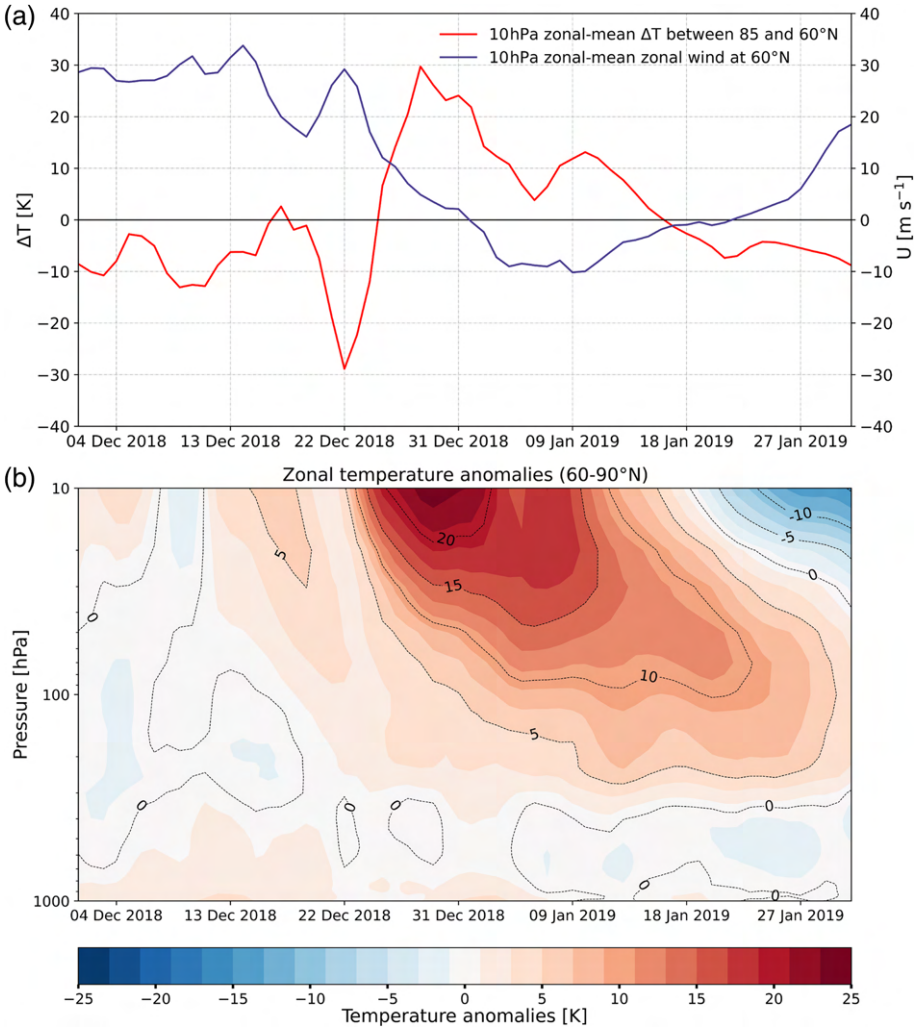


Figure 8. (a) Zonal-mean zonal wind at 60°N (dark blue line) and zonal-mean temperature difference between 85°N and 60°N (red line) at 10hPa. (b) Vertical profile of area-weighted zonal mean (60–90°N) temperature anomalies for December 2018 to January 2019.

On 29 December 2018, ECMWF HRES and ENS predicted the first of the three precipitation peaks (4–6 January 2019) in the Northern Alps as being extreme (Figure 11). The pattern of the blocking high over the eastern North Atlantic stayed remarkably persistent in the period of 7–13 January 2019 when the second and third precipitation peaks occurred.

Discussion and conclusions

In this study, we have identified several factors that contributed to the heavy Alpine snowfall of January 2019. The main characteristics of this event are summarised as follows:

- ZAMG evaluated the 17-day snowfall from 30 December to 15 January 2019 as exceptional in some regions of the Austrian Alps. At several stations, like Hochfilzen and Seefeld in Tyrol, and Abtenau in Salzburg, the total fresh snow amounts measured over 17 days broke 100-year records.
- The snowfall was associated with a northwesterly to northerly flow, which transported water vapour from the North Atlantic toward the Alps. The flow was underpinned by a blocking high over the eastern North Atlantic and a low-pressure system over Eastern Europe. Due to the orographic effect of the mountains, large amounts of snow accumulated on the northern side of the Alps.
- A major SSW occurred in early January 2019. During the SSW, the polar vortex was displaced southward over the North Atlantic region and split into two vortices, with one lobe residing over eastern Canada and another over northwestern Siberia. During these events, the geopotential height anomalies were coupled between the

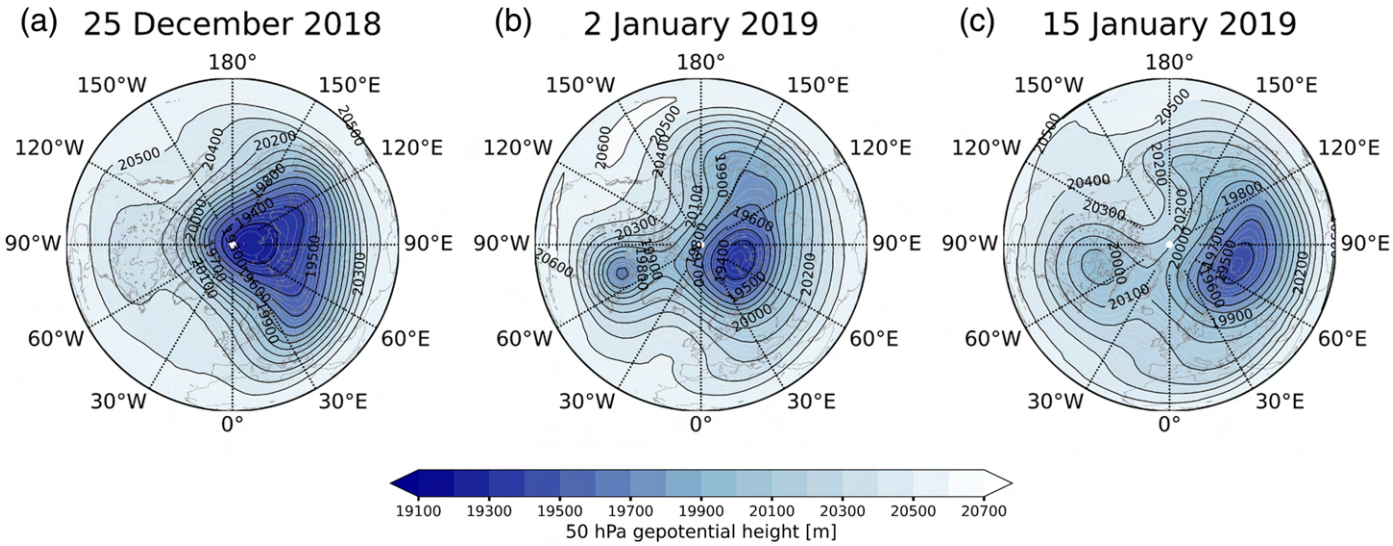


Figure 9. Polar vortex evolution in terms of 50hPa geopotential height on three selected dates in winter 2018/2019. Panels show (a) vortex prior to before splitting, (b) vortex split and (c) further split with the two smaller vortices displaced apart.

14778696, 2022, 1, Downloaded from https://rmets.onlinelibrary.wiley.com/doi/10.1002/wea.4020 by CochraneAustria, Wiley Online Library on [28/10/2024]. See the Terms and Conditions (https://onlinelibrary.wiley.com/terms-and-conditions) on Wiley Online Library for rules of use; OA articles are governed by the applicable Creative Commons License

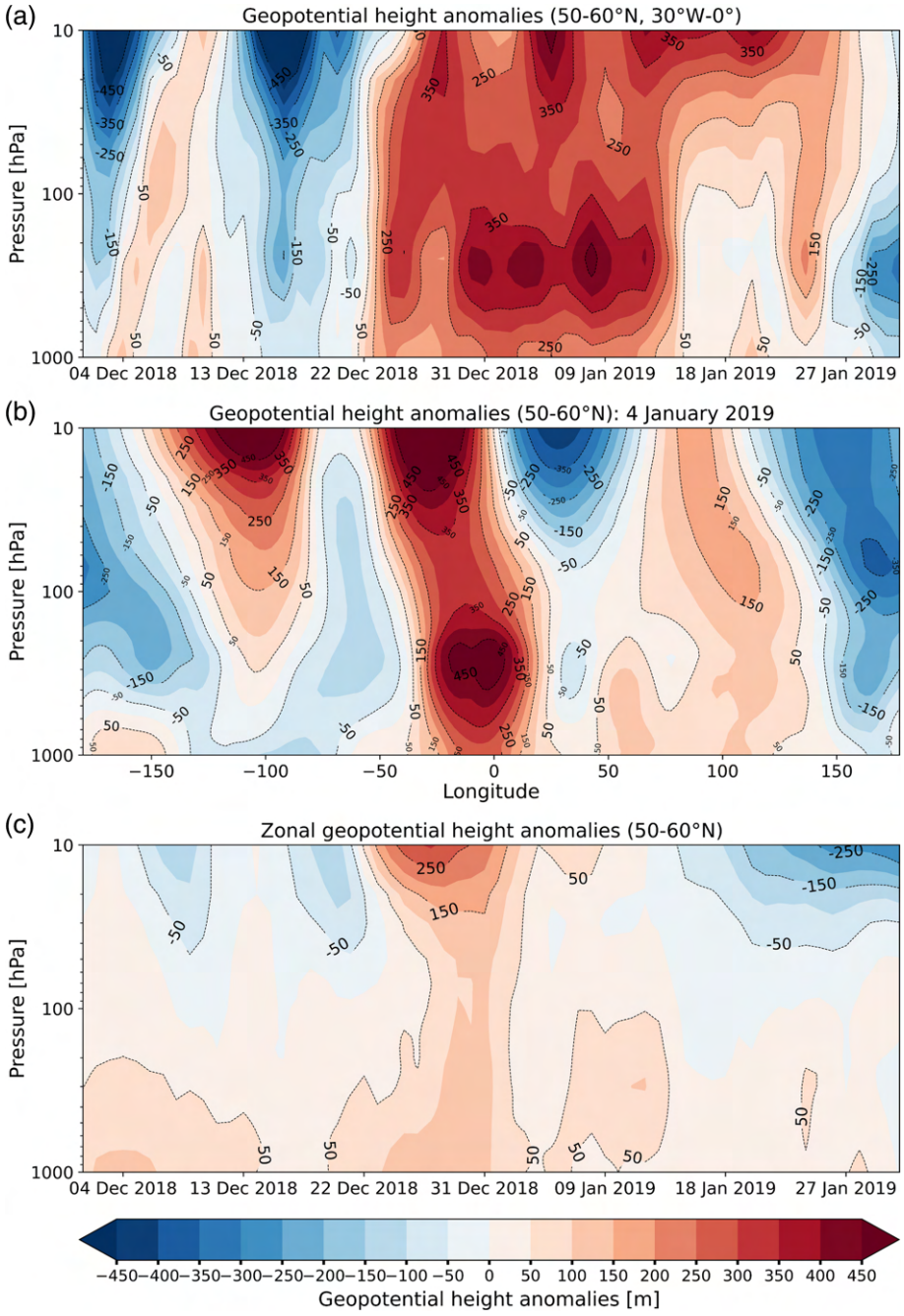


Figure 10. GPH anomalies (a) averaged over the region 50–60°N and 30°W–0°W for December 2018 to January 2019, (b) shown for all longitudes on 4 January 2019, and for comparison (c) the zonal-mean over the region 50–60°N.

lower troposphere and stratosphere over the North-Atlantic region, where the blocking was located. The reported couplings suggest a possible connection between the evolution of the block and the stratospheric polar vortex split. Blocking may have helped split the vortex due to enhanced upward wave propagation, and subsequent displacement of the daughter vortices could have enhanced the tropospheric troughs on either side of the blocking.

- The accurate location and persistence of the blocking high were only predicted after the stratospheric polar vortex split occurred. It is an open question whether this was just due to reduced lead time or due to improved predictability of the model after assimilating details of the polar vortex split and subsequent SSW once they had been observed. At the regional level, the total amount of snowfall was not precisely resolved, making the forecast of local hazards and impacts (e.g. avalanche risk, snow load) challenging.

The results of this study highlight the importance of further investigation of the connection between winter blocking events and SSWs, which may offer the potential for improved predictions of winter weather. Particularly, investigating the evolution of the zonal asymmetry of the vortex in relation to surface weather may prove helpful in this respect. Future changes in the frequency and intensity of heavy snowfall events remain uncertain. The variability of the amount of snow in the Alps is critically dependent on the Euro-Atlantic flow regimes. According to Scherrer *et al*. (2004), European blocking regimes explain half of the Alpine snow variability. Given that the European Alps are exposed to the Atlantic and Mediterranean climatic regimes, heavy precipitation, associated with intensified moisture fluxes from these regions, as the result of increasing sea surface temperatures cannot be ruled out. A better understanding of the changes in blocking under a warming climate is therefore fundamental to assess changes in heavy snowfall episodes.

Acknowledgements

We acknowledge ECMWF (Reading, UK) and Copernicus Climate Change Service for access to the ERA5 reanalysis data, and ZAMG (Vienna, Austria) for access to station data and SNOWGRID. We thank Christian Pehsl (ZAMG, Graz, Austria) and Jacob Abermann (University of Graz, Austria) for fruitful discussions and help on snow data. This work was funded by the Austrian Science Fund (FWF) under research grant W 1256 (Doctoral Programme Climate Change – Uncertainties, Thresholds and Coping Strategies).

References

Baldwin MP, **Dunkerton TJ**. 2001. Stratospheric harbingers of anomalous weather regimes. *Science* **294**: 581–584.

Barnes EA, **Polvani LM**, **Sobel AH**. 2013. Model projections of atmospheric steering of Sandy-like superstorms. *Proc. Natl. Acad. Sci. USA* **110**(38): 15211–15215.

Brunner L. 2018. A new perspective on atmospheric blocking from observations – detection, analysis, and impacts. PhD thesis. Scientific Report No. 76-2018. Wegener Center Verlag, Graz, Austria. ISBN: 978-3-9504501-3-2.

Brunner L, **Steiner AK**. 2017. A global perspective on atmospheric blocking using GPS radio occultation – one decade of observations. *Atmos. Meas. Tech.* **10**: 4727–4745.

Burroughs WJ. 2000. Alpine snow records. *Weather* **55**: 84–92.

Butler AH, **Sjoberg JP**, **Seidel DJ *et al***. 2017. A sudden stratospheric warming compendium. *Earth Syst. Sci. Data* **9**: 63–76.

Butler AH, **Lawrence ZD**, **Lee SH *et al***. 2020. Differences between the 2018 and 2019 stratospheric polar vortex split events. *Q. J. R. Meteorol. Soc.* **146**: 3503–3521.

Charlton AJ, **Polvani LM**. 2007. A new look at stratospheric sudden warmings. Part I: climatology and modeling benchmarks. *J. Clim.* **20**(3): 449–469.

14778696, 2022, 1, Downloaded from https://rmets.onlinelibrary.wiley.com/doi/10.1002/wea.4020 by CochraneAustria, Wiley Online Library on [28/10/2024]. See the Terms and Conditions (https://onlinelibrary.wiley.com/terms-and-conditions) on Wiley Online Library for rules of use; OA articles are governed by the applicable Creative Commons License

RIGHTSLINK
RMetS Royal Meteorological Society

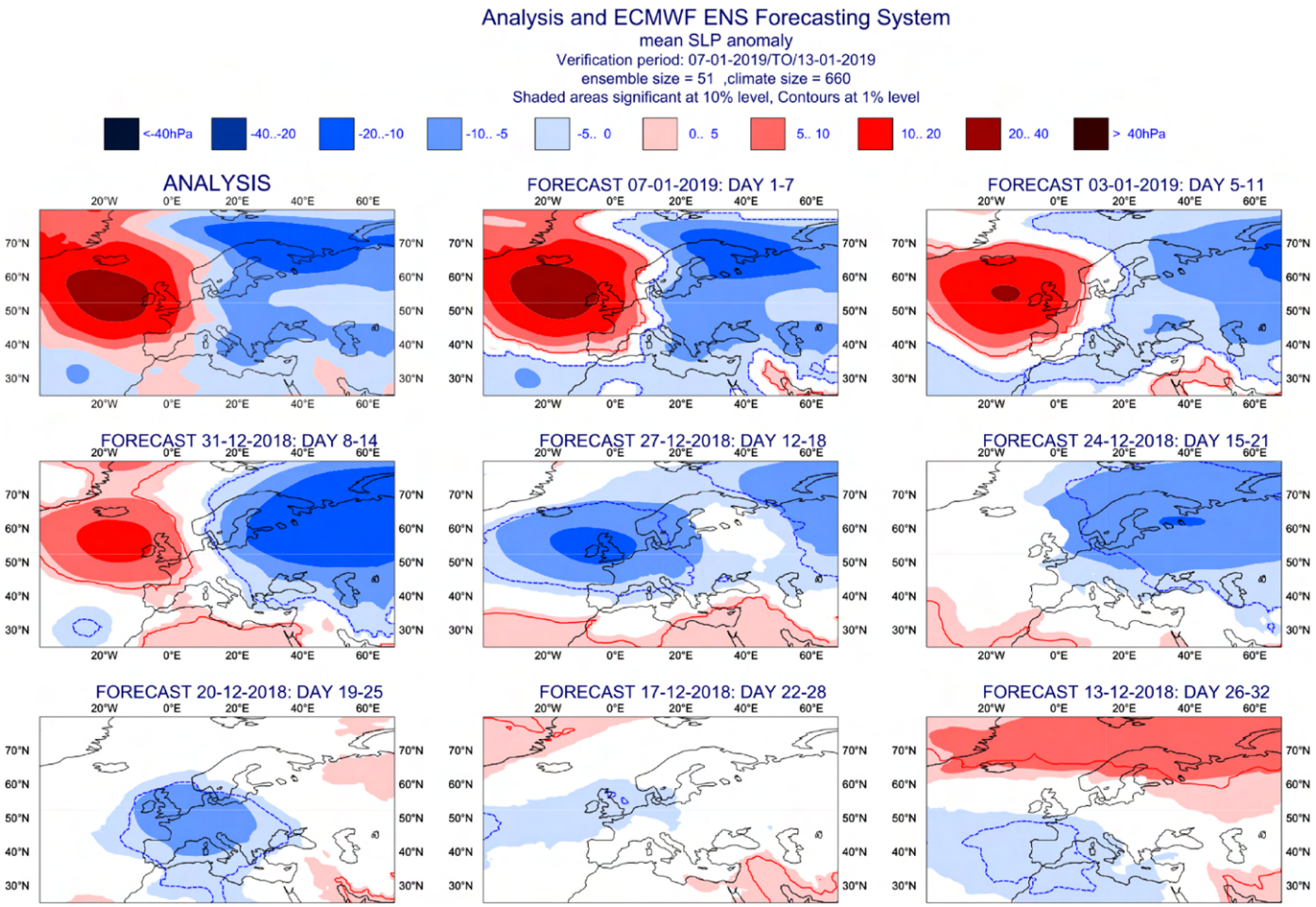


Figure 11. Weekly-mean ECMWF analysis and ENS forecast sea level pressure anomalies relative to the past 20-year model climate for 7 January 2019 to 13 January 2019. Eight forecasts are shown for that week (bottom right to top middle panel), showing how well the anomalies were predicted compared with the analysis. Shaded areas are significant at 10% level, contours at 1% level. The areas where the ensemble forecast is not significantly different from the ensemble climatology are blank.

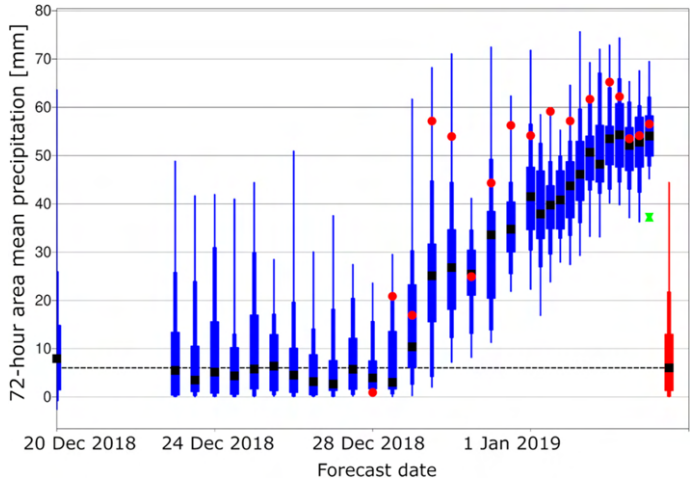


Figure 12. Evolution of ECMWF ENS and HRES forecasts of 72-hour area mean precipitation (4–6 January 2019) for the Northern Alps (47–48°N; 10–15°E). The blue box-and-whiskers indicate the 1st, 10th, 25th, 75th, 90th and 99th percentile, black dots the ensemble median, red dots the HRES forecast, and red box-and-whisker the model climate. The green cross corresponds to the mean precipitation for Austria according to ECMWF high-density observations (HDOBS).

Domeisen DIV, **Grams CM**, **Papritz L**. 2020. The role of North Atlantic–European weather regimes in the surface impact of sudden stratospheric warming events. *Weather Clim. Dynam.* **1**: 373–388.

ECMWF. 2021. Operational configurations of the ECMWF Integrated Forecasting System (IFS). https://www.ecmwf.int/en/forecasts/documentation-and-support [Accessed 6 April 2021].

Froidevaux P, **Martius O**. 2016. Exceptional integrated vapour transport toward orography: an important precursor to severe floods in Switzerland. *Q. J. R. Meteorol. Soc.* **142**: 1997–2012.

Hersbach H, **Bell B**, **Berrisford P *et al***. 2020. The ERA5 global reanalysis. *Q. J. R. Meteorol. Soc.* **146**: 1999–2049.

Karpechko AY, **Charlton-Perez A**, **Balmaseda AM *et al***. 2018. Predicting sudden stratospheric warming 2018 and its climate impacts with a multimodel ensemble. *Geophys. Res. Lett.* **45**: 13538–13546.

King AD, **Butler AH**, **Jucker M *et al***. 2019. Observed relationships between sudden stratospheric warmings and European climate extremes. *J. Geophys. Res. Atmos.* **124**: 13943–13961.

Kolstad EW, **Breiteig T**, **Scaife AA**. 2010. The association between stratospheric weak polar vortex events and cold air outbreaks in the Northern Hemisphere. *Q. J. R. Meteorol. Soc.* **136**: 886–893.

Lawinenwarndienst (LWD) Steiermark. 2020. *Enorme Schneemengen, Gefahrenstufe 5, "sehr große" Lawinengefahr in den Nordalpen!* https://www.lawine-steiermark.at/aktuelles/aktuelle-ereignisse/enorme-schneemengen-gefahrenstufe-5-sehr-grosse-lawinengefahr-in-den-nordal [accessed 6 April 2021].

14778696, 2022, 1, Downloaded from https://rmets.onlinelibrary.wiley.com/doi/10.1002/wea.4020 by CochraneAustria, Wiley Online Library on [28/10/2024]. See the Terms and Conditions (https://onlinelibrary.wiley.com/terms-and-conditions) on Wiley Online Library for rules of use; OA articles are governed by the applicable Creative Commons License

Lee S, **Butler A**. 2020. The 2018–2019 Arctic stratospheric polar vortex. *Weather* **75**: 52–57.

Martius O, **Polvani LM**, **Davies HC**. 2009. Blocking precursors to stratospheric sudden warming events. *Geophys. Res. Lett.* **36**: L14806

Olefs M, **Schöner W**, **Suklitsch M *et al***. 2013. SNOWGRID – a new operational snow cover model in Austria. *Proceedings of the International Snow Science Workshop*. Grenoble – Chamonix Mont Blanc, Grenoble, France.

Pasquier JT, **Pfahl S**, **Grams CM**. 2019. Modulation of atmospheric river occurrence and associated precipitation extremes in the North Atlantic Region by European weather regimes. *Geophys. Res. Lett.* **46**: 1014–1023.

Pelly JL, **Hoskins BJ**. 2003. A new perspective on blocking. *J. Atmos. Sci.* **60**: 743–755.

Radlherr A, **Winkler A**, **Bauer M**. 2019. Meteorologische Analyse der intensiven Schneefallperiode im Jänner 2019 (Meteorological analysis of the intensive snowfall period during January 2019). *Journal for Torrent, Avalanche, Landslide and Rock Fall* **183**.

Rao J, **Garfinkel CI**, **Chen H *et al***. 2019. The 2019 New Year stratospheric sudden warming and its real-time predictions in multiple S2S models. *J. Geophys. Res. Atmos.* **124**: 11155–11174.

Rao J, **Garfinkel CI**, **White IP**. 2020. Predicting the downward and surface influence of the February 2018 and January 2019 sudden stratospheric warming events in subseasonal to seasonal (S2S) models. *J. Geophys. Res. Atmos.* **125**: e2019JD031919.

Rex DF. 1950. Blocking action in the middle troposphere and its effect upon regional climate I: an aerological study of blocking action. *Tellus* **2**(3): 196–211.

Scherrer SC, **Appenzeller C**, **Laternser M**. 2004. Trends in Swiss Alpine snow days: the role of local- and large-scale climate variability. *Geophys. Res. Lett.* **31**: L13215

Schöner W, **Koch R**, **Matulla C *et al***. 2019. Spatiotemporal patterns of snow depth within the Swiss-Austrian Alps for the past half century (1961 to 2012) and linkages to climate change. *Int. J. Climatol.* **39**: 1589–1603.

Sillmann J, **Croci-Maspoli M**, **Kallache M *et al***. 2011. Extreme cold winter temperatures in Europe under the influence of North Atlantic atmospheric blocking. *J. Clim.* **24**(22): 5899–5913.

Sodemann H, **Zubler E**. 2009. Seasonal and inter-annual variability of the moisture sources for Alpine precipitation during 1995–2002. *Int. J. Climatol.* **30**: 947–961.

Sousa PM, **Trigo RM**, **Barriopedro D *et al***. 2017. Responses of European precipitation distributions and regimes to different blocking locations. *Clim. Dyn.* **38**(3-abr): 1141–1160.

Thompson DWJ, **Wallace JM**. 1998. The Arctic oscillation signature in the wintertime geopotential height and temperature fields. *Geophys. Res. Lett.* **25**: 1297–1300.

Tibaldi S, **Molteni F**. 1990. On the operational predictability of blocking. *Tellus A* **42**(3): 343–365.

Tyrlis E, **Hoskins BJ**. 2008. Aspects of a Northern Hemisphere atmospheric blocking climatology. *J. Atmos. Sci.* **65**(5): 1638–1652.

Woollings T, **Hoskins B**. 2008. Simultaneous Atlantic-Pacific blocking and the Northern Annular Mode. *Q. J. R. Meteorol. Soc.* **134**: 1635–1646.

Correspondence to: K. Yessimbet

kamilya.yessimbet@uni-graz.at

© 2021 The Authors. Weather published by John Wiley & Sons Ltd on behalf of the Royal Meteorological Society.

This is an open access article under the terms of the Creative Commons Attribution License, which permits use, distribution and reproduction in any medium, provided the original work is properly cited.

doi: 10.1002/wea.4020

Paper II. Pathways of influence between Northern Hemisphere blocking and stratospheric polar vortex variability

Kamilya Yessimbet[1,2], Theodore G. Shepherd[3,4], Albert C. Ossó[1], and Andrea K. Steiner[1,2]

[1]Wegener Center for Climate and Global Change, University of Graz, Graz, Austria
[2]FWF-DK Climate Change, University of Graz, Graz, Austria
[3]Department of Meteorology, University of Reading, Reading, UK
[4]Jülich Supercomputing Centre, Forschungszentrum Jülich, Jülich, Germany

Geophysical Research Letters, 49, e2022GL100895
doi: doi.org/10.1029/2022GL100895

© 2022 The Authors. Weather published by John Wiley & Sons Ltd on behalf of the Royal Meteorological Society. This is an open access article under the terms of the Creative Commons Attribution License.

Check for updates

AGU ADVANCING EARTH AND SPACE SCIENCE

Geophysical Research Letters

RESEARCH LETTER
10.1029/2022GL100895

Pathways of Influence Between Northern Hemisphere Blocking and Stratospheric Polar Vortex Variability

Kamilya Yessimbet[1,2], Theodore G. Shepherd[3,4], Albert C. Ossó[1], and Andrea K. Steiner[1,2]

[1]Wegener Center for Climate and Global Change, University of Graz, Graz, Austria, [2]FWF-DK Climate Change, University of Graz, Graz, Austria, [3]Department of Meteorology, University of Reading, Reading, UK, [4]Jülich Supercomputing Centre, Forschungszentrum Jülich, Jülich, Germany

Abstract We apply a causal inference-based framework to test and quantify previously suggested causal relationships between Northern Hemisphere blocking, upward wave-activity fluxes and stratospheric polar vortex (SPV) variability using reanalysis data. We show that the influence of blocking on the polar vortex is entirely mediated by upward wave-activity fluxes, as the classical view would suggest. However, the causal pathway is not completely straightforward. In contrast to the vortex-weakening effect of European blocking, the vortex-strengthening effect of west Pacific blocking on lower stratospheric wave-activity fluxes is only partially mediated by upper tropospheric wave-activity fluxes. In addition, only two-thirds of the effect of upper tropospheric wave-activity fluxes on polar vortex variability is mediated by lower stratospheric wave-activity fluxes. We also show that sudden stratospheric warmings are not entirely explainable in terms of upward wave-activity fluxes. These findings help clarify the pathways of influence between blocking and SPV variability.

Plain Language Summary Blocking has been thought to influence the wintertime stratospheric polar vortex (SPV) via its effect on upward propagating planetary waves. Yet there has been debate about the exact pathways of influence. In this study, we use reanalysis data to examine and quantify previously suggested causal relationships between Northern Hemisphere blocking, upper tropospheric wave-activity fluxes, lower stratospheric wave-activity fluxes, SPV variability, and sudden stratospheric warmings. By making the causal reasoning explicit in the statistical analysis we can quantify indirect (mediated) and direct pathways of influence. We confirm the classical view that upward wave-activity fluxes determine the influence of blocking on the polar vortex. However, we show that the pathway is not the simple causal chain described above. For example, only two-thirds of the effect of upper tropospheric wave-activity fluxes on polar vortex variability is mediated by lower stratospheric wave-activity fluxes. These non-mediated pathways suggest that additional causal factors play a role in how blocking affects polar vortex variability and sudden stratospheric warmings.

Key Points:

- The pathways of influence between European and west Pacific blocking and polar vortex variability are quantified using causal inference
- Both upper tropospheric and lower stratospheric wave-activity fluxes mediate these pathways, and both are needed for a full description
- Our results suggest additional causal factors play a role in how blocking affects polar vortex variability and sudden stratospheric warmings

Supporting Information:

Supporting Information may be found in the online version of this article.

Correspondence to:

K. Yessimbet,
kamilya.yessimbet@uni-graz.at

Citation:

Yessimbet, K., Shepherd, T. G., Ossó, A. C., & Steiner, A. K. (2022). Pathways of influence between Northern Hemisphere blocking and stratospheric polar vortex variability. *Geophysical Research Letters*, *49*, e2022GL100895. https://doi.org/10.1029/2022GL100895

Received 17 AUG 2022
Accepted 11 NOV 2022

Author Contributions:

Conceptualization: Kamilya Yessimbet, Theodore G. Shepherd
Data curation: Kamilya Yessimbet
Formal analysis: Kamilya Yessimbet
Funding acquisition: Andrea K. Steiner
Investigation: Kamilya Yessimbet
Methodology: Kamilya Yessimbet, Theodore G. Shepherd
Resources: Andrea K. Steiner
Supervision: Theodore G. Shepherd, Albert C. Ossó, Andrea K. Steiner
Validation: Kamilya Yessimbet, Theodore G. Shepherd, Albert C. Ossó, Andrea K. Steiner
Visualization: Kamilya Yessimbet

© 2022. The Authors.
This is an open access article under the terms of the Creative Commons Attribution License, which permits use, distribution and reproduction in any medium, provided the original work is properly cited.

1. Introduction

The dynamical coupling between the troposphere and stratosphere has historically been explained from the established properties of stationary, planetary-scale Rossby waves and their interaction with the mean flow (Matsuno, 1970). These waves originate mainly in the troposphere and, as they propagate into the stratosphere, transfer angular momentum vertically, causing the stratospheric mean flow to decelerate (Andrews et al., 1987; Shepherd, 2002). The nonlinear interactions between these waves and the polar vortex drive wintertime Arctic stratospheric polar vortex (SPV) variability, which manifests in extreme cases as a sudden stratospheric warming (SSW)—a breakdown of the polar vortex, accompanied by rapid adiabatic heating in the polar stratosphere (Hitchcock et al., 2013).

The detailed mechanisms of SSW initiation are still not fully understood, but all studies agree on the importance of sustained absorption of stratospheric wave activity for vortex disruption (Baldwin et al., 2021). SSWs are often thought to be forced by anomalously strong wave-activity sources originating in the troposphere (e.g., Garfinkel et al., 2010; Martius et al., 2009). Some authors have argued that the stratosphere controls the upward wave propagation and determines the occurrence of SSWs, for example, through resonance and nonlinear effects responsible for the rapid amplification of wave activity in the stratosphere (Baldwin et al., 2021; Birner & Albers, 2017; de la Cámara et al., 2017). However, even if SSWs are not always dependent on tropospheric sources of variability, this does not mean that they are unaffected by these sources.

Writing – original draft: Kamilya Yessimbet
Writing – review & editing: Theodore G. Shepherd, Albert C. Ossó, Andrea K. Steiner

In this respect, tropospheric blocking has often been considered a precursor to SSWs (Attard & Lang, 2019; Colucci & Kelleher, 2015; Martius et al., 2009; Nishii et al., 2011). These studies suggest a geographically dependent blocking influence on the enhancement/suppression of upward wave-activity propagation into the stratosphere through constructive/destructive interference between climatological stationary waves and the anomalous waves generated by blocking. For example, blocking over Europe and the Euro-Atlantic region tends to constructively interfere with the climatological wave pattern and enhance the upward wave-activity propagation, contributing to a warmer polar vortex and an increased probability of SSWs (Attard & Lang, 2019). In contrast, blocking over the west Pacific suppresses upward wave-activity propagation through destructive interference with the climatological pattern. As noted earlier, this focus on tropospheric wave-activity forcing does not exclude the possibility of stratospheric mechanisms playing a role in the effect of west Pacific blocking, for example, via the wave reflection mechanism (Kodera et al., 2016).

The anomalous upward wave-activity propagation signal associated with blocking is often considered to propagate from the upper troposphere around 200–300 hPa to the lower stratosphere around 100 hPa (Attard & Lang, 2019; Colucci & Kelleher, 2015; Martius et al., 2009). Recently, Weinberger et al. (2021) suggested that atmospheric variability above the tropopause, especially in the vertical gradients of buoyancy frequency, is a crucial factor controlling the extent of the upward propagation to 100 hPa. Relatedly, Attard and Lang (2019) observed that the signal associated with blocking did not depend on a single synoptic event (blocking or extratropical cyclone) alone and suggested that stratospheric conditions are precursors to the 100-hPa signal. Several questions thus remain open on what conditions are essential for anomalous wave-activity propagation between the troposphere and the stratosphere, and what is the role of blocking in this.

Various statistical analysis methods and climate modeling have been used to investigate the relationship between blocking, wave-activity propagation and SSWs (e.g., de la Cámara et al., 2017; Nishii et al., 2011). A widely applied statistical method is cross-correlation analysis, assuming a linear relationship between the different processes (e.g., Polvani & Waugh, 2004). However, the results can be highly biased by autocorrelation and indirect effects (Kretschmer et al., 2016; Runge et al., 2014). To overcome these issues, we apply a causal inference theory-based approach to examine the plausible causal connections between blocking, upward wave-activity propagation, and SPV changes and quantify the strength of the connections in reanalysis data. This relatively novel method within climate dynamics, described in Section 2.1, allows to overcome spurious correlations and identifies direct and indirect effects within the assumed causal network (Kretschmer et al., 2016, 2021; Runge et al., 2014).

Motivated by earlier results, we study the previously suggested causal relationships and ask the following questions:

1. Is the effect of blocking (either European or west Pacific) on lower stratospheric wave-activity fluxes (at 100 hPa) entirely mediated by its effect on upper tropospheric wave-activity fluxes (at 300 hPa)?
2. Is the effect of upper tropospheric wave-activity fluxes on polar vortex variability entirely mediated by its effect on lower stratospheric wave-activity fluxes?
3. Is the effect of blocking (either European or west Pacific) on polar vortex variability entirely mediated by its effect on upper tropospheric and lower stratospheric wave-activity fluxes?
4. Are SSWs explainable entirely by anomalies in upper tropospheric and lower stratospheric wave-activity fluxes?

Our choices of the different causal elements are based on previous literature to ensure continuity with that literature. The hypothesized causal model reflecting the above linkages is shown schematically in Figure 1a. In this study, we aim to quantify the strength of the causal relationships from the data and test if the above hypotheses are supported by the data, or if there appear to be other factors or pathways of influence.

2. Data and Methods

This study is based on the European Centre for Medium Range Weather Forecasts (ECMWF) ERA5 reanalysis data (Bell et al., 2021; Hersbach et al., 2020). The data is averaged daily from November to March for the period 1950–2019 and utilized on a horizontal grid resolution of 2.5° × 2.5°. Anomalies are computed by removing a commonly used 60-year (1950–2010) daily mean climatology, then normalized by the daily standard deviation.

19448007, 2022, 23, Downloaded from https://agupubs.onlinelibrary.wiley.com/doi/10.1029/2022GL100895 by CochraneAustria, Wiley Online Library on [24/07/2023]. See the Terms and Conditions (https://onlinelibrary.wiley.com/terms-and-conditions) on Wiley Online Library for rules of use; OA articles are governed by the applicable Creative Commons License

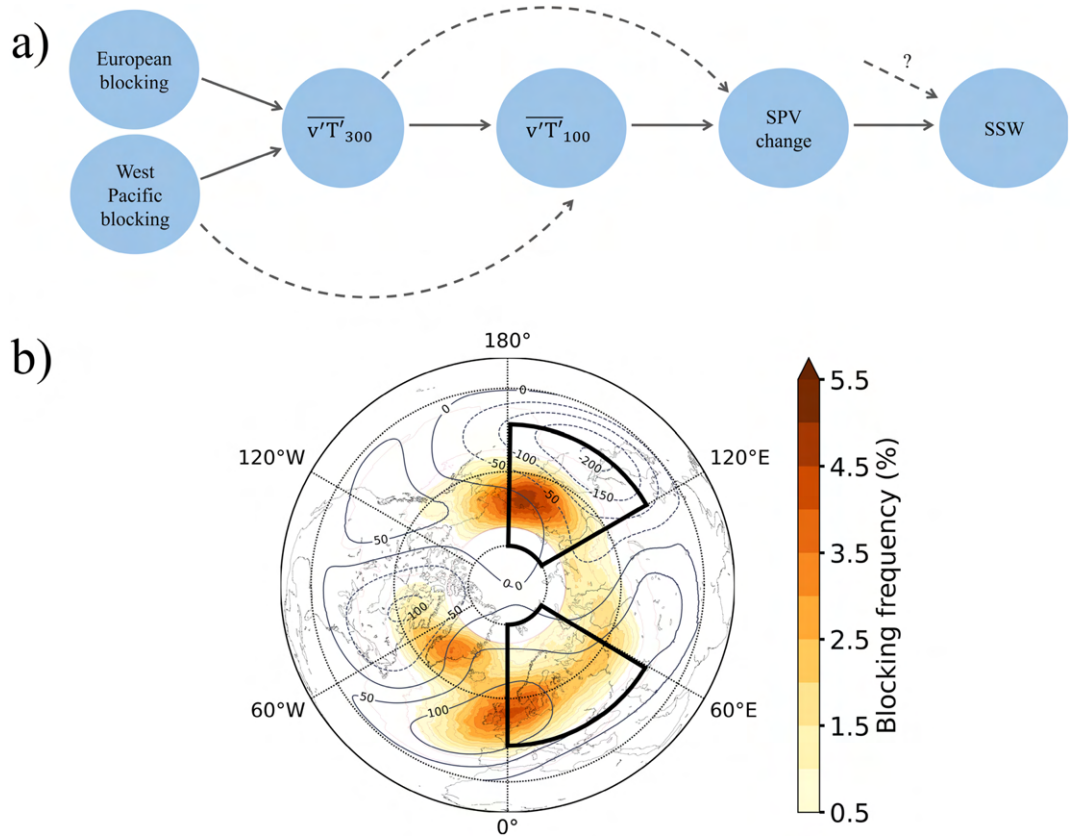


Figure 1. (a) Schematic view of the hypothesized causal model. The nodes represent the main processes: blocking either over Europe or the west Pacific, upper-tropospheric heat flux anomaly, lower-stratospheric heat flux anomaly, stratospheric polar vortex change and sudden stratospheric warming. Solid arrows represent hypothesized causal relationships between the processes and indicate the direction of influence. Dashed arrows represent the additional causal pathways identified in this analysis. (b) Shading shows the climatological blocking frequency expressed as a percentage of blocked days per grid point for the November to March season from 1950 to 2010. Contours indicate the zonally asymmetric component of the 500-hPa geopotential height climatology. Solid boxes define the European and west Pacific blocking regions.

We have re-done the analysis using a wintertime averaged climatology, and the results are essentially the same. Throughout the paper, standardised anomalies are used.

To quantify the vertical wave-activity flux, we use a 45°–75°N average of the zonal-mean meridional eddy heat flux (hereafter heat flux), which is proportional to the vertical component of the Eliassen-Palm flux vector (Edmon et al., 1980). The heat flux $\overline{v'T'}$ is calculated by zonally averaging the product of meridional wind v and temperature T deviations from their respective zonal averages (the overbar represents the zonal average and the prime deviations from the zonal averages). Following Weinberger et al. (2021), we consider the upward wave-activity propagation between the troposphere and the stratosphere using standardised heat flux anomalies at 300 and 100 hPa, which represent the lower and upper limits of the primary communication layer between the upper troposphere and the bottom of the polar vortex, respectively.

For simplicity, we use total heat fluxes for both 300 and 100 hPa. We have tested our analysis using 1–3 zonal wavenumber filtering; the results are essentially the same as for the total heat fluxes.

To determine polar vortex changes, we use the zonal-mean zonal wind, $\overline{u}$, at 10 hPa and 60°N and calculate the wind tendency, du, over 5 days, hereafter referred to as the SPV change. SSWs are detected using the commonly accepted wind reversal definition, in which the central date of an SSW is considered to be the day in which $\overline{u}$ becomes negative (Butler et al., 2017). A minimum timescale of 20 days separation is used between SSW events, and final SSW events are excluded. This leads to a total of 44 events over the time period considered. However, the sampling constraints of our time-lag analysis reduce the total number of SSW events to 37 and 30 (Figures 3a and 3b).

19448007, 2022, 23, Downloaded from https://agupubs.onlinelibrary.wiley.com/doi/10.1029/2022GL100895 by CochraneAustria, Wiley Online Library on [24/07/2023]. See the Terms and Conditions (https://onlinelibrary.wiley.com/terms-and-conditions) on Wiley Online Library for rules of use; OA articles are governed by the applicable Creative Commons License

19448007, 2022, 23, Downloaded from https://agupubs.onlinelibrary.wiley.com/doi/10.1029/2022GL100895 by CochraneAustria, Wiley Online Library on [24/07/2023]. See the Terms and Conditions (https://onlinelibrary.wiley.com/terms-and-conditions) on Wiley Online Library for rules of use; OA articles are governed by the applicable Creative Commons License

Following the blocking detection methodology described by Brunner and Steiner (2017) and Brunner (2018), blocking events are identified based on the reversal of 500-hPa geopotential height gradients. The three-step algorithm considers first the reversal of meridional 500-hPa gradients within the 45° to 80°N latitude band, then requires that the reversed gradients span at least 15° longitude and persist within a 10° longitude and 5° latitude extent for at least 5 consecutive days. Additionally, to identify persistent blocking events, it is required that the previous criterion is satisfied for more than 4 consecutive days.

The geographical definitions of European (0°–59°E) and west Pacific (120°–179°E) blocking are chosen following Attard and Lang (2019), who found that these two blocking regions are associated with statistically significant heat flux anomalies. Figure 1b shows the climatological blocking frequency for the winter season and highlights the two selected geographical regions. Our blocking detection methodology identifies 220 European blocks and 183 west Pacific blocks over the time period considered.

To test our hypothesis about the underlying causal mechanisms and quantify the relationships from the data, we use a causal network approach proposed by Kretchmer et al. (2021) and based on causal inference theory (Pearl, 2009a, 2009b). A causal network approach assumes a hypothetical causal model represented in graphical networks consisting of links that connect nodes, that is, conditionally dependent processes (Pearl, 2013). The graphical representation enables the identification of direct and indirect links, which is essential for generating explanations. The interest lies in quantifying the causal effects of those links, where information flows in the direction of the causal influence.

In this work, we test the hypothesis that the causal relationships have a chain structure. A causal chain network consists of a minimum of three variables, that is, $X \rightarrow Z \rightarrow Y$, where X is the independent variable, Y is the dependent variable, and Z is the mediating variable. When controlling for the mediator, the relationship between X and Y becomes nonsignificant, equivalently X and Y become independent conditional on Z, that is, $P(X \cap Y|Z) = P(X|Z)$ $P(Y|Z)$, where P denotes probability density functions (Kretschmer et al., 2016; Pearl, 2009b). For example, in the chain depicted in Figure 1a, we assume that $\overline{v'T'}_{300}$ affects the SPV only through $\overline{v'T'}_{100}$, that is, $\overline{v'T'}_{100}$ is the mediator. If the effect of $\overline{v'T'}_{300}$ on SPV change becomes nonsignificant when $\overline{v'T'}_{100}$ is controlled for, then full mediation would be confirmed. On the other hand, if the effect remains significant, this suggests there is another pathway from $\overline{v'T'}_{300}$ to the SPV which avoids $\overline{v'T'}_{100}$, at least the way it is expressed in this network.

In the case of linear relationships of continuous variables, multiple linear regression analysis (MLR) is used to estimate causal effects, and "controlling for" is achieved by including the mediator variable in the regression model. In our case, we have a mixture of continuous variables (heat fluxes and SPV change) and categorical variables (blocking and SSWs). This reflects the way these different flow elements are most commonly described in the scientific literature, to ensure a meaningful connection with that literature.

3. Results

3.1. Causal Effect of Blocking on Lower Stratospheric Heat Flux Anomalies

We first test for evidence of the statistical relationship between blocks and heat flux anomalies. We construct a composite of daily standardised heat flux anomalies 1–20 days before and after the onset of European and west Pacific blocks. We found no correlation between the occurrence of European and west Pacific blocks, so they can be considered as independent drivers. Consistent with the results of Attard and Lang (2019), European blocks are accompanied by positive heat flux anomalies, while west Pacific blocks are accompanied by negative heat flux anomalies (Figure 2a). At 300 hPa, statistically significant positive and negative heat flux anomalies, respectively, precede the blocking onset. Heat flux anomalies at 100 hPa lag those at 300 hPa, indicating their upward propagation coinciding with the blocking formation. Overall, the composite analysis supports the hypothesized causal relationships discussed in Section 1.

We then seek to establish whether the causal effect of blocking (European and west Pacific) on the heat flux in the lower stratosphere at 100 hPa is entirely mediated by its effect on the heat flux in the upper troposphere at 300 hPa. First, the time scales of the processes involved are determined. In Figure 2a, the peaks between the 300 and 100 hPa heat flux anomalies coincide within 5–7 days. The following analysis uses a 5-day average for the heat flux anomaly time series, as the sensitivity tests showed the strongest causal effect with this choice.

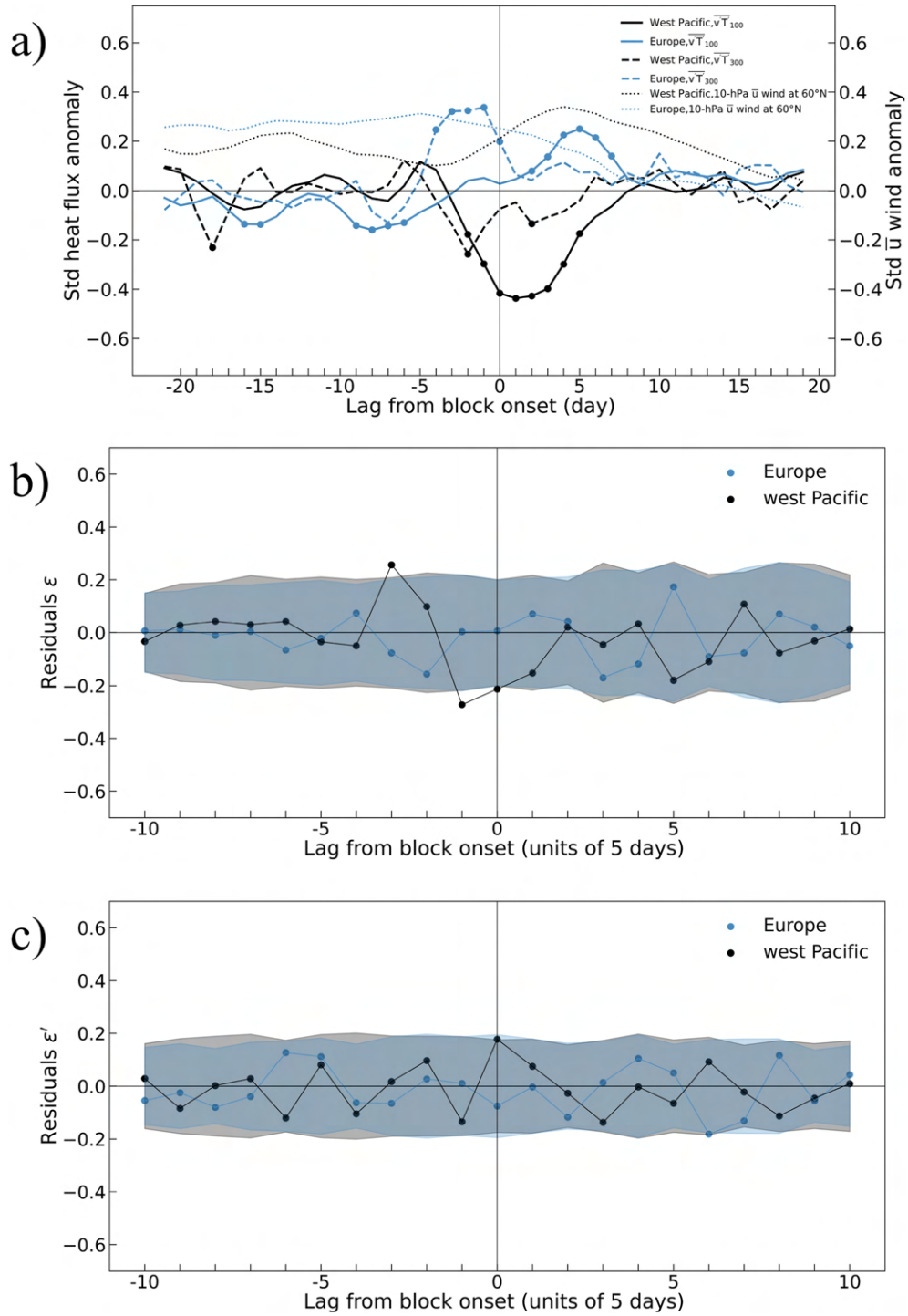


Figure 2. (a) Composite time series of the standardised 100-hPa heat flux anomaly (solid), 300-hPa heat flux anomaly (dashed), and 10-hPa zonal-mean zonal wind anomaly at 60°N (dotted) relative to the onset of European or west Pacific blocking. Dots indicate statistical significance above the 95% confidence level according to a two-tailed Student *t* test (the null hypothesis is that the composite mean at each lag is statistically indistinguishable from zero). Lag is in units of days. Composite of residuals obtained by (b) regressing the 5-day averaged 100-hPa standardised heat flux anomaly on the 5-day averaged 300-hPa standardised heat flux anomaly, and (c) regressing the 5-day averaged standardised stratospheric polar vortex change du on 5-day averaged 100-hPa and 300-hPa standardised heat flux anomalies, plotted relative to the onset of European or west Pacific blocking. Shading indicates the noise level, that is, 95% confidence range for the null hypothesis according to a two-tailed Student *t* distribution. Lag is in units of 5 days.

19448007, 2022, 23, Downloaded from https://agupubs.onlinelibrary.wiley.com/doi/10.1029/2022GL100895 by CochraneAustria, Wiley Online Library on [24/07/2023]. See the Terms and Conditions (https://onlinelibrary.wiley.com/terms-and-conditions) on Wiley Online Library for rules of use; OA articles are governed by the applicable Creative Commons License

19448007, 2022, 23, Downloaded from https://agupubs.onlinelibrary.wiley.com/doi/10.1029/2022GL100895 by CochraneAustria, Wiley Online Library on [24/07/2023]. See the Terms and Conditions (https://onlinelibrary.wiley.com/terms-and-conditions) on Wiley Online Library for rules of use; OA articles are governed by the applicable Creative Commons License

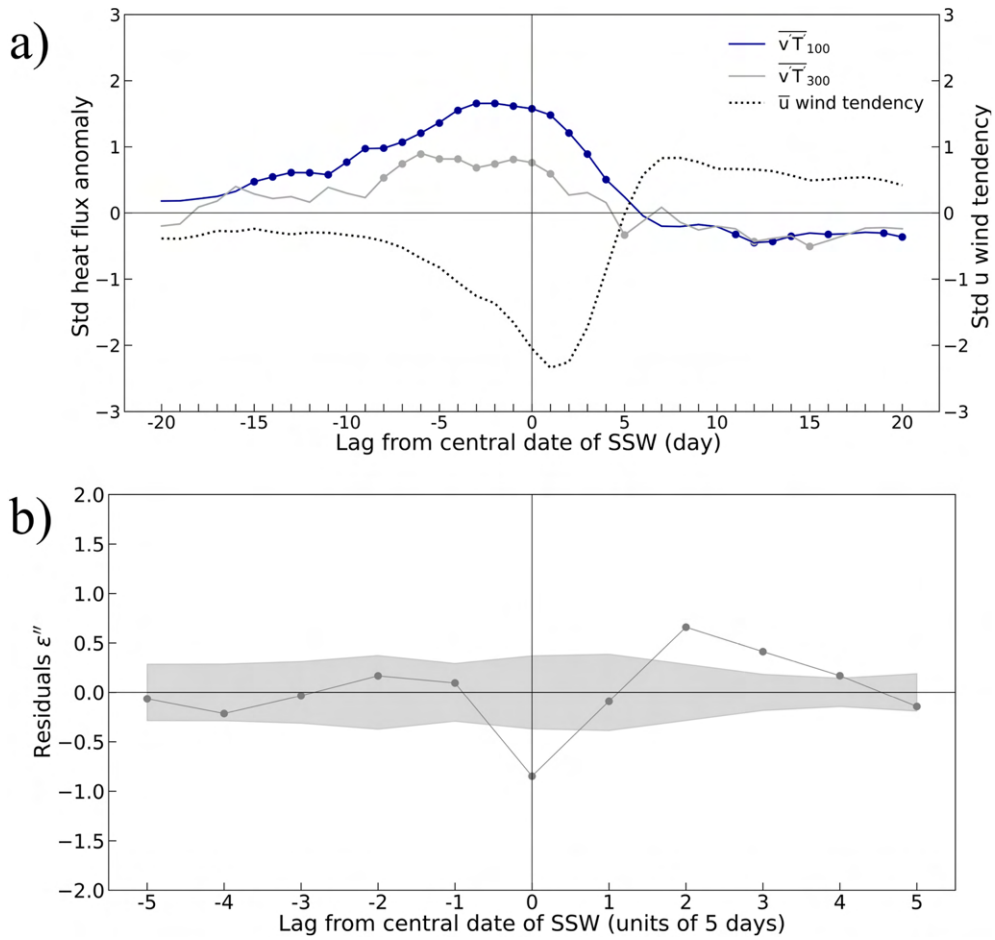


Figure 3. (a) Composite of the 100- and 300-hPa standardised heat flux anomalies, and the stratospheric polar vortex (SPV) change, relative to the onset of sudden stratospheric warming (SSW) events. Dots indicate statistical significance above the 95% confidence level according to a two-tailed Student *t* test (the null hypothesis is that the composite mean at each lag is statistically indistinguishable from zero). Lag is in units of days. (b) Composite of residuals obtained by regressing the 5-day averaged standardised SPV change du on the 5-day averaged 100- and 300-hPa standardised heat flux anomalies, plotted relative to the onset of SSW events. Shading indicates the noise level, that is, 95% confidence range for the null hypothesis according to a two-tailed Student *t* distribution. Lag is in units of 5 days.

Quantifying the causal effect in the chain can be done by regressing the 100-hPa heat flux anomaly on blocking and controlling for the mediating effect of 300-hPa heat flux by including it in the regression model. However, a technical complication is that the blocking index is a categorical variable while the other variables are continuous. Therefore, we first estimate the causal effect of the 300-hPa heat flux anomaly on the 100-hPa heat flux anomaly with time lag $\tau = +1$ (i.e., 5 days) by simply regressing the latter on the former. Choosing a lag of 5 days between variables was found to be the optimal lag choice for our analysis, after we ran sensitivity tests for lags of 1, 3, 5, and 10 days. It also makes physical sense in terms of Rossby-wave propagation timescales. A standardised causal effect is estimated as 0.33 in the regression model formulated as

$$\overline{v'T'}_{100,\ t+\tau} = 0.33\,\overline{v'T'}_{300,\ t} + \varepsilon, \tag{1}$$

where ε is the residual.

In the next step, we analyze the obtained residuals by plotting the lag-composite evolution of the residuals relative to the blocking onset to determine if blocking has an effect on the residuals (Figure 2b). This is effectively the same as if we regressed the residuals on the blocking index to determine the regression coefficient or causal effect, that is, performing a sequential linear regression. A random distribution of the residuals indicates that the effect of blocking on the 100-hPa heat flux anomaly is fully mediated by its effect on the 300-hPa heat

19448007, 2022, 23, Downloaded from https://agupubs.onlinelibrary.wiley.com/doi/10.1029/2022GL100895 by CochraneAustria, Wiley Online Library on [24/07/2023]. See the Terms and Conditions (https://onlinelibrary.wiley.com/terms-and-conditions) on Wiley Online Library for rules of use; OA articles are governed by the applicable Creative Commons License

flux anomaly. Figure 2b shows the residuals spread over 50 days before and after the onset of European and west Pacific blocking. Recall that lag 1 corresponds to 5 days. For European blocks the residuals appear to be randomly distributed around zero, supporting the hypothesized pathway in this case. However, for west Pacific blocks, there appears to be a negative signal immediately preceding block onset. This suggests that in this case the residuals contain a structure not accounted for in our model, meaning there may be another pathway of influence or a more complex time dependence which cannot be captured with a single time lag.

Given the limited length of the winter season, using the 50 days before and after block onset in Figure 2b, compared with only 20 days in Figure 2a, reduces the number of blocks considered to 77 European blocks and 88 west Pacific blocks. We have performed a sensitivity test, re-doing the calculation leading to Figure 2b using only the 25 days before and after block onset, which increases the number of blocks considered to 181 European blocks and 154 west Pacific blocks. The results are included in Figure S1a in Supporting Information S1, and confirm the conclusion derived from Figure 2b.

3.2. Causal Effect of Blocking and Heat Flux Anomalies on SPV Changes

We now assess the relationship between blocking, heat flux anomalies and SPV changes. We first test whether the effect of the 300-hPa heat flux anomaly on the SPV is entirely mediated by its effect on the 100-hPa heat flux, as depicted in Figure 1a. We use a MLR model to quantify the standardised causal effect of a 300-hPa heat flux anomaly on the SPV change du when controlling for the 100-hPa heat flux anomaly as a mediator. The model is formulated as

$$\mathrm{du}_{t+\tau} = -0.62\,\overline{\mathrm{v}'\mathrm{T}'}_{100,\,t+\tau} - 0.10\,\overline{\mathrm{v}'\mathrm{T}'}_{300,\,t} + \varepsilon' \tag{2}$$

where ε' is the residual, and the lag τ is in units of 5 days. Note that the 95% confidence intervals on the regression coefficients are approximately ± 0.035. This result indicates a direct pathway from $\overline{\mathrm{v}'\mathrm{T}'}_{300}$ to du which avoids $\overline{\mathrm{v}'\mathrm{T}'}_{100}$. To estimate the relative strength of the direct and indirect pathways from $\overline{\mathrm{v}'\mathrm{T}'}_{300}$ to du, we employ the path tracing rule. The direct pathway has a standardised strength of -0.10. The strength of the indirect pathway is the regression coefficient of du on $\overline{\mathrm{v}'\mathrm{T}'}_{100}$, -0.62. multiplied by the correlation between $\overline{\mathrm{v}'\mathrm{T}'}_{300}$ and $\overline{\mathrm{v}'\mathrm{T}'}_{100}$, 0.32, which gives -0.20. The correlation between $\overline{\mathrm{v}'\mathrm{T}'}_{300}$ and du is the sum of the strength of the direct and indirect pathways, namely -0.30. Thus, one-third of the influence of $\overline{\mathrm{v}'\mathrm{T}'}_{300}$ on du occurs via the direct pathway, and two-thirds is mediated by $\overline{\mathrm{v}'\mathrm{T}'}_{100}$.

To test if the effect of blocking on SPV changes is mediated via its effect on the 300- and 100-hPa heat flux anomalies, we repeat the residual analysis as in Section 3.1. Figure 2c shows the composite of residuals $\boldsymbol{\varepsilon}'$ relative to blocking onset. It is observed that the residuals are distributed relatively evenly around zero for both European and west Pacific blocking. The same sensitivity test used for Figure 2b is applied here to increase the number of blocking events considered. The results are included in Figure S1b in Supporting Information S1, and confirm the conclusion derived from Figure 2c. This suggests that once we consider the complete causal chain from blocking to SPV and condition on the upper tropospheric and lower stratospheric heat fluxes, their effect controls away the effect of blocking on the SPV. This confirms the classical view that the influence of blocking on the SPV is entirely mediated by upward wave-activity fluxes represented by the standard metrics. However, using only the upper tropospheric or lower stratospheric wave-activity fluxes alone does not fully capture the pathway.

We finally try to understand the contribution of the heat fluxes to the occurrence of SSWs. Figure 3a summarizes the results of the composite heat flux anomalies and wind tendency 1–20 days before and after the SSW central date.

Significant positive standardized heat flux anomalies (about 2 standard deviations) appear first around lag -15, preceding the central date. This enhanced peak in heat flux is accompanied by an increased negative wind tendency, indicating preconditioning of the SPV followed by a breakdown. This suggests as expected that anomalous upward wave-activity propagation precedes SSWs, consistent with the existing literature (Baldwin et al., 2021).

19448007, 2022, 23, Downloaded from https://agupubs.onlinelibrary.wiley.com/doi/10.1029/2022GL100895 by CochraneAustria, Wiley Online Library on [24/07/2023]. See the Terms and Conditions (https://onlinelibrary.wiley.com/terms-and-conditions) on Wiley Online Library for rules of use; OA articles are governed by the applicable Creative Commons License

We now ask whether the SSW occurrence is fully explainable by the heat fluxes. To this end, we perform the same residual analysis as in Figures 2b and 2c, but now composited relative to the SSW central dates (Figure 3b). This is an inverse regression, as we condition on the target variable. We see that the strong features in du at and just after the SSW central date in Figure 3a are weakened, but are still there. Using the same logic as for the analysis in Section 3.1, we can conclude that SSWs are not fully explainable from the heat fluxes. This could suggest an alternative causal factor, which would certainly not be inconsistent with the literature. However, it could also reflect a confounding factor. Monnin et al. (2022) showed that the seasonal dependence of the climatological strength of the SPV induces a seasonal dependence of the relationship between SSWs and other variables, which can be considered a statistical artifact. (In causal statistics, this is known as a "collider bias.") However, it is not possible to determine whether that effect might be playing a role here, due to the small sample size of SSWs in the reanalysis record. Note that the lag relations evident in Figure 3a suggest that there might be a time lag of about 5 days between the upper stratospheric heat flux and the SPV change associated with SSWs. We have performed a sensitivity test, re-doing the calculation leading to Figure 3b using a regression analysis with a 5-day time lag between these two quantities. The results are included in Figure S2 in Supporting Information S1, and confirm the conclusion derived from Figure 3b.

4. Discussion and Conclusions

In the present study, we apply a causal inference-based framework to examine the effect of blocking on Northern Hemisphere polar stratospheric variability through upward propagating wave activity. We test a hypothesized causal chain for blocking in Europe and the west Pacific using causal reasoning. The paper considers two main aspects: first, we test the evidence for a causal relationship between blocking and lower-stratospheric heat flux, and then, whether this is linked to changes in SPV and the occurrence of SSWs.

Our findings are generally consistent with the proposed hypotheses, but not entirely so. Our first analysis supports the assumption that the influence of European blocking on the lower stratospheric heat flux is fully mediated (within our sampling uncertainties) by its influence on the upper tropospheric heat flux. This does not hold for west Pacific blocking, however, meaning there is another pathway (or pathways) of influence on the lower stratospheric heat flux. This may indicate that the mechanisms of vertical influence differ for European and west Pacific blocking. West Pacific blocking has been linked to regional wave reflection, where upward propagating waves are reflected downward due to conditions in the stratosphere (Kodera et al., 2016; Matthias & Kretschmer, 2020). Wave reflection has also been addressed by Weinberger et al. (2021). They suggest that near-reflecting conditions above the tropopause are crucial for determining the upward wave propagation from 300 to 100 hPa. A possible causal variable accounting for the factor determining the upward wave propagation would be the refractive index (Matsuno, 1970; Weinberger et al., 2021). The inclusion of the refractive index in the causal network may potentially explain the difference in results for the two types of blocking. Therefore, wave reflection should be considered in the causal network of the stratosphere-troposphere coupling mechanism, which should be undertaken in future studies.

Our further results suggest that the influence of blocking on the SPV is fully mediated by its effect on the heat fluxes. This is true for both types of blocking. However, neither the upper tropospheric nor the lower stratospheric heat fluxes are sufficient on their own to fully capture this pathway. In particular, only two-thirds of the influence of the upper tropospheric heat fluxes on the SPV is mediated by the lower stratospheric heat fluxes. Answering the question about the effect of blocking and heat fluxes on the occurrence of SSWs is more challenging, partly because of the small number of SSWs in the observed record, and partly because of the potentially confounding factor of the seasonal cycle on any relationship between atmospheric variables and SSWs (Monnin et al., 2022). It is possible that this question could be addressed using hindcasts from seasonal prediction models, which can provide a much larger sample size for statistical analysis.

Overall, we have analyzed the pathways of influence between European and west Pacific blocking and polar vortex variability in line with the previously proposed hypotheses that blocking is an important source of anomalous wave activity flux which disturbs the polar vortex. Our findings, which are summarized in Figure 1a, help clarify the pathways of influence between blocking and SPV variability. The broader purpose of this paper was to demonstrate how the causal inference approach can be applied to identify and quantify these kinds of causal relationships. This approach can overcome the ambiguity of correlation analysis and provide a complementary

method for hypothesis testing. More generally, our study adds to the large body of literature addressing the connection between blocking and SSWs and the mechanisms of troposphere-stratosphere coupling.

Data Availability Statement

ECMWF's ERA5 reanalysis data are freely available at https://www.ecmwf.int/en/forecasts/datasets/reanalysis-datasets/era5.

Acknowledgments
This work was funded by the Austrian Science Fund (FWF) under research Grant W1256 (Doctoral Programme Climate Change: Uncertainties, Thresholds and Coping Strategies, http://dk-climate-change.uni-graz.at). We acknowledge ECMWF (Reading, UK) and Copernicus Climate Change Service for access to the ERA5 reanalysis data. The Visitors Programme at the University of Reading's Department of Meteorology is thanked for hosting an extended research visit by the first author. We thank the two reviewers for their constructive comments.

References

Andrews, D. G., Holton, J. R., & Leovy, C. B. (1987). Middle atmosphere dynamics. *International geophysics series* (Vol. 40). Academic Press.
Attard, H. E., & Lang, A. L. (2019). Troposphere–stratosphere coupling following tropospheric blocking and extratropical cyclones. *Monthly Weather Review*, *147*(5), 1781–1804. https://doi.org/10.1175/MWR-D-18-0335.1
Baldwin, M. P., Ayarzagüena, B., Birner, T., Butchart, N., Butler, A. H., Charlton-Perez, A. J., et al. (2021). Sudden stratospheric warmings. *Reviews of Geophysics*, *59*(1), e2020RG000708. https://doi.org/10.1029/2020RG000708
Bell, B., Hersbach, H., Simmons, A., Berrisford, P., Dahlgren, P., Horányi, A., et al. (2021). The ERA5 global reanalysis: Preliminary extension to 1950. *Quarterly Journal of the Royal Meteorological Society*, *147*(741), 4186–4227. https://doi.org/10.1002/qj.4174
Birner, T., & Albers, J. R. (2017). Sudden stratospheric warmings and anomalous upward wave activity flux. *Sola*, *13A*, 8–12. https://doi.org/10.2151/sola.13A-002
Brunner, L. (2018). *A new perspective on atmospheric blocking from observations—Detection, analysis, and impacts* (PhD thesis). Scientific Report No. 76-2018. Wegener Center Verlag.
Brunner, L., & Steiner, A. K. (2017). A global perspective on atmospheric blocking using GPS radio occultation—One decade of observations. *Atmospheric Measurement Techniques*, *10*(12), 4727–4745. https://doi.org/10.5194/amt-10-4727-2017
Butler, A. H., Sjoberg, J. P., Seidel, D. J., & Rosenlof, K. H. (2017). A sudden stratospheric warming compendium. *Earth System Science Data*, *9*(1), 63–76. https://doi.org/10.5194/essd-9-63-2017
Colucci, S. J., & Kelleher, M. E. (2015). Diagnostic comparison of tropospheric blocking events with and without sudden stratospheric warming. *Journal of the Atmospheric Sciences*, *72*(6), 2227–2240. https://doi.org/10.1175/JAS-D-14-0160.1
de la Cámara, A., Albers, J. R., Birner, T., Garcia, R. R., Hitchcock, P., Kinnison, D. E., & Smith, A. K. (2017). Sensitivity of sudden stratospheric warmings to previous stratospheric conditions. *Journal of the Atmospheric Sciences*, *74*(9), 2857–2877. https://doi.org/10.1175/JAS-D-17-0136.1
Edmon, H. J., Jr., Hoskins, B. J., & McIntyre, M. E. (1980). Eliassen–Palm cross sections for the troposphere. *Journal of the Atmospheric Sciences*, *37*(12), 2600–2616. https://doi.org/10.1175/1520-0469(1980)037<2600:EPCSFT>2.0.CO;2
Garfinkel, C. I., Hartmann, D. L., & Sassi, F. (2010). Tropospheric precursors of anomalous northern hemisphere stratospheric polar vortices. *Journal of Climate*, *23*(12), 3282–3299. https://doi.org/10.1175/2010JCLI3010.1
Hersbach, H., Bell, B., Berrisford, P., Hirahara, S., Horányi, A., Muñoz-Sabater, J., et al. (2020). The ERA5 global reanalysis. *Quarterly Journal of the Royal Meteorological Society*, *146*(730), 1999–2049. https://doi.org/10.1002/qj.3803
Hitchcock, P., Shepherd, T. G., & Manney, G. L. (2013). Statistical characterization of arctic polar-night jet oscillation events. *Journal of Climate*, *26*(6), 2096–2116. https://doi.org/10.1175/JCLI-D-12-00202.1
Kodera, K., Mukougawa, H., Maury, P., Ueda, M., & Claud, C. (2016). Absorbing and reflecting sudden stratospheric warming events and their relationship with tropospheric circulation. *Journal of Geophysical Research: Atmospheres*, *121*(1), 80–94. https://doi.org/10.1002/2015JD023359
Kretschmer, M., Adams, S. V., Arribas, A., Prudden, R., Robinson, N., Saggioro, E., & Shepherd, T. G. (2021). Quantifying causal pathways of teleconnections. *Bulletin of the American Meteorological Society*, *102*(12), E2247–E2263. https://doi.org/10.1175/BAMS-D-20-0117.1
Kretschmer, M., Coumou, D., Donges, J. F., & Runge, J. (2016). Using causal effect networks to analyse different Arctic drivers of mid-latitude winter circulation. *Journal of Climate*, *29*(11), 4069–4081. https://doi.org/10.1175/JCLI-D-15-0654.1
Martius, O., Polvani, L. M., & Davies, H. C. (2009). Blocking precursors to stratospheric sudden warming events. *Geophysical Research Letters*, *36*(14), L14806. https://doi.org/10.1029/2009GL038776
Matsuno, T. (1970). Vertical propagation of stationary planetary waves in the winter northern hemisphere. *Journal of the Atmospheric Sciences*, *27*(6), 871–883. https://doi.org/10.1175/1520-0469(1970)027<0871:VPOSPW>2.0.CO;2
Matthias, V., & Kretschmer, M. (2020). The influence of stratospheric wave reflection on North American cold spells. *Monthly Weather Review*, *148*(4), 1675–1690. https://doi.org/10.1175/MWR-D-19-0339.1
Monnin, E., Kretschmer, M., & Polichtchouk, I. (2022). The role of the timing of sudden stratospheric warmings for precipitation and temperature anomalies in Europe. *International Journal of Climatology*, *42*(6), 3448–3462. https://doi.org/10.1002/joc.7426
Nishii, K., Nakamura, H., & Orsolini, Y. J. (2011). Geographical dependence observed in blocking high influence on the stratospheric variability through enhancement and suppression of upward planetary-wave propagation. *Journal of Climate*, *24*, 6408–6423. https://doi.org/10.1175/JCLI-D-10-05021.1
Pearl, J. (2009a). Causal inference in statistics: An overview. *Statistics Surveys*, *3*, 96–146. https://doi.org/10.1214/09-SS057
Pearl, J. (2009b). *Causality: Models, reasoning, and inference* (2nd ed.). Cambridge University Press.
Pearl, J. (2013). Linear models: A useful "microscope" for causal analysis. *Journal of Causal Inference*, *1*, 155–170. https://doi.org/10.1515/jci-2013-0003
Polvani, L. M., & Waugh, D. W. (2004). Upward wave activity flux as a precursor to extreme stratospheric events and subsequent anomalous surface weather regimes. *Journal of Climate*, *17*(18), 3548–3554. https://doi.org/10.1175/1520-0442(2004)017<3548:UWAFAA>2.0.CO;2
Runge, J., Petoukhov, V., & Kurths, J. (2014). Quantifying the strength and delay of climatic interactions: The ambiguities of cross correlation and a novel measure based on graphical models. *Journal of Climate*, *27*(2), 720–739. https://doi.org/10.1175/JCLI-D-13-00159.1
Shepherd, T. G. (2002). Issues in stratosphere-troposphere coupling. *Journal of the Meteorological Society of Japan*, *80*(4B), 769–792. https://doi.org/10.2151/jmsj.80.769
Weinberger, I., Garfinkel, C. I., White, I. P., & Birner, T. (2021). The efficiency of upward wave propagation near the tropopause: Importance of the form of the refractive index. *Journal of the Atmospheric Sciences*, *78*(8), 2605–2617. https://doi.org/10.1175/JAS-D-20-0267.1

19448007, 2022, 23, Downloaded from https://agupubs.onlinelibrary.wiley.com/doi/10.1029/2022GL100895 by CochraneAustria, Wiley Online Library on [24/07/2023]. See the Terms and Conditions (https://onlinelibrary.wiley.com/terms-and-conditions) on Wiley Online Library for rules of use; OA articles are governed by the applicable Creative Commons License

Paper III. Observational perspective on sudden stratospheric warmings and blocking from Eliassen–Palm fluxes

Kamilya Yessimbet[1,2], Andrea K. Steiner[1,2], Florian Ladstädter[1], and Albert Ossó[1]

[1]Wegener Center for Climate and Global Change, University of Graz, Graz, Austria
[2]FWF-DK Climate Change, University of Graz, Graz, Austria

Atmos. Chem. Phys., 24, 10893–10919
doi: doi.org/10.5194/acp-24-10893-2024

This is an open access article under the terms of the Creative Commons Attribution License.

Atmos. Chem. Phys., 24, 10893–10919, 2024
https://doi.org/10.5194/acp-24-10893-2024
© Author(s) 2024. This work is distributed under
the Creative Commons Attribution 4.0 License.

Atmospheric Chemistry and Physics
Open Access
EGU

Observational perspective on sudden stratospheric warmings and blocking from Eliassen–Palm fluxes

Kamilya Yessimbet[1,2], Andrea K. Steiner[1,2], Florian Ladstädter[1], and Albert Ossó[1]

[1]Wegener Center for Climate and Global Change, University of Graz, 8010 Graz, Austria
[2]FWF-DK Climate Change, University of Graz, 8010 Graz, Austria

Correspondence: Kamilya Yessimbet (kamilya.yessimbet@uni-graz.at)

Received: 4 December 2023 – Discussion started: 25 January 2024
Revised: 31 May 2024 – Accepted: 13 July 2024 – Published: 27 September 2024

Abstract. In this study, we examine eight major boreal sudden stratospheric warming (SSW) events between 2007 and 2019 to understand the vertical coupling between the troposphere and stratosphere as well as the relationship between SSWs and blocking events using global navigation satellite system (GNSS) radio occultation (RO) observations. Our study covers the main aspects of SSW events, including the vertical structure of planetary-wave propagation, static stability, geometry of the polar vortex, and occurrence of blocking events. To analyze wave activity and atmospheric circulation, we compute the quasi-geostrophic Eliassen–Palm (EP) flux and geostrophic winds. The results show that the observations agree with theory and previous studies in terms of the primary dynamic features and provide a detailed view of their vertical structure. We observe a clear positive peak of upward EP flux in the stratosphere prior to all SSW events. In seven out of eight events, this peak is preceded by a clear peak in the troposphere. Within the observed timeframe, we identify two types of downward dynamic interactions and the emergence of blocking events. During the 2007 and 2008 "reflecting" events, we observe a displacement of the polar vortex along with a downward propagation of wave activity from the stratosphere to the troposphere during vortex recovery, coinciding with the formation of blocking in the North Pacific region. Conversely, in the other six SSW "absorbing" events from 2009 to 2019, which were characterized by a vortex split, we observe wave absorption and the subsequent formation of blocking in the Euro-Atlantic region. The analysis of the static stability demonstrates an enhancement of the polar tropopause inversion layer as the result of SSWs, which was stronger for the absorbing events. Overall, our study provides an observational view of the synoptic and dynamic evolution of the major SSWs, their link to blocking, and the impact on the polar tropopause.

1 Introduction

In winter, dynamical coupling between the troposphere and stratosphere, in particular the stratospheric polar vortex (SPV), is an important source of surface climate variability. The coupling is mediated by wave–mean flow interactions and often occurs via the downward progression of zonal-mean anomalies following large SPV anomalies (Baldwin and Dunkerton, 2001). These downward anomalies can induce a change in the tropospheric circulation with patterns that resemble the annular modes (Baldwin and Dunkerton, 1999, 2001). In another view, the downward influence is mediated by the reflection of planetary wave activity from the stratosphere into the troposphere (Hines, 1974; Geller and Alpert, 1980; Perlwitz and Harnik, 2004; Matthias and Kretschmer, 2020; Messori et al., 2022).

In this study, we focus on connections between sudden stratospheric warming (SSW) events, i.e., extreme cases of SPV variability, and atmospheric blocking, i.e., persistent high-pressure systems that interrupt the regular westerly flow at midlatitudes. We adopt two distinctive classifications for SSWs. Depending on the SPV geometry, the first classification categorizes them into displacement and split events. In the displacement type of SSWs, the polar vortex is dis-

placed away from the pole, and in the split type, the polar vortex breaks up into daughter vortices (Butler et al., 2017). The second classification divides SSWs into reflecting and absorbing events based on the planetary-wave activity evolution (Kodera et al., 2016). Reflecting SSW events are characterized by the downward reflection of planetary waves from the stratosphere into the troposphere, whereas absorbing events indicate non-reflecting stratospheric conditions, implying wave absorption by the stratosphere, during SSW recovery. While the former classification describes the SPV behavior during the mature phase of SSWs, the latter describes the behavior of planetary-wave activity during the recovery phase of SSWs, with a more pronounced focus on their impact on the troposphere.

In terms of the impacts on the troposphere, reflecting SSW events have been linked to the occurrence of North Pacific blocking, while absorbing SSWs have been associated with a hemispheric near-surface pattern of relatively high pressure over the polar region and low pressure in the midlatitudes that resembles the negative phase of the Arctic Oscillation (AO) (Kodera et al., 2016). Some studies have suggested that the split and displacement types of SSW events may also lead to different tropospheric responses (Mitchell et al., 2013). However, other studies, such as Maycock and Hitchcock (2015), have not found significant differences in the tropospheric impacts of the split and displacement events.

The atmospheric layer where the main dynamic coupling occurs is the upper troposphere and lower stratosphere (UTLS). An accurate representation of the vertical structure of the UTLS is known to be important for the resolution of atmospheric dynamics and circulation in coupled climate models (Gerber and Manzini, 2016). This, in part, underpins the rationale for employing global navigation satellite system (GNSS) radio occultation (RO) data – which are known for their stability, accuracy, and high vertical resolution within the UTLS (Steiner et al., 2020) – in our study. There have been previous studies resolving important aspects of atmospheric dynamics from RO data, such as Leroy and Anderson (2007), in which the quasi-geostrophic Eliassen–Palm (EP) flux was calculated; Scherllin-Pirscher et al. (2014) and Verkhoglyadova et al. (2014), in which geostrophic winds were calculated; Healy et al. (2020), in which quasi-biennial oscillation (QBO) zonal winds were retrieved; and Pilch Kedzierski et al. (2020), in which Rossby waves were studied.

In this study, we utilize globally distributed direct measurements of geopotential height and temperature fields from RO data. These measurements are used to compute geostrophic winds, the blocking index, the quasi-geostrophic EP flux, and the static stability. The computed parameters are then used as a basis for our synoptic and dynamic analysis of SSW events that occurred between 2007 and 2019. Our main objective is to characterize the dynamics induced by these SSW events and examine their links to blocking events from a observational perspective. We focus on the analysis of the vertical aspects of the EP flux, as it plays a critical role in understanding how the stratospheric circulation responds to the upward propagation of planetary-wave activity from the troposphere (Yessimbet et al., 2022a). Due to its high vertical resolution, RO is shown in this study to be particularly suitable for providing information for the dynamic and synoptic analysis of SSW events and blocking events (e.g., Brunner et al., 2016).

We describe the RO dataset and detail the methods employed in Sects. 2 and 3, respectively. Section 4 presents the results for all investigated SSW events from 2006 to 2019 with a detailed analysis of two representative SSW events in February 2008 and January 2019. Finally, we discuss and draw conclusions about our findings in Sect. 5.

2 Data

This study employs measurements from GNSS RO collected by various satellite missions, including CHAMP (Wickert et al., 2001), SAC-C (Hajj et al., 2004), GRACE (Beyerle et al., 2005; Wickert et al., 2005), MetOp (Luntama et al., 2008), and Formosat-3/COSMIC (Anthes, 2011). The GNSS RO method is based on the detection of radio signals transmitted by GNSS satellites, which are refracted by the Earth's atmosphere as they propagate through it to low Earth orbit (LEO) satellites. The measured signal phase changes are converted to bending angle profiles and further to refractivity by an Abel transform. At high altitudes, the Abel integral requires initialization with background data. Thermodynamic parameters are then computed under the assumption of a dry atmosphere ("dry" parameters). In moist air conditions (lower to middle troposphere, specifically in the tropics), the retrieval of the (physical) temperature or humidity requires prior knowledge of the state of the atmosphere (e.g., Kursinski et al., 1995, 1996; Healy and Eyre, 2000). Due to the background data involved, the retrieved RO temperature data exhibit larger uncertainties in the lowermost moist parts of the troposphere and at high altitudes (above about 30 km). For an overview of the retrieval process and the structural uncertainties involved, see, e.g., Steiner et al. (2011, 2020). The RO measurements are of high quality, with minimal structural uncertainty within the UTLS region, as highlighted by Scherllin-Pirscher et al. (2017) and Steiner et al. (2020).

In this work, we use the geopotential height and physical temperature as a function of pressure, as processed by the Wegener Center for Climate and Global Change (WEGC) with the Occultation Processing System (OPS) version 5.6 (Angerer et al., 2017; Steiner et al., 2020) using the phase delay data derived at the University Corporation for Atmospheric Research COSMIC Data Analysis and Archive Center (UCAR/CDAAC).

Geostrophic-wind fields can be derived from RO geopotential-height fields (Scherllin-Pirscher et al., 2014, 2017). RO geostrophic-wind and gradient-wind fields were

found to capture all the main wind features in our study. Compared to atmospheric analyses, wind differences are generally small ($2\,\mathrm{m\,s^{-1}}$) except near the subtropical jet (up to $10\,\mathrm{m\,s^{-1}}$). There, RO winds underestimate the actual winds due to the geostrophic- and gradient-wind approximations, while RO retrieval errors have negligible effects (Scherllin-Pirscher et al., 2014).

The number of daily RO profiles retrieved from different missions varied over the period from 2006 to 2019, with the highest number of profiles occurring from 2007 to 2010 (>2500 profiles per day) and the number of profiles decreasing (from more than 2500 to less than 2000 profiles) from 2012 onwards (Fig. S1 in the Supplement) as the lifetimes of some of the RO missions were exceeded (Fig. 5; Angerer et al., 2017).

Utilizing data from the available records spanning 2006 to 2019, we focus on the daily wintertime period from November to March. The vertical grid consists of 147 pressure levels from 1000 to 10 hPa (the levels are 200 m apart – i.e., equidistant in altitude space – up to 20 km and 500 m apart above that). To generate $2.5° \times 2.5°$ gridded bins from the profile data, we employ a spatial and temporal weighting methodology. This involves applying Gaussian weighting according to the latitude–longitude distances of each profile in relation to the bin center, taking all profiles within 600 km from the center into account. An additional temporal Gaussian weighting of ± 2 d around the given day is also applied. With this, we reduce the number of missing grid points while maintaining as much measurement information as possible. Thus, in the range of vertical pressure levels from 10 to 850 hPa, there are fewer than 10 missing grid points in the daily gridded fields, with the number increasing towards the surface. For any remaining missing grid points, we use bilinear interpolation to fill in these gaps.

3 Method

This study applies a geostrophic approximation to derive winds directly from geopotential heights, as it balances the pressure gradient with Coriolis forces. RO measurements allow the retrieval of geopotential height as an independent vertical coordinate. The computation of geostrophic winds is based on Scherllin-Pirscher et al. (2014).

To study wave activity, we calculate the quasi-geostrophic EP flux based on Edmon et al. (1980). According to the definition of the EP flux for spherical geometry, the meridional F_ϕ and vertical F_p components are defined as

$$\boldsymbol{F} = \left(F_\phi, F_p\right) = a\cos\phi \left(-\overline{u'v'}, f\frac{\overline{v'\theta'}}{\frac{\partial\bar{\theta}}{\partial p}} \right), \tag{1}$$

where a denotes the equatorial radius of the Earth, p denotes the logarithm of the pressure, ϕ is the latitude, and θ is the potential temperature. The Coriolis parameter f equals

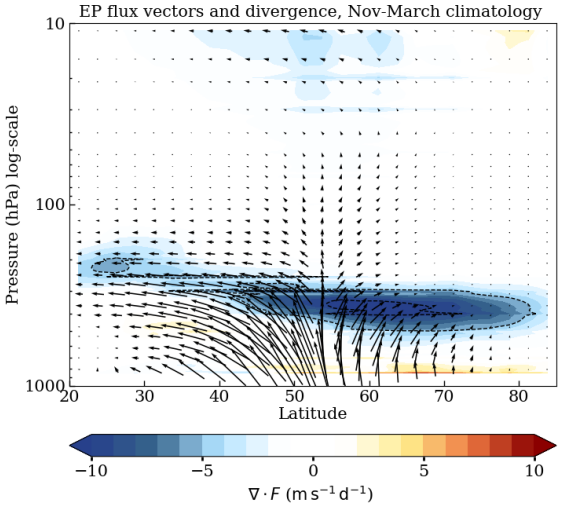


Figure 1. Climatological Eliassen–Palm flux vectors and divergence (shading) for November to March from 2006 to 2019. The vectors are plotted for every fifth pressure level.

$2\Omega\sin\phi$, where Ω is the Earth's angular velocity, u and v are the geostrophic meridional and zonal winds, the overlines denote zonal averages, and primes indicate deviations from zonal averages. Divergence of the EP flux, $\nabla\cdot\boldsymbol{F} \equiv \frac{\partial F_\phi}{\partial_\phi} + \frac{\partial F_p}{\partial_p}$, scaled by $\frac{1}{a\cos\phi}$, indicates an acceleration of the zonal flow. The climatological EP flux for winter 2006 to 2019 is shown in Fig. 1, where a convergence zone (blue shading) with upward-directed EP flux vectors is observed in the upper troposphere, which means that the wave activity is intensified in the wintertime upper troposphere. For display purposes, EP flux vectors are scaled as follows:

$$\left(\boldsymbol{F}_\phi, \boldsymbol{F}_p\right) = \cos\varphi\left(\frac{F_\phi}{a\,\pi}, \frac{F_p}{10^5}\right), \tag{2}$$

according to commonly used methods (NOAA's Physical Sciences Laboratory, 2023).

The 3D wave activity flux, the Plumb flux, presented in Appendix B, is computed according to Plumb (1985; Eq. 5.7). In addition, we also compute the eddy meridional heat flux $\overline{v'T'}$ at 100 hPa and averaged over 45–75° N, similar to Kodera et al. (2016), who used it as a proxy for the vertical wave propagation between the troposphere and the stratosphere to characterize reflecting and absorbing SSW events. The computation of anomalies is performed by subtracting the 2007–2019 daily mean climatology. A standard algorithm based on 500 hPa geopotential-height gradients and described in Brunner and Steiner (2017) and Brunner (2018) is used to calculate the blocking index. Two distinct blocking regions have been defined based on the highest frequencies of blocking during the wintertime: the North Pacific (160° E to 160° W) and Euro-Atlantic (30° W to 45° E).

To examine further effects of the different SSW types, we compute the static stability in the form of the Brunt–Väisälä

frequency, N^2, defined as follows:

$$N^2 = -\frac{pg^2 \frac{\partial\theta}{\partial p}}{RT\theta}, \quad (3)$$

where g denotes the gravitational acceleration ($g = 9.81\,\mathrm{m\,s^{-2}}$), R is the gas constant of dry air ($R = 287\,\mathrm{J\,kg^{-1}\,K^{-1}}$), and T is the temperature.

In our analysis, we also make comparisons of key parameters such as the zonally averaged parameters, zonal-mean zonal wind, and $\overline{v'T'}$ (Figs. S2 and S3) between RO and reanalyses (e.g., ERA5), which confirm the consistency and the reliability of the RO-based dynamics.

For the definition of major SSW events, we adopt a commonly used definition from Butler et al. (2017), which defines the central date of an SSW event as the day when the zonal-mean zonal wind at 10 hPa and 60° N, $\overline{u}$, changes from westerly to easterly. The diagnosed central SSWs are compared with the list of major midwinter SSWs in reanalysis products in the SSW Compendium dataset (NOAA CSL, 2024).

4 Results

Section 4.1 describes the commonalities in the key dynamics of the 2007 and 2008 winters. To illustrate this, we show the results of the analysis of the 2008 winter as a representative case study. Similarly, Sect. 4.2 presents the 2019 SSW event as an example to describe the commonalities between the 2009, 2010, 2013, 2016, and 2018 events. In Sect. 4.3, we analyze the vertical wave activity and static stability for all SSW events from 2007 to 2019.

4.1 Type I: SSW events in 2007 and 2008

One of the main commonalities of the 2008 and 2007 events was the SPV displacement. Figure 2a shows the vortex evolution during the main phases of the winter of 2008. During December and January, the vortex remained strong and symmetrically centered at the North Pole. In February, the vortex began to weaken, losing its symmetry and finally shifting from the pole towards Eurasia. The vortex weakening was marked by warming, with stratospheric polar-cap (65–90° N) temperature anomalies exceeding the climatological mean and showing short-term fluctuation (Fig. 3a, b). While the vortex was displaced, positive polar-cap temperature anomalies propagated downwards to around 70 hPa. On 22 February, $\overline{u}$ turned easterly (Fig. 3c), marking the central date of a major SSW event. The reversal of $\overline{u}$ lasted for 6 d, followed by a period of recovery and gradual cooling. A similar pattern was observed in the winter of 2007, with a vortex displacement and $\overline{u}$ reversal on 24 February that lasted only 4 d and was also accompanied by fluctuating stratospheric polar-cap temperature anomalies (Figs. A1a, A2a, b).

Another common feature of the 2008 and 2007 SSW events was a relatively short (about 12 and 13 d) pulse of wave activity propagation (responsible for the $\overline{u}$ reversal) and its significant decrease (marked by a negative $\overline{v'T'}$) during the first week of the SSW recovery phase. The onset of the SSW recovery phase is defined as the date when the maximum North Pole (80–90° N) temperature anomalies at 50 hPa are reached (Kodera et al., 2016).

For the 2008 event, $\overline{v'T'}$ at 100 hPa and averaged across 45–75° N is shown in Fig. 3c. The behavior of $\overline{v'T'}$ is coherent with that of $\overline{u}$: as $\overline{v'T'}$ increases, indicating the upward propagation of planetary-wave activity, the wind speed decreases. From the beginning of February, a weakening of $\overline{u}$ occurred concurrent with the occurrence of two consecutive $\overline{v'T'}$ peaks with a 2 d lag between them. The 2 d lag between these two pulses may be an indication that the upward wave activity was suppressed and then resumed. The reversal of $\overline{u}$ occurred during the second $\overline{v'T'}$ peak, which lasted the 12 d from 15 to 26 February. In the first week of the SSW recovery phase, the $\overline{v'T'}$ was characterized by negative values.

The time–height representation of the vertical component of EP flux as a function of pressure $F_p$is shown in Fig. 3d. From 7 February, there was a negative F_p anomaly below 300 hPa, indicating an intensification of wave activity. Following this, a mildly negative F_p pattern was observed, first between 300 and 100 hPa and then above 20 hPa with a delay of 2 d. Another (less intense) negative F_p anomaly appeared below 400 hPa on 15 February and later extended to about 100 hPa, which indicates the upward propagation of wave activity. Between 18 February and the central date of the SSW event, a pronounced negative F_p anomaly was noticeable above 100 hPa. Following the central SSW date, a substantial positive F_p anomaly became apparent below 300 hPa before being succeeded by a minor positive F_p anomaly within the stratosphere. Starting from 29 February, the second peak of the positive F_p anomaly maximized below the 300 hPa level and extended throughout the entirety of the atmospheric column. These instances of positive F_p anomaly peaks were consistent with the negative $\overline{v'T'}$ peak observed from 27 February to 6 March, as illustrated in Fig. 3c. The negative $\overline{v'T'}$ peak suggests a substantial reduction in the propagation of planetary-wave activity into the stratosphere or a downward propagation of wave activity due to the reflection of these waves from the stratosphere into the troposphere.

The negative $\overline{v'T'}$ peak from 27 February to 6 March coincided with the occurrence of blocking in the North Pacific, as shown in Fig. 3e. Note that for the 2007 SSW event, there was also a negative $\overline{v'T'}$ peak concurrent with the development of North Pacific blocking (Fig. A2c, e). In Fig. 2b, the manifestation of North Pacific blocking is evident through a positive 500 hPa geopotential-height anomaly from 27 to 29 February. Notably, the arrangement of the 500 hPa geopotential-height anomaly field corresponded to that of the 50 hPa field. The barotropic low-pressure system over eastern Eurasia indicated a polar-vortex shift toward Eurasia. This

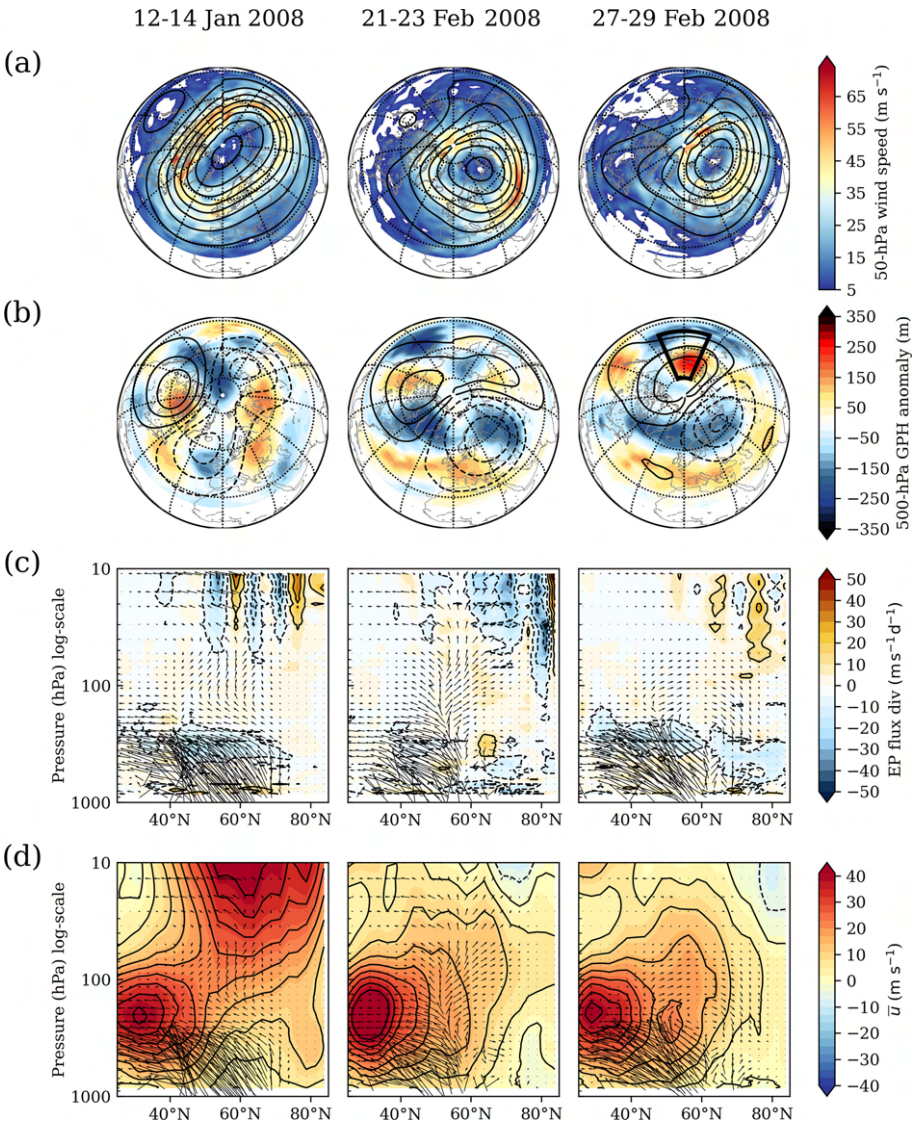


Figure 2. Evolution of the 2008 SSW, as shown by the results at three dates: before the SPV displacement (left), during its displacement (center), and during its recovery (right). **(a)** 50 hPa wind speed (shading) and 50 hPa geopotential height (contours). **(b)** 500 hPa geopotential-height anomaly (shading) and 50 hPa geopotential-height anomaly (contours). The black box indicates the North Pacific blocking region selected. **(c)** Meridional cross-sections of Eliassen–Palm flux vectors and divergence (shading). **(d)** Meridional cross-sections of Eliassen–Palm flux vectors and zonal wind (shading). The vectors are plotted for every fifth pressure level.

alignment underscores a connection between stratospheric and tropospheric conditions.

For a more detailed analysis of the vertical propagation of wave activity and its impact on the circulation, the meridional cross-sections of the divergence and vectors of the 3 d averaged EP flux and $\overline{u}$ for the main phases of the 2008 SPV are shown in Fig. 2c and d. Throughout the SPV's displacement and disruption phase, there was a notable enhancement of EP flux convergence and the upward propagation of EP flux vectors. As the EP flux progressively propagated into the stratosphere and northward of 75° N, it resulted in a slowing down of the stratospheric $\overline{u}$ at the pole. From 21 to 23 February, it can be observed that easterly winds are already present in the upper stratosphere, while westerly winds prevail in the middle and lower stratosphere. According to Perlwitz and Harnik (2003) and Kodera et al. (2008), this negative wind shear indicates favorable conditions for the reflection of upward-propagating wave packets. When these wave packets encounter a transition from lower regions (with westerly winds that support the upward propagation of the wave packets) to higher regions (with easterly winds which oppose that propagation), an effective barrier to upward propagation is formed, resulting in the reflection of part of the wave energy. Between 27 and 29 February, the downward propagation of

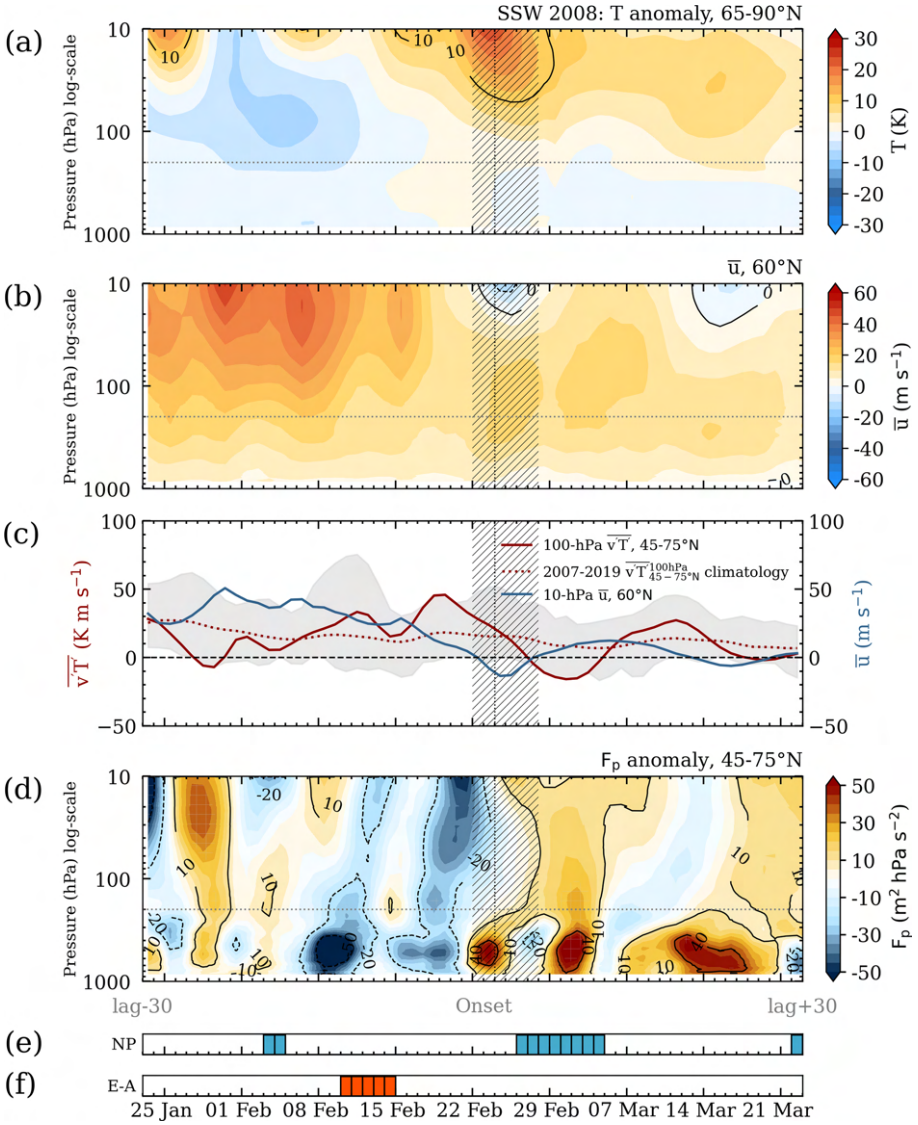


Figure 3. Time–height evolution of **(a)** the area-weighted temperature anomaly averaged over 65–90° N, **(b)** the zonal wind at 60° N, and **(c)** the 100 hPa eddy meridional heat flux averaged over 45–75° N (solid red line), its daily climatology (dotted red line), and the zonal-mean zonal wind at 60° N and 10 hPa (solid blue line). Grey shading covers the region between the daily minimum and maximum of the heat flux for the period 2007–2019. Time–height evolution of **(d)** the anomaly of the vertical component of the Eliassen–Palm flux averaged over 45–75° N, **(e)** blocking index for the North Pacific region, and **(f)** blocking index for the Euro-Atlantic region. The hatched region indicates dates when the zonal-mean zonal wind at 60° N and 10 hPa is negative, and the vertical dotted line indicates the day when the polar (80–90° N) temperature anomaly reaches its maximum, i.e., the start of the SSW recovery phase. The dotted horizontal line indicates 200 hPa (the approximate level of the extratropical tropopause). The time interval shown is ±30 d from the central date (22 February) of the 2008 SSW.

the EP flux can be observed together with an acceleration of $\overline{u}$ in the stratosphere, indicating that wave reflection is taking place. During those days, it can also be observed that the EP flux divergence in the stratosphere from 10 to 70 hPa is maximized between 70 and 80° N. According to Shaw et al. (2010), the presence of a localized positive EP flux divergence can act as an indicator of a reflecting condition within the atmosphere. A similar EP flux evolution is observed for the 2007 event (Fig. A1c, d).

In addition to the EP flux analysis, to further examine the evidence for the relationship between the downward propagation of wave activity and North Pacific blocking, we analyzed the evolution of the 3D Plumb flux (Fig. B1). Starting from 21–23 February (Fig. B1b), and particularly on 27–29 February 2008 (Fig. B1c), a downward propagation of wave activity between about 250 and 300° E is observed along with a trough centered over 300° E and a positive barotropic geopotential-height anomaly between 150 and

200° E (North Pacific). This is observed together with the eastward tilt of the trough, implying downward propagation of the Rossby waves, aligning with the findings of Kodera et al. (2008). This in turn induced the formation of the North Pacific ridge, which then led to the formation of the North Pacific blocking.

The above analysis finds that the main characteristics of the 2008 and 2007 SSW events are consistent with the characteristics of reflecting SSWs, which in turn is consistent with the findings of Kodera et al. (2008, 2016). On this basis, we classify these SSW events as reflecting events.

4.2 Type II: SSW events from 2009 to 2019

One of the main features of the SSW events that occurred between 2009 and 2019 was the SPV split. The 2010, 2013, 2016, and 2019 events were of mixed type, in which the vortex displaces and then splits (see Figs. 4a, A5a, A7a, and A9a). The 2009 and 2018 SSW events were of the split type (Figs. A3a, A11a). Figure 4a shows the SPV evolution of the 2019 event. A displacement of the vortex towards Eurasia was initiated around mid-December 2018. Beginning on 22 December, the displaced vortex elongated towards the North Atlantic. On 2 January, the vortex reversed and split into two lobes and then continued to split apart until the middle of January.

In the weeks following the vortex displacement in December 2018, the polar-cap temperature anomaly in the stratosphere increased significantly and exhibited a marked downward propagation, extending to approximately 200 hPa (Fig. 5a). The long-lasting deep warming is another commonality of the 2009–2019 SSW events (Figs. A2a, A4a, A6a, A8a, A10a, and A12a). Consistent with the polar-cap temperature variability, the reversal of $\overline{u}$ lasted several weeks in these years, which contrasts with the short duration of the SPV reversal in the 2007–2008 events. The only exception was the 2016 SSW event, during which the SPV did not undergo a recovery phase as it was a final warming event. Nevertheless, this event, with its major SSW characteristics, merits its inclusion in our analysis, and it has also been the focus of previous studies such as Manney and Lawrence (2016).

Another interesting feature of these events is the prolonged and gradual wave activity propagation into the stratosphere. The evolution of $\overline{u}$ and $\overline{v'T'}$ in 2019 is shown in Fig. 5c. The $\overline{v'T'}$ peaked on 22 December during the displacement of the vortex, after which $\overline{u}$ began to weaken. Subsequently, as January commenced, the $\overline{v'T'}$ peak underwent a gradual reduction. This was followed by an acceleration of $\overline{u}$ and the eventual recovery of the SPV. Similarly, in 2010, 2013, and 2016, the $\overline{v'T'}$ peaked during the vortex displacement and gradually decreased during $\overline{u}$ reversal (Figs. A6c, A8c, and A10c). In these events, several successive and overlapping peaks in $\overline{v'T'}$ are responsible for the continuous and long-lasting upward wave propagation (about 40 d). In the split events of 2009 and 2018, the peaks in $\overline{v'T'}$ were enhanced before the vortex split and lasted for 38 and 24 d, respectively (Figs. A4c and A12c). They then gradually decreased until the vortex recovered.

In the time–height view of F_p for the 2019 event (Fig. 5d), the enhanced wave activity pattern first appeared around 4 to 13 December in the troposphere below 300 hPa. This was followed by mildly negative F_p in the whole atmospheric column. Around 23 December, the negative F_p peaked in the stratosphere, extending vertically upward from about 200 hPa. This was preceded by a tropospheric F_p enhancement with a delay of about 8 d. From 25 December, there was another wave activity pattern in the troposphere below 200 hPa, which continued until 1 January. After the reversal of $\overline{u}$, the troposphere featured a more divergent state, indicating a decrease in wave activity. In the 2009–2018 events, the negative F_p peak in the stratosphere is preceded by a negative F_p peak in the troposphere by a few days before either the SPV displacement (2010, 2013, and 2016) or the SPV split (2009 and 2018 events).

As for the tropospheric response, Euro-Atlantic blocking was observed in the troposphere during the SPV split from late December to mid-January, as shown by the positive 500 hPa geopotential-height anomaly over the Euro-Atlantic in Fig. 4b.

The blocking index captures Euro-Atlantic blocking from 9 to 11 January in Fig. 5f. It can also be observed that the Euro-Atlantic blocking coincided with the configuration of the positive 50 hPa geopotential-height anomaly centered over the North Pole and extended towards the North Atlantic, suggesting a vertical stratosphere–troposphere connection (Fig. 4b). Butler et al. (2020) described that strongly positive stratospheric polar-cap geopotential anomalies or the negative phase of the Northern Annular Mode (NAM) index were observed from the end of December until mid-January 2019 along with North Atlantic blocking. A possible link between this blocking and the SPV configuration in January 2019 is also suggested by Yessimbet et al. (2022b). Similarly, the 2009–2018 SSW events also featured Euro-Atlantic blocking shortly after the SPV split (Figs. A4e–f, A6e–f, A8e–f, A10e–f, and A12e–f), and the geopotential-height configuration resembled a negative AO pattern (Figs. A3b, A5b, A7b, A9b, and A11b).

A closer look at the EP flux during the first week of the recovery phase of the 2019 SSW reveals a continuous upward direction of wave propagation from the troposphere to the stratosphere, as shown in Fig. 4c and d. The large EP flux convergence zone in the stratosphere in early January led to a deceleration of $\overline{u}$. As the EP flux vectors propagated poleward and upward, the $\overline{u}$ at the pole became easterly and extended downward. To further investigate the relationship between the North Atlantic blocking and the details of wave activity propagation, the 3D Plumb flux evolution and vertically resolved geopotential-height anomalies are shown in Fig. B2. Along with the onset of North Atlantic blocking formation, it can be observed that the wave activity is enhanced outward

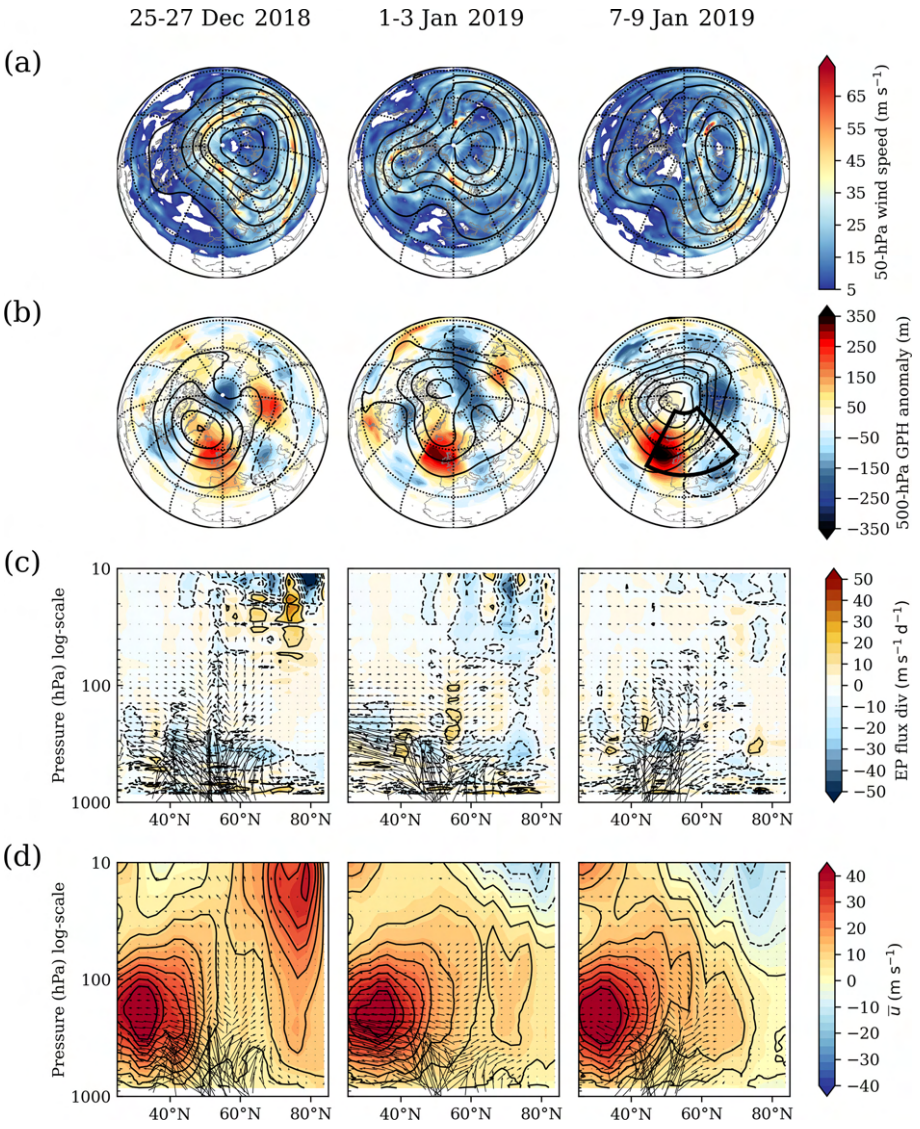


Figure 4. Same as for Fig. 2, but for the 2019 SSW. The 3 d averaged parameters are shown for three dates: during the SPV displacement (left), during the split (center), and after the SPV split (right). The black box indicates the selected Euro-Atlantic blocking region.

from the positive geopotential-height anomalies centered between 50 and 0° W. This suggests that wave packets originating from the North Atlantic block propagate into the stratosphere, thereby contributing to vortex weakening and further SSW development. Overall, the continuous upward propagation of the wave activity (shown by EP flux) into the stratosphere and a deep downward descent of a reversed $\overline{u}$ from the stratosphere into the troposphere during the SSW recovery are also typical for the 2009–2018 events (Figs. A3c–d, A5c–d, A7c–d, A9c–d, and A11c–d).

The characteristics of the SSW events that occurred between 2009 and 2019 align with the description of absorbing SSW events as outlined by Kodera et al. (2016). On this basis, we classify the SSW events from 2009 to 2019 as absorbing.

4.3 Time–height view of the wave activity for 2007–2019 SSW events

Figure 6 displays the time–height evolution of the F_p anomaly averaged over 45–75° N along with the blocking index within a ±30 d timeframe relative to each of the SSW events between 2007 and 2019.

Before each SSW, there was a pronounced increase in wave activity (indicated by blue shading) in the stratosphere, often extending below 100 hPa. In almost all events, an increase in stratospheric wave activity was preceded by an increase in tropospheric wave activity by several days, indicating upward wave activity propagation. The exception was the 2007 event, during which the stratospheric enhancement occurred without a strong signal of tropospheric wave activity

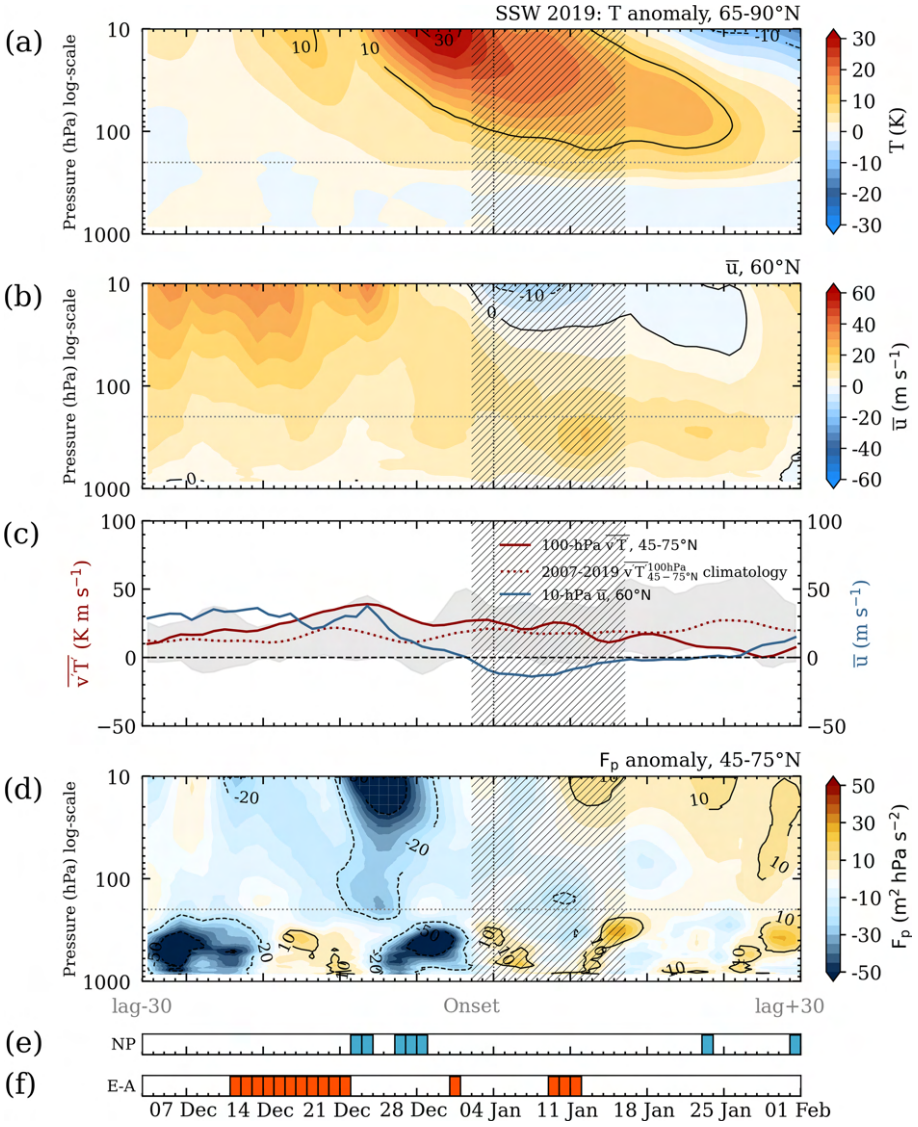


Figure 5. Same as for Fig. 3, but for the 2019 SSW. The time interval is shown for ±30 d from the central date (2 January).

enhancement preceding it. However, approximately 20 d before that, another notable intensification of wave activity was initially observed in the troposphere and then in the stratosphere above 70 hPa, which suggests the preconditioning of the SPV.

Comparing all individual events, the upward wave propagation signals associated with SSW were less pronounced and shorter in 2007 and 2008, as was the duration of the $\overline{u}$ reversal in these years. In the other six events, the wave activity propagation signals prior to $\overline{u}$ reversal were more pronounced and longer.

The strongest signal of increased wave activity shortly before the SPV split was observed in 2009. For 2010, 2013, and 2019, there was an increase in F_p in the 2 weeks prior to $\overline{u}$ reversal, coinciding with the SPV displacement. At the end of January and beginning of February 2016, there was an intensification of the F_p, which occurred during a minor SSW event reported by Dörnbrack et al. (2018). In 2018, there were three episodes of F_p enhancement, each separated by an interval of about 2 weeks before the split of the SPV. The first enhancement was continuous throughout the atmospheric column, with a few days lag between the tropospheric and stratospheric anomalies. The second enhancement was observed in the troposphere and then in the stratosphere above 100 hPa, with no vertical continuity between the two regions. These two signals were not sufficient to weaken the vortex and trigger an SSW event. The third F_p anomaly intensification signal was the strongest, with clear signs of upward wave propagation before the SPV split. Interestingly, a closer look at the 2018 SSW event (Fig. A12) reveals that only vertically continuous signals (marked by 100 hPa $\overline{v'T'}$ peaks) coincide with $\overline{u}$ weakening. The same is true for all

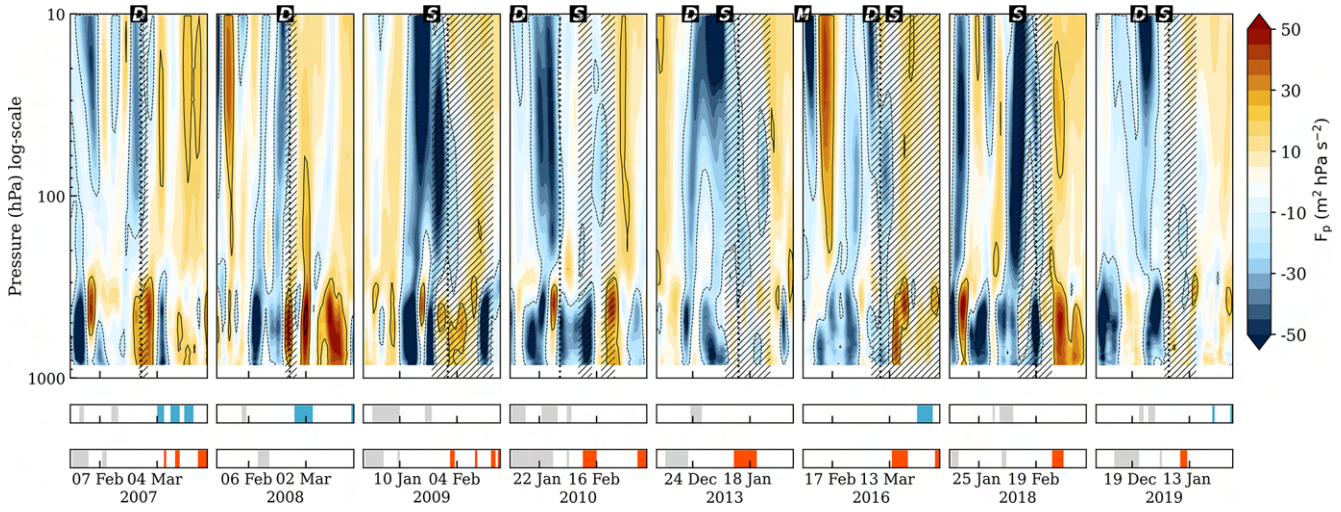


Figure 6. Time–height evolution of the anomaly of the vertical component of the Eliassen–Palm flux (45–75° N) within a ±30 d timeframe relative to each of the SSW events from 2007 to 2019. Hatched regions indicate dates when the zonal-mean zonal wind at 60° N and 10 hPa is negative, and the vertical dotted lines indicate the start of the SSW recovery phase. The letters "D" and "S" indicate the approximate start of the SPV displacement and split, respectively. The letter "M" indicates a minor SSW event. The lower panels show the blocking index for the North Pacific (blue) and the blocking index for the Euro-Atlantic region (orange). The blocking events before the SSWs are greyed out.

other SSW events, which may indicate that the propagation or amplification of wave activity in the lower stratosphere (around 100 hPa) is more important for the weakening of SPV than its amplification in the middle and upper stratosphere.

Regarding the blocking events, in both the 2007 and 2008 events, the North Pacific blocking became apparent shortly after the $\overline{u}$ recovery. For the other SSW events, we find that the Euro-Atlantic blocking is observed immediately after the onset of the SSW recovery and during and after (for the 2018 event) the reversal of $\overline{u}$.

To better understand the differences between the SSW events, we also analyzed the evolution of the zonally averaged polar (75–90° N) static-stability anomalies (Fig. 7). In the 2009–2019 SSW events, an increase in the static-stability anomaly near 300 hPa can be observed as $\overline{u}$ reverses. This static-stability enhancement indicates a strengthening of the tropopause inversion layer (TIL) in the polar region in the aftermath of SSWs. This observation confirms the findings of Grise et al. (2010), who demonstrated that the magnitude of the TIL is enhanced following SSWs. Also, the case studies of Wargan and Coy (2016) (using reanalyses) and Wang et al. (2016) (using Formosat-3/COSMIC RO measurements) described an enhancement of the static stability in the vicinity of the polar tropopause following the 2009 SSW event.

In our observations, the 2009 and 2013 SSW events had the strongest enhancement of the polar TIL magnitude. We also note the decreasing enhancement of the static stability from the stratosphere to the tropopause level during the onset of the SSWs, which is observed in the static-stability anomalies for the 2009, 2016, 2018, and 2019 SSWs and in its absolute value for all SSWs (Fig. S4a). This shows that the absorbing SSW events in 2009–2019 had stronger and more prolonged impacts (in terms of thermal heating) on the UTLS and the enhancement of the polar TIL than the reflecting events in 2007 and 2008 did. For the reflecting events, the magnitude of TIL enhancement is much weaker compared to the absorbing events. In 2008, the enhancement of the static-stability anomaly occurred in late March during the final $\overline{u}$ reversal.

5 Discussion and conclusions

The main objective of this study was to characterize the synoptic and dynamic conditions of SSWs and to investigate the link to blocking events from an observational perspective. We used GNSS RO observations for these analyses as the dataset resolves the relevant features to provide information on the stratosphere–troposphere coupling.

Within the timeframe of available RO data spanning from 2007 to 2019, we examined a total of eight major SSW events, including a final SSW event in 2016. To characterize SSWs, we analyzed RO temperature and geopotential-height profiles on isobaric surfaces, which also served as a basis for deriving daily geostrophic winds and quasi-geostrophic EP fluxes. We also computed the blocking index to assess blocking events.

The results showed that the RO data resolve all the main dynamic features of SSWs and troposphere–stratosphere coupling phenomena reasonably well. While the geostrophic-wind speed near the upper-tropospheric subtropical jet and at the SPV level may be slightly underestimated,

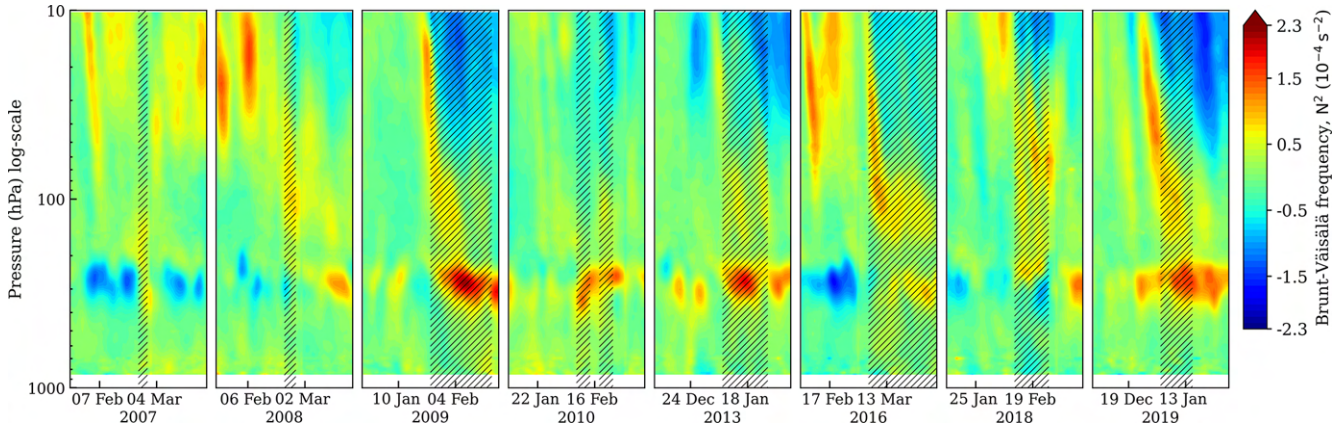


Figure 7. Time–height evolution of the anomalous static stability or the Brunt–Väisälä frequency, N^2 (75–90° N), within a ±30 d timeframe relative to each of the SSW events from 2007 to 2019. Hatched regions indicate dates when the zonal-mean zonal wind at 60° N and 10 hPa is negative.

as noted by Scherllin-Pirscher et al. (2014), our study showed that the SPV evolution is well captured. Analyzing the evolution of the SPV, we classified the SSW events into distinct categories – specifically, displacement, split, and mixed-type events. The 2007 and 2008 SSW events were identified as displacement events, while the 2009 and 2018 events were classified as split events and the 2010, 2013, 2016, and 2019 as mixed-type events. A case in point is the 2019 SSW event, which agrees with the findings of Lee and Butler (2020).

Furthermore, our study shows that the key patterns of quasi-geostrophic EP fluxes are well captured and consistent with established theory and the existing literature. Building on the analysis of EP flux evolution, we have classified the SSW events into two categories: reflecting and absorbing events. Thus, the 2007 and 2008 SSW events were categorized as reflecting and the remaining events between 2009 and 2019 as absorbing. For the reflecting SSWs, our observations revealed a short duration of the $\overline{u}$ reversal and a concurrent downward propagation of EP flux during the initial week of the SSW recovery phase. The analysis of the 3D Plumb flux showed that the downward-propagating wave packets induced a trough over eastern Canada and North America and the formation of a ridge over the North Pacific, leading to the onset of North Pacific blocking. On the other hand, absorbing SSW events exhibited a more prolonged $\overline{u}$ reversal and upward propagation of the EP flux. During the recovery phase, these events were accompanied by the formation of blocking in the Euro-Atlantic region and a geopotential-height configuration resembling a negative AO pattern. Enhanced wave activity originating from the North Atlantic blocking was observed to propagate into the stratosphere, thereby potentially contributing to vortex weakening and further SSW development.

These observations agree with the findings of Perlwitz and Harnik (2004), who suggested that there are two types of stratospheric winter conditions, reflective and non-reflective, which are characterized by different downward dynamic interactions similar to those observed in our study.

Although the reflecting events of 2007 and 2008 were also classified as displacement events and the absorbing events of 2009–2019 as split and mixed events, the relatively limited number of SSW events studied does not allow statistical conclusions to be drawn concerning the consistent alignment of these two classification types. As highlighted in the Introduction, these classifications are rooted in distinct phases of an SSW. The classification based on the polar-vortex geometry is for the mature phase, whereas the classification based on the propagation of planetary-wave activity is for the recovery phase of SSWs.

Nevertheless, we show that reflecting and absorbing SSW events differ in the magnitude of the downward impact (manifested, e.g., in the TIL variability, downward propagation of the easterly wind, and temperature anomalies) and correspond to specific divergent tropospheric responses. Reflecting events connected to vortex displacement are observed to trigger downward wave propagation that induces blocking over the North Pacific region, while absorbing events connected to vortex splitting are associated with blocking over the North Atlantic and upward wave propagation. The magnitude of the downward impact may be one of the factors to consider when addressing the open question of whether displacement or split events trigger different responses in the tropospheric circulation.

Concerning the vertical structure of the quasi-geostrophic EP flux, we observed a consistent pattern of an enhanced upward EP flux (F_p) preceding the $\overline{u}$ reversal in each SSW event. We also observed evidence of upward propagation of wave activity as, prior to each SSW, F_p intensified in the troposphere before intensifying in the stratosphere. This aligns with the hypothesis that an increase in stratospheric wave activity is typically preceded by a burst of wave activity within the troposphere (Polvani and Waugh, 2004). Interestingly,

this contradicts the results of Jucker (2016), who, based on an idealized general circulation model (GCM), did not observe any tropospheric enhancement of wave activity propagating into the stratosphere prior to SSWs. It is worth emphasizing that the peak in wave activity amplification exhibited distinct temporal characteristics for reflecting and absorbing SSW events. Specifically, the amplification peak was shorter for reflecting SSWs than for absorbing events. This suggests the relevance of considering the timescales associated with wave activity pulses. This aspect agrees with the finding of Sjoberg and Birner (2012), who suggested that longer-duration wave activity pulses are more effective at generating SSWs than shorter yet stronger pulses.

In addition, the analysis of polar static-stability anomalies showed that the SSWs are followed by an enhanced polar TIL, which was strongest for the 2009 and 2013 SSW events and weakest for the 2007 and 2008 events. This indicates that the strength of the TIL is influenced by the magnitude of the SSW and its downward impact. Given that TIL enhancement can further influence stratosphere–troposphere coupling and tropospheric circulation, this further emphasizes the distinction between SSW events and their downward influences.

In conclusion, our findings underscore the applicability of GNSS RO for the exploration of atmospheric circulation dynamics. Due to its high vertical resolution, GNSS RO has the potential to study the interplay between tropopause structure and wave activity propagation. A detailed study of the relationship between tropopause structure and wave activity propagation that is relevant to SSW events should be performed in future GNSS RO studies.

Appendix A: SSWs in 2007, 2009, 2010, 2013, 2016, and 2018

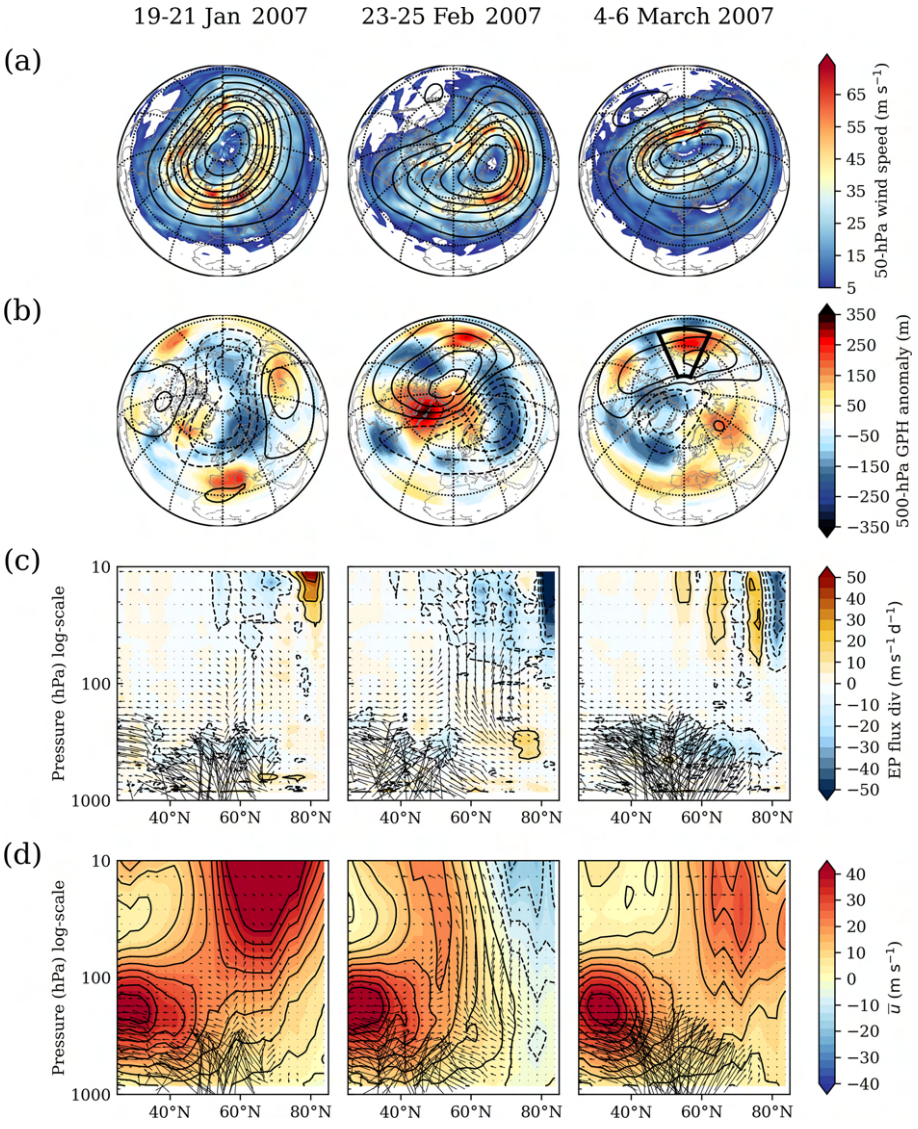


Figure A1. Evolution of the 2007 SSW, as shown by the results for three dates: before the SPV displacement (left), during its displacement (center), and during its recovery (right). **(a)** 50 hPa wind speed (shading) and 50 hPa geopotential height (contours). **(b)** 500 hPa geopotential-height anomaly (shading) and 50 hPa geopotential-height anomaly (contours). The black box indicates the selected North Pacific blocking region. **(c)** Meridional cross-sections of Eliassen–Palm flux vectors and divergence (shading). **(d)** Meridional cross-sections of Eliassen–Palm flux vectors and zonal wind (shading). The vectors are plotted for every fifth pressure level.

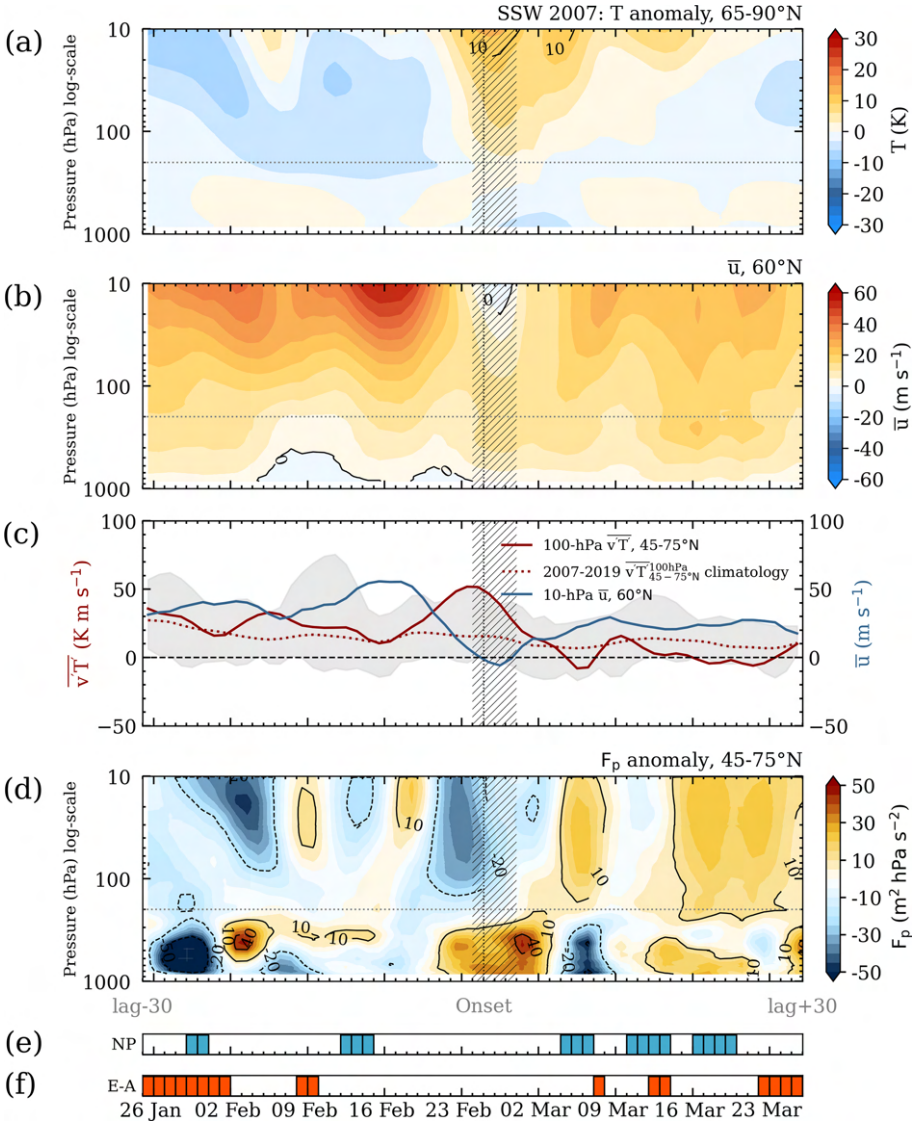


Figure A2. Time–height evolution of **(a)** the area-weighted temperature anomaly averaged over 65–90° N, **(b)** the zonal wind at 60° N, and **(c)** the 100 hPa eddy meridional heat flux averaged over 45–75° N (solid red line), its daily climatology (dotted red line), and the zonal-mean zonal wind at 60° N and 10 hPa (solid blue line). Grey shading covers the region between the daily minimum and maximum of the heat flux for the period 2007–2019. Time–height evolution of **(d)** the anomaly of the vertical component of the Eliassen–Palm flux averaged over 45–75° N, **(e)** the blocking index for the North Pacific region, and **(f)** the blocking index for the Euro-Atlantic region. The hatched region indicates dates when the zonal-mean zonal wind at 60° N and 10 hPa is negative, and the vertical dotted line indicates the day when the polar (80–90° N) temperature anomaly reaches its maximum, i.e., the start of the SSW recovery phase. The dotted horizontal line indicates 200 hPa (the approximate level of the extratropical tropopause). The time interval shown is ±30 d from the central date (24 February) of the 2007 SSW.

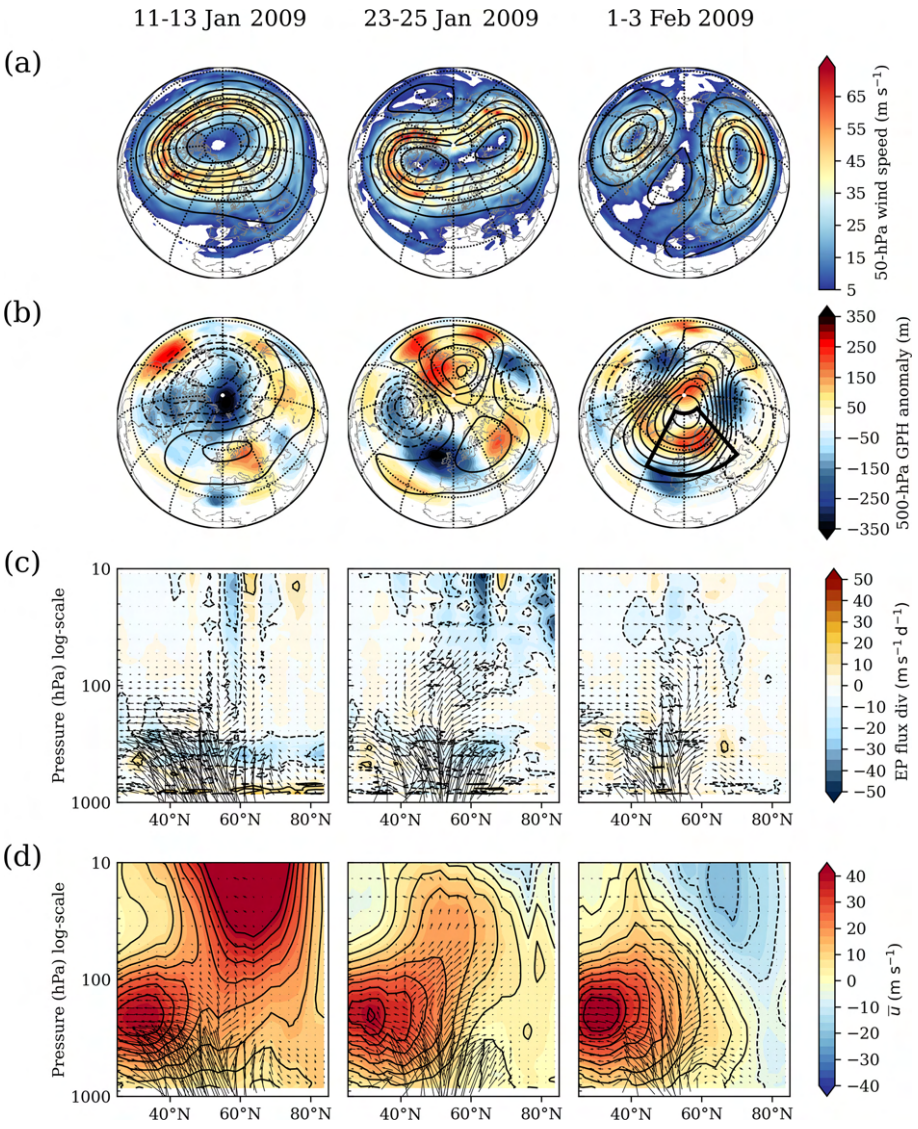


Figure A3. Same as Fig. A1 but for the 2009 SSW. The 3 d averaged parameters are shown for three dates: before the SPV split (left), during the split (center), and after the split (right). The black box indicates the selected Euro-Atlantic blocking region.

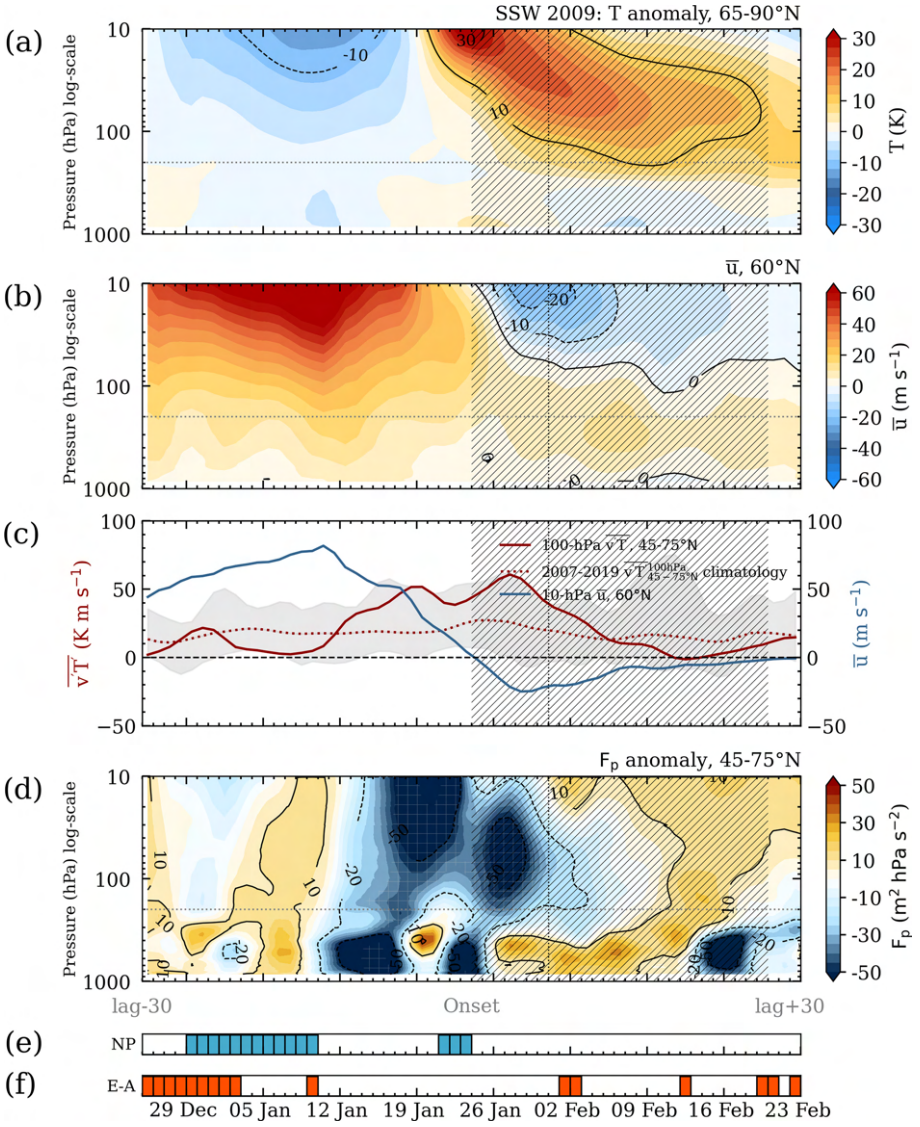


Figure A4. Same as Fig. A2 but for the 2009 SSW. The time interval shown is ±30 d from the central date (24 January).

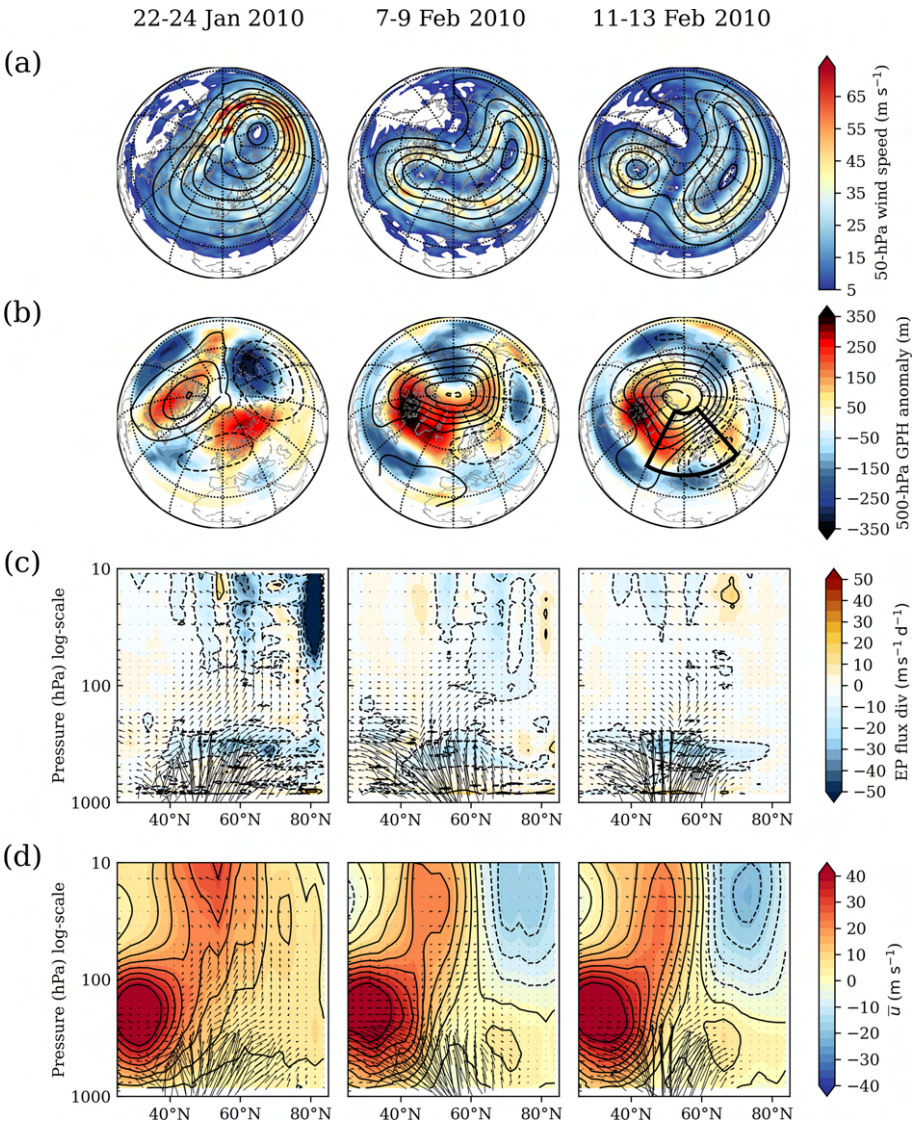


Figure A5. Same as Fig. A1 but for the 2010 SSW. The 3 d averaged parameters are shown for three dates: during the SPV displacement (left), during the split (center), and after the split (right). The black box indicates the defined Euro-Atlantic blocking region.

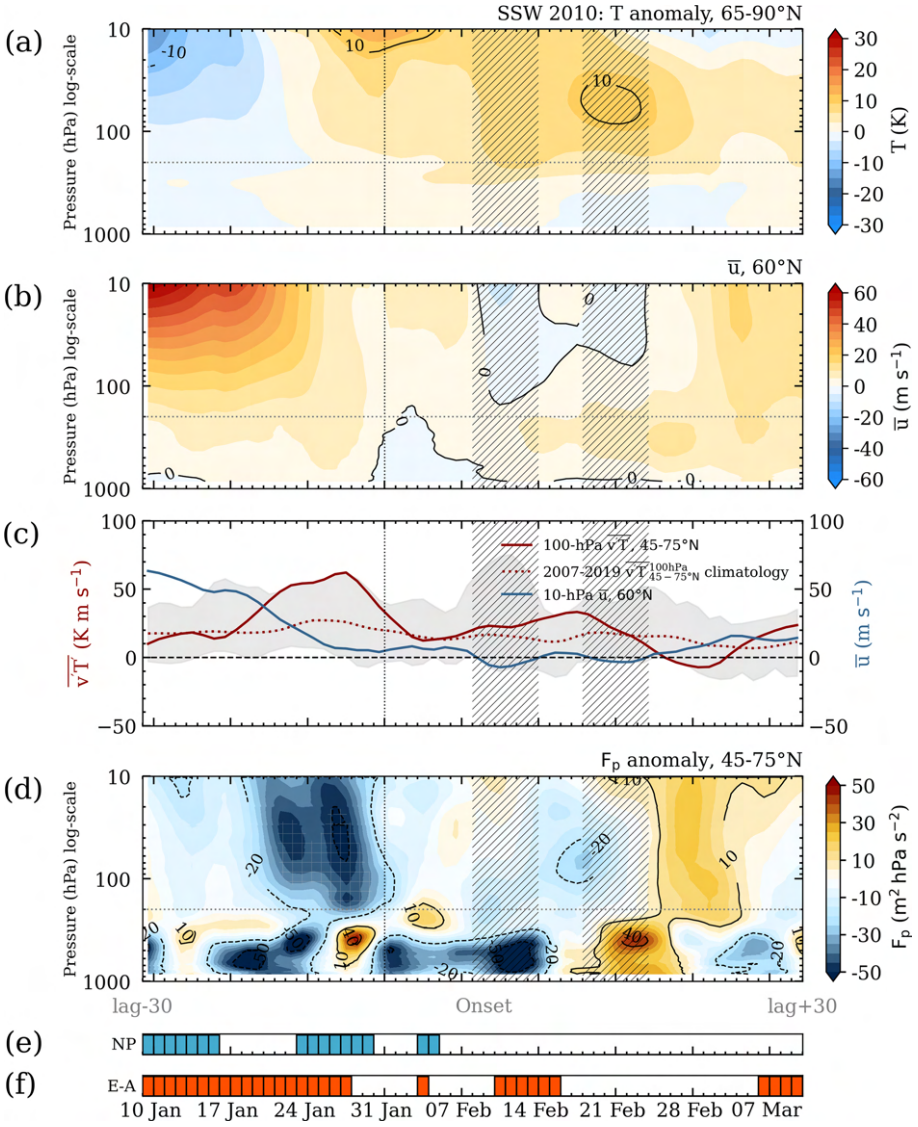


Figure A6. Same as Fig. A2 but for the 2010 SSW. The time interval shown is ±30 d from the central date (8 February).

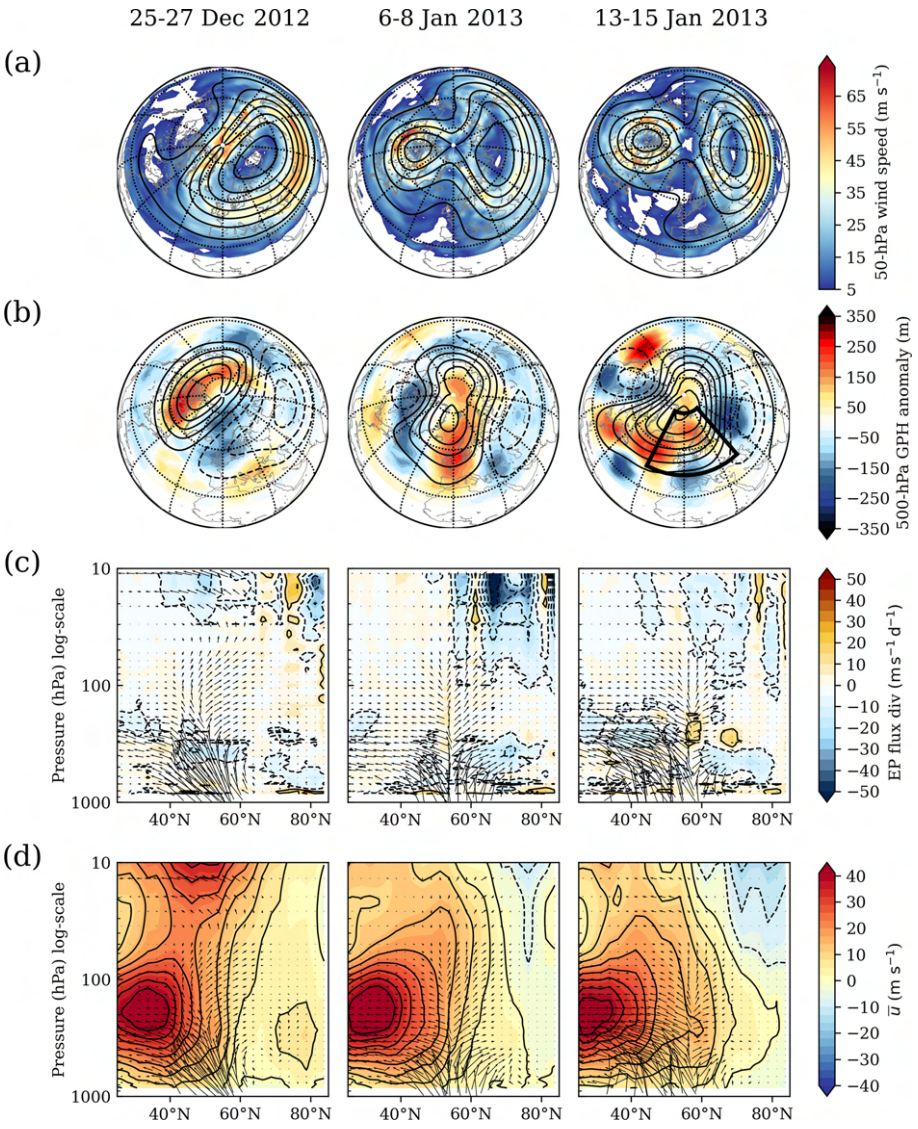


Figure A7. Same as Fig. A1 but for the 2013 SSW. The 3 d averaged parameters are shown for three dates: during the SPV displacement (left), during the split (center), and after the split (right). The black box indicates the defined Euro-Atlantic blocking region.

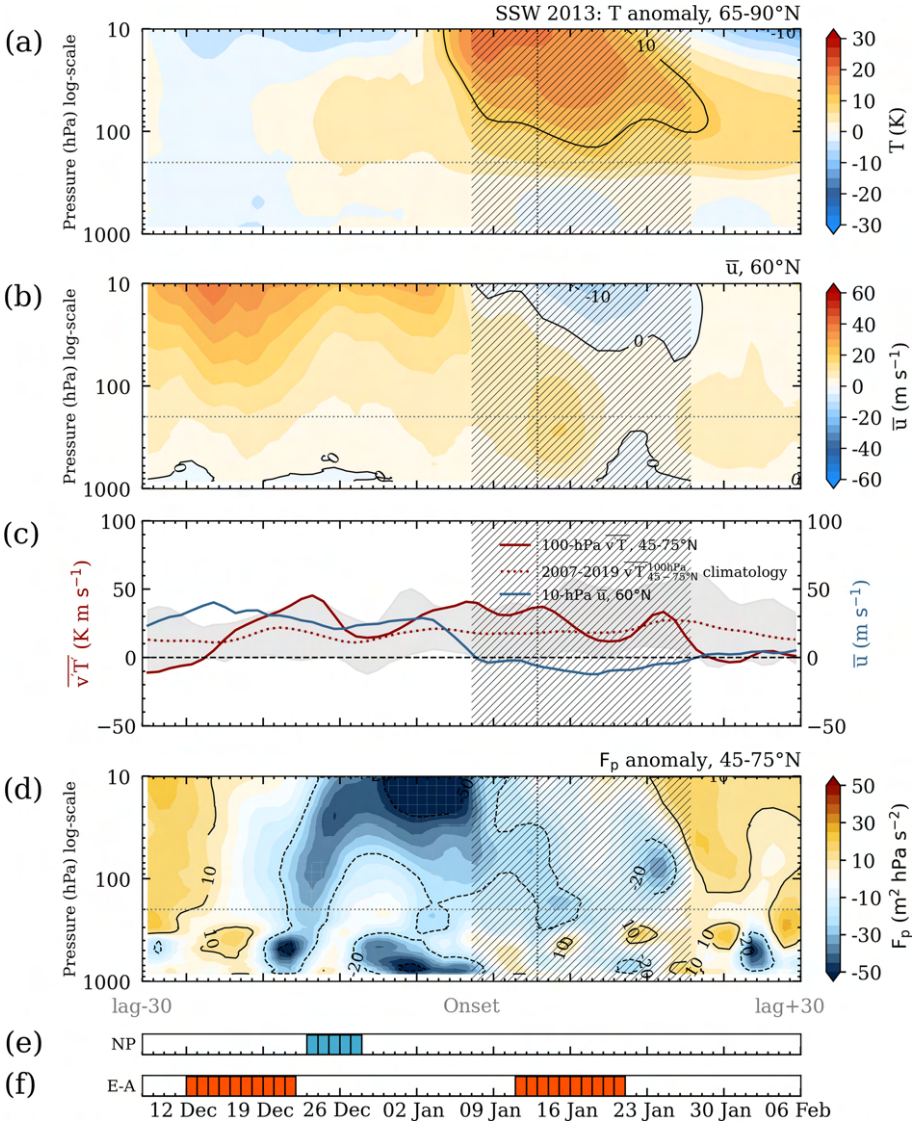


Figure A8. Same as Fig. A2 but for the 2013 SSW. The time interval shown is ±30 d from the central date (7 January).

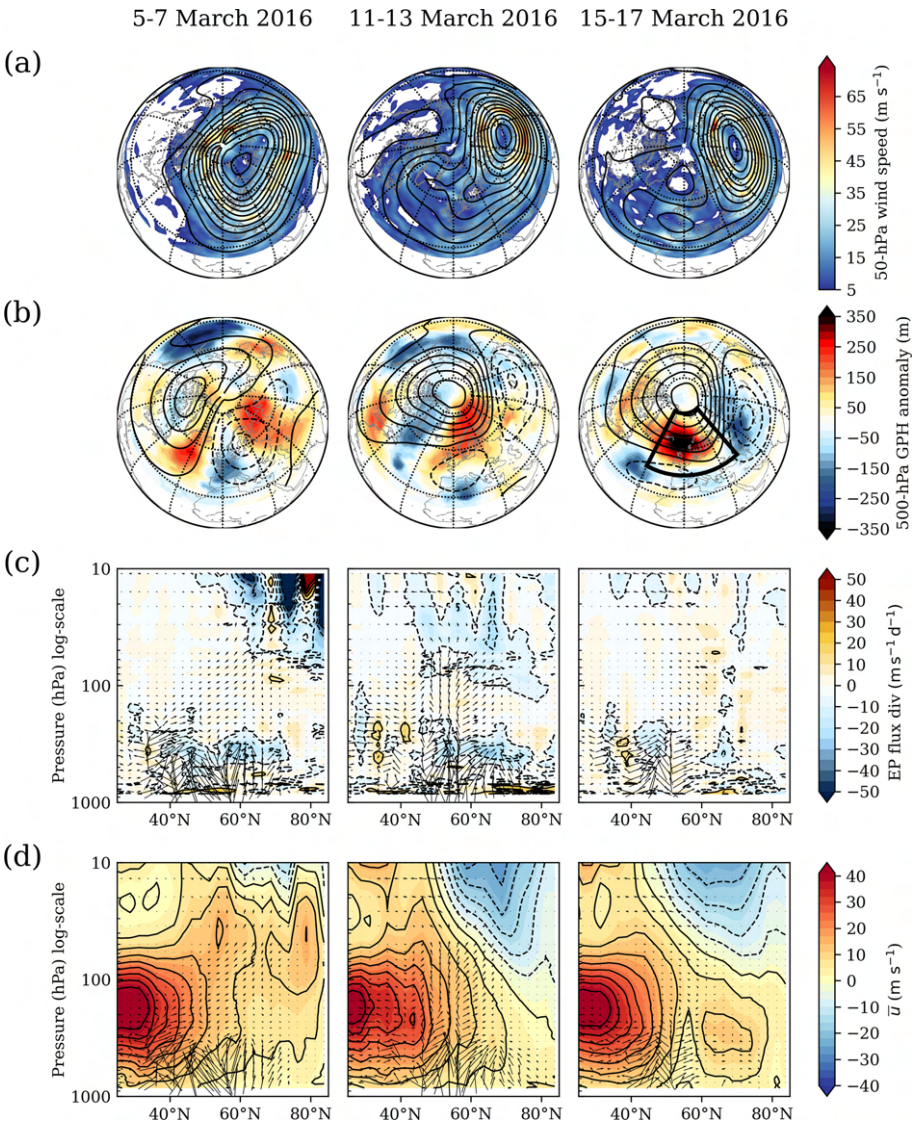


Figure A9. Same as Fig. A1 but for the 2016 SSW. The 3 d averaged parameters are shown for three dates: during the SPV displacement (left), during the split (center), and after the split (right). The black box indicates the defined Euro-Atlantic blocking region.

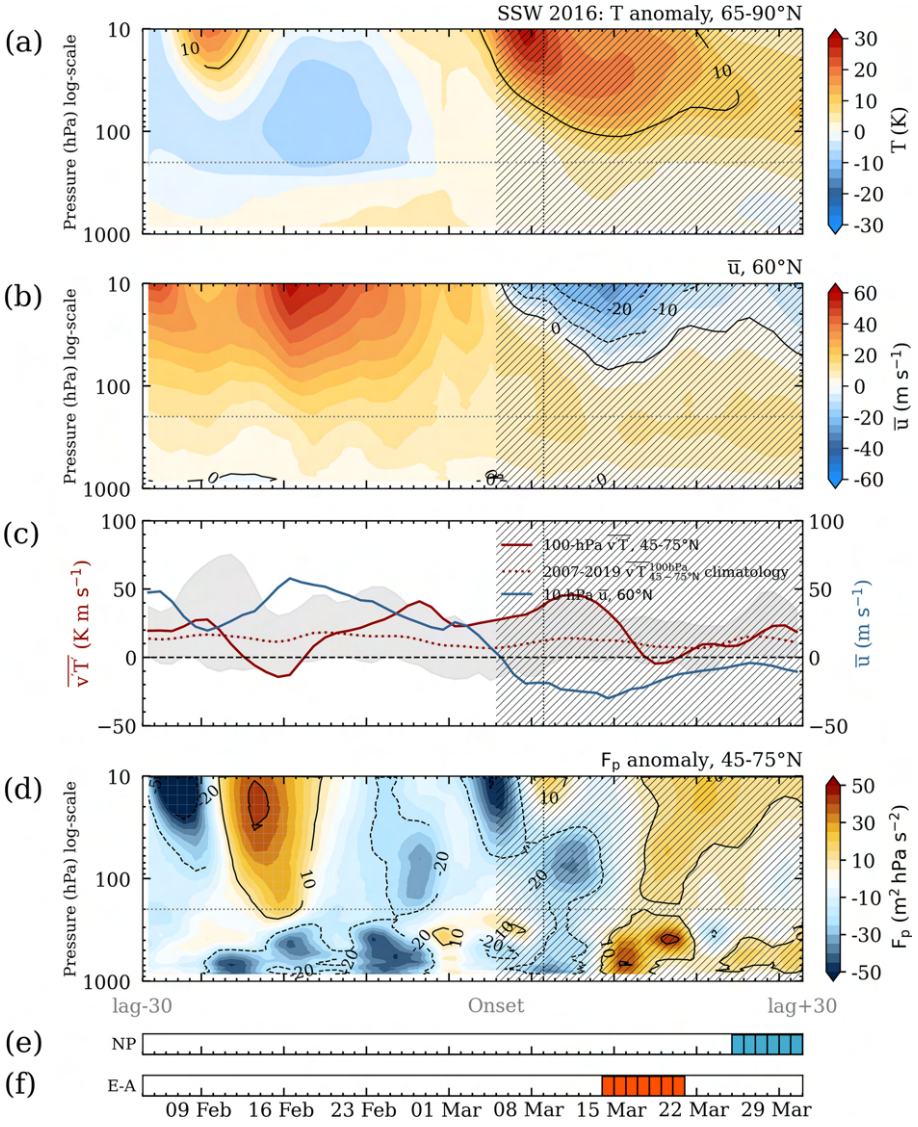


Figure A10. Same as Fig. A2 but for the 2016 SSW. The time interval shown is ±30 d from the central date (5 March).

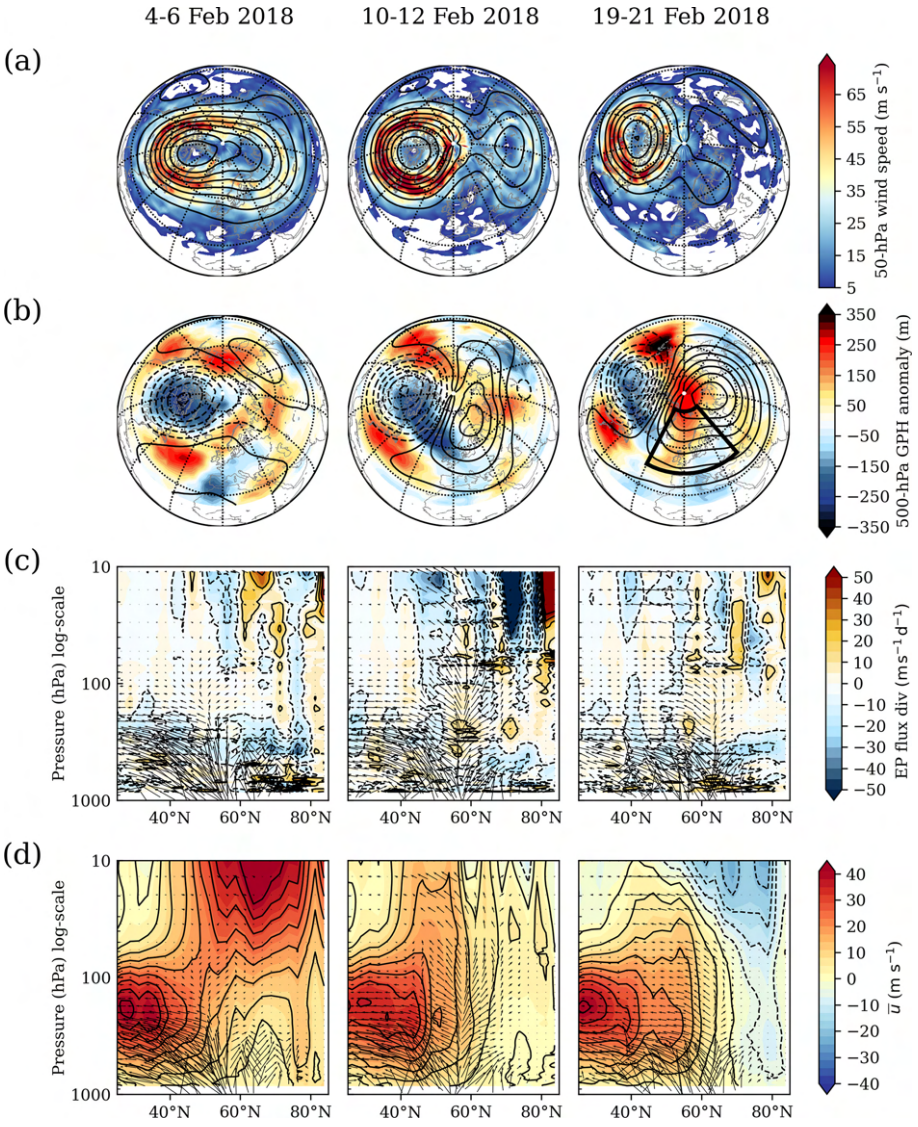


Figure A11. Same as Fig. A1 but for the 2018 SSW. The 3 d averaged parameters are shown for three dates: before the SPV split (left), during the split (center), and after the split (right). The black box indicates the defined Euro-Atlantic blocking region.

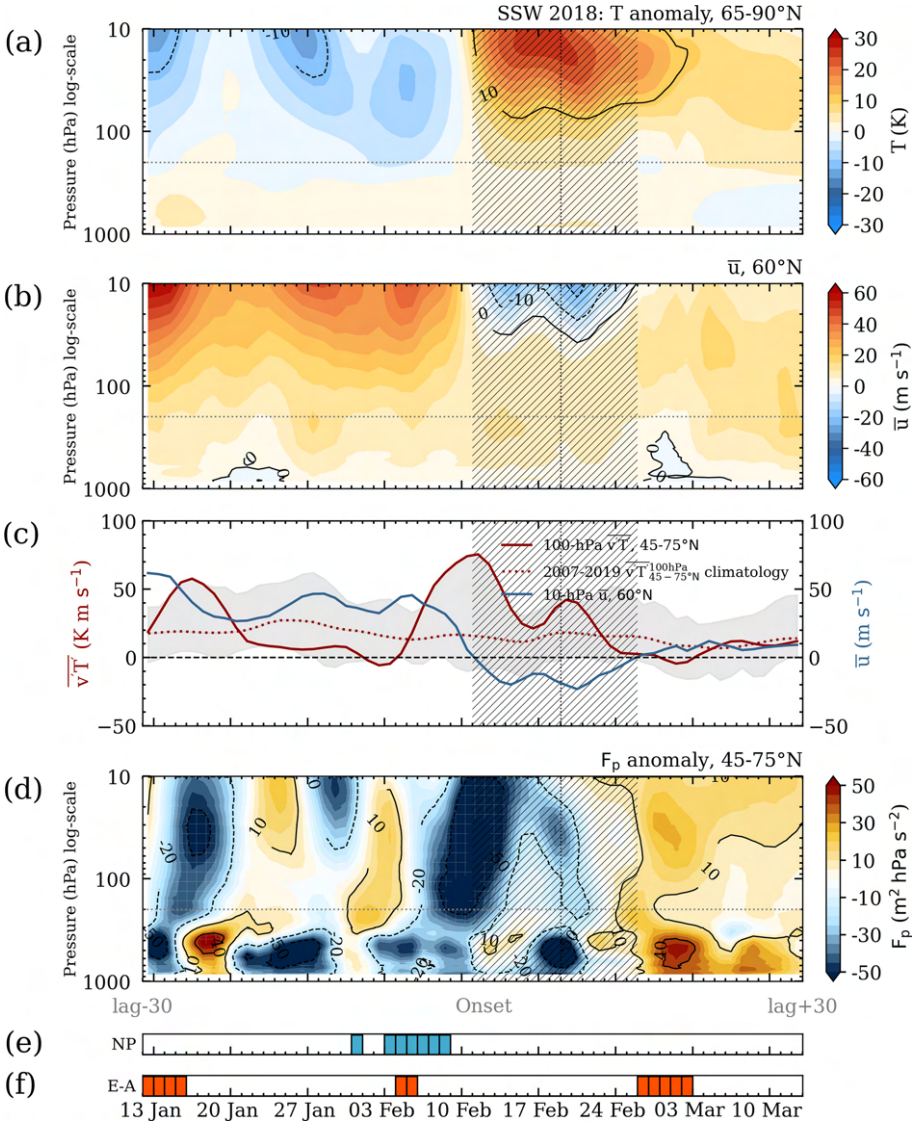


Figure A12. Same as Fig. A2 but for the 2018 SSW. The time interval shown is ±30 d from the central date (11 February).

Appendix B: Plumb flux

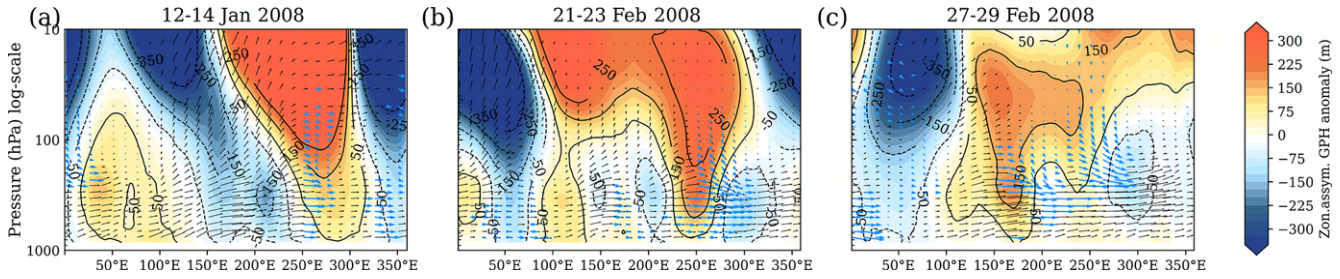


Figure B1. Evolution of the vertical and zonal components of the 3D Plumb flux (arrows) for the 2008 SSW before the SPV displacement (12–14 January), during its displacement (21–23 February), and during its recovery (27–29 February). The vectors are plotted for every fifth longitude and pressure level. Blue vectors denote where the vertical component of the Plumb flux is negative. Shading indicates the zonally asymmetric component of the geopotential-height anomaly.

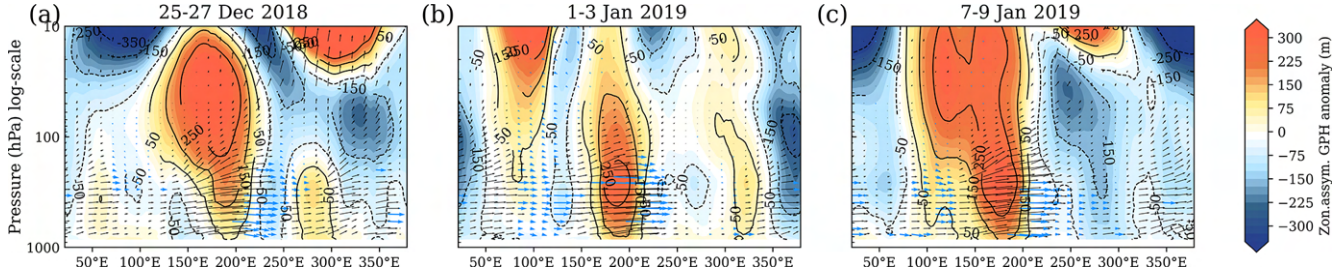


Figure B2. Evolution of the vertical and zonal components of the 3D Plumb flux (arrows) for the 2019 SSW during the SPV displacement (25–27 December 2018), during its split (1–3 January), and after the split (7–9 January). The vectors are plotted for every fifth longitude and pressure level. Blue vectors denote where the vertical component of the Plumb flux is negative. Shading indicates the anomaly of the zonally asymmetric component of the geopotential height.

Data availability. The Wegener Center (WEGC) GNSS RO record OPSv5.6 profiles are available at https://doi.org/10.25364/WEGC/OPS5.6:2020.1 (EOPAC Team, 2020).

Supplement. The supplement related to this article is available online at: https://doi.org/10.5194/acp-24-10893-2024-supplement.

Author contributions. KY contributed to the development of the theory, performed the computational implementation and data analysis, produced all figures, and wrote the first draft of the paper. AKS provided the initial design for this study. FL provided the gridded RO dataset. All authors contributed to the design of the study and figures, the discussion of the results, and the revision of the text. AKS, FL, and AO provided guidance and advice on all aspects of the study.

Competing interests. The contact author has declared that none of the authors has any competing interests.

Disclaimer. Publisher's note: Copernicus Publications remains neutral with regard to jurisdictional claims made in the text, published maps, institutional affiliations, or any other geographical representation in this paper. While Copernicus Publications makes every effort to include appropriate place names, the final responsibility lies with the authors. For the purpose of open access, the author has applied a CC BY public copyright license to any author-accepted manuscript version arising from this submission.

Acknowledgements. We thank the WEGC EOPAC team for providing the OPSv5.6 data profiles. We are grateful to Barbara Scherllin-Pirscher and Lukas Brunner for providing the software used in our study to estimate the geostrophic winds and blocking indices, respectively.

Financial support. This work was funded by the Austrian Science Fund (FWF) under research grant (grant no. W1256) (the doctoral program Climate Change: Uncertainties, Thresholds and Coping Strategies). The authors also acknowledge financial support by the University of Graz.

Review statement. This paper was edited by Peter Haynes and reviewed by three anonymous referees.

References

Angerer, B., Ladstädter, F., Scherllin-Pirscher, B., Schwärz, M., Steiner, A. K., Foelsche, U., and Kirchengast, G.: Quality aspects of the Wegener Center multi-satellite GPS radio occultation record OPSv5.6, Atmos. Meas. Tech., 10, 4845–4863, https://doi.org/10.5194/amt-10-4845-2017, 2017.

Anthes, R. A.: Exploring Earth's atmosphere with radio occultation: contributions to weather, climate and space weather, Atmos. Meas. Tech., 4, 1077–1103, https://doi.org/10.5194/amt-4-1077-2011, 2011.

Baldwin, M. P. and Dunkerton, T. J.: Propagation of the Arctic Oscillation from the stratosphere to the troposphere, J. Geophys. Res., 104, 30937–30946, https://doi.org/10.1029/1999JD900445, 1999.

Baldwin, M. P. and Dunkerton, T. J.: Stratospheric Harbingers of Anomalous Weather Regimes, Science, 294, 581–584, https://doi.org/10.1126/science.1063315, 2001.

Beyerle, G., Schmidt, T., Michalak, G., Heise, S., Wickert, J., and Reigber, C.: GPS radio occultation with GRACE: Atmospheric profiling utilizing the zero difference technique, Geophys. Res. Lett., 32, L13806, https://doi.org/10.1029/2005GL023109, 2005.

Brunner, L.: A new perspective on atmospheric blocking from observations – Detection, analysis, and impacts, PhD thesis, Wegener Center Verlag, Scientific Report No. 76-2018, 2018.

Brunner, L. and Steiner, A. K.: A global perspective on atmospheric blocking using GPS radio occultation – one decade of observations, Atmos. Meas. Tech., 10, 4727–4745, https://doi.org/10.5194/amt-10-4727-2017, 2017.

Brunner, L., Steiner, A. K., Scherllin-Pirscher, B., and Jury, M. W.: Exploring atmospheric blocking with GPS radio occultation observations, Atmos. Chem. Phys., 16, 4593–4604, https://doi.org/10.5194/acp-16-4593-2016, 2016.

Butler, A. H., Sjoberg, J. P., Seidel, D. J., and Rosenlof, K. H.: A sudden stratospheric warming compendium, Earth Syst. Sci. Data, 9, 63–76, https://doi.org/10.5194/essd-9-63-2017, 2017.

Butler, A. H., Lawrence, Z. D., Lee, S. H., Lillo, S. P., and Long, C. S.: Differences between the 2018 and 2019 stratospheric polar vortex split events, Q. J. Roy. Meteor. Soc., 146, 3503–3521, https://doi.org/10.1002/qj.3858, 2020.

Dörnbrack, A., Gisinger, S., Kaifler, N., Portele, T. C., Bramberger, M., Rapp, M., Gerding, M., Faber, J., Žagar, N., and Jelić, D.: Gravity waves excited during a minor sudden stratospheric warming, Atmos. Chem. Phys., 18, 12915–12931, https://doi.org/10.5194/acp-18-12915-2018, 2018.

Edmon Jr., H. J., Hoskins, B. J., and McIntyre, M. E.: Eliassen–Palm cross sections for the troposphere, J. Atmos. Sci., 37, 2600–2616, https://doi.org/10.1175/1520-0469(1980)037<2600:EPCSFT>2.0.CO;2, 1980.

EOPAC Team: GNSS Radio Occultation Record (OPS 5.6 2001–2019), Wegener Center Data Record, University of Graz, Austria [data set], https://doi.org/10.25364/WEGC/OPS5.6:2020.1, 2020.

Geller, M. A. and Alpert, J. C.: Planetary Wave Coupling between the Troposphere and the Middle Atmosphere as a Possible Sun-Weather Mechanism, J. Atmos. Sci., 37, 1197–1215, https://doi.org/10.1175/1520-0469(1980)037<1197:PWCBTT>2.0.CO;2, 1980.

Gerber, E. P. and Manzini, E.: The Dynamics and Variability Model Intercomparison Project (DynVarMIP) for CMIP6: assessing the stratosphere–troposphere system, Geosci. Model Dev., 9, 3413–3425, https://doi.org/10.5194/gmd-9-3413-2016, 2016.

Grise, K. M., Thompson, D. W. J., and Birner T.: A Global Survey of Static Stability in the Stratosphere and Upper Troposphere, J. Climate, 23, 2275–2292, https://doi.org/10.1175/2009JCLI3369.1, 2010.

Hajj, G. A., Ao, C. O., Iijima, B. A., Kuang, D., Kursinski, E. R., Mannucci, A. J., Meehan, T. K., Romans, L. J., de la Torre Juarez, M., and Yunck, T. P.: CHAMP and SAC-C atmospheric occultation results and intercomparisons. J. Geophys. Res.-Atmos., 109, D06109, https://doi.org/10.1029/2003JD003909, 2004.

Healy, S. B. and Eyre, J. R.: Retrieving temperature, water vapour and surface pressure information from refractive-index profiles derived by radio occultation: A simulation study, Q. J. Roy. Meteor. Soc., 126, 1661–1683, https://doi.org/10.1002/qj.49712656606, 2000.

Healy, S. B., Polichtchouk, I., and Horányi, A.: Monthly and zonally averaged zonal wind information in the equatorial stratosphere provided by GNSS radio occultation, Q. J. Roy. Meteor. Soc., 146, 3612–3621, https://doi.org/10.1002/qj.3870, 2020.

Hines, C. O.: A Possible Mechanism for the Production of Sun-Weather Correlations, J. Atmos. Sci., 31, 589–591, https://doi.org/10.1175/1520-0469(1974)031<0589:APMFTP>2.0.CO;2, 1974.

Jucker, M.: Are Sudden Stratospheric Warmings Generic? Insights from an Idealized GCM, J. Atmos. Sci., 73, 5061–5080, https://doi.org/10.1175/JAS-D-15-0353.1, 2016.

Kodera, K., Mukougawa, H., and Itoh S.: Tropospheric impact of reflected planetary waves from the stratosphere, Geophys. Res. Lett., 35, L16806, https://doi.org/10.1029/2008GL034575, 2008.

Kodera, K., Mukougawa, H., Maury, P., Ueda, M., and Claud, C.: Absorbing and reflecting sudden stratospheric warming events and their relationship with tropospheric circulation, J. Geophys. Res.-Atmos., 121, 80–94, https://doi.org/10.1002/2015JD023359, 2016.

Kursinski, E. R., Hajj, G. A., Hardy, K. R., Romans, L. J., and Schofield, J. T.: Observing tropospheric water vapor by radio occultation using the Global Positioning System, Geophys. Res. Lett., 22, 2365–2368, https://doi.org/10.1029/95GL02127, 1995.

Kursinski, E. R., Hajj, G. A., Bertiger, W. I., Leroy, S. S., Meehan, T. K., Romans, L. J., Schofield, J. T., McCleese, D. J., Melbourne, W. G., Thornton, C. L., Yunck, T. P., Eyre, J. R., and Nagatani, R. N.: Initial Results of Radio Occultation Observations of Earth's Atmosphere Using the Global Positioning System, Science, 271, 1107–1110, 1996.

Lee, S. H. and Butler, A. H.: The 2018–2019 Arctic stratospheric polar vortex, Weather, 75, 52–57, https://doi.org/10.1002/wea.3643, 2020.

Leroy, S. S. and Anderson, J. G.: Estimating Eliassen–Palm flux using COSMIC radio occultation, Geophys. Res. Lett., 34, L10810, https://doi.org/10.1029/2006GL028263, 2007.

Luntama, J.-P., Kirchengast, G., Borsche, M., Foelsche, U., Steiner, A., Healy, S. B., von Engeln, A., O'Clerigh, E., and Marquardt, C.: Prospects of the EPS GRAS mission for operational atmo-

spheric applications, B. Am. Meteorol. Soc., 89, 1863–1875, https://doi.org/10.1175/2008BAMS2399.1, 2008.

Manney, G. L. and Lawrence, Z. D.: The major stratospheric final warming in 2016: dispersal of vortex air and termination of Arctic chemical ozone loss, Atmos. Chem. Phys., 16, 15371–15396, https://doi.org/10.5194/acp-16-15371-2016, 2016.

Matthias, V. and Kretschmer, M.: The influence of stratospheric wave reflection on North American cold spells, Mon. Weather Rev., 148, 1675–1690, https://doi.org/10.1175/MWR-D-19-0339.1, 2020.

Maycock, A. C. and Hitchcock, P.: Do split and displacement sudden stratospheric warmings have different annular mode signatures?, Geophys. Res. Lett., 42, 10943–10951, https://doi.org/10.1002/2015GL066754, 2015.

Messori, G., Kretschmer, M., Lee, S. H., and Wendt, V.: Stratospheric downward wave reflection events modulate North American weather regimes and cold spells, Weather Clim. Dynam., 3, 1215–1236, https://doi.org/10.5194/wcd-3-1215-2022, 2022.

Mitchell, D. M., Gray, L. J., Anstey, J., Baldwin, M. P., and Charlton-Perez, A. J.: The influence of stratospheric vortex displacements and splits on surface climate, J. Climate, 26, 2668–2682,https://doi.org/10.1175/JCLI-D-12-00030.1, 2013.

NOAA CSL: Chemistry & Climate Processes: SSWC, https://csl.noaa.gov/groups/csl8/sswcompendium/majorevents.html, last access: 1 May 2024.

NOAA's Physical Sciences Laboratory: https://psl.noaa.gov/data/epflux/, last access: 30 November 2023.

Perlwitz, J. and Harnik, N.: Observational evidence of a stratospheric influence on the troposphere by planetary wave reflection, J. Climate, 16, 3011–3026, https://doi.org/10.1175/1520-0442(2003)016<3011:OEOASI>2.0.CO;2, 2003.

Perlwitz, J. and Harnik, N.: Downward coupling between the stratosphere and troposphere: The relative roles of wave and zonal mean processes, J. Climate, 17, 4902–4909, https://doi.org/10.1175/JCLI-3247.1, 2004.

Pilch Kedzierski, R., Matthes, K., and Bumke, K.: New insights into Rossby wave packet properties in the extratropical UTLS using GNSS radio occultations, Atmos. Chem. Phys., 20, 11569–11592, https://doi.org/10.5194/acp-20-11569-2020, 2020.

Plumb, R. A.: On the three-dimensional propagation of stationary waves. J. Atmos. Sci., 42, 217–229, https://doi.org/10.1175/1520-0469(1985)042<0217:OTTDPO>2.0.CO;2, 1985.

Polvani, L. M. and Waugh, D. W.: Upward wave activity flux as a precursor to extreme stratospheric events and subsequent anomalous surface weather regimes, J. Climate, 17, 3547–3553, https://doi.org/10.1175/1520-0442(2004)017<3548:UWAFAA>2.0.CO;2, 2004.

Scherllin-Pirscher, B., Steiner, A. K., and Kirchengast, G.: Deriving dynamics from GPS radio occultation: Three-dimensional wind fields for monitoring the climate, Geophys. Res. Lett., 41, 7367–7374, https://doi.org/10.1002/2014GL061524, 2014.

Scherllin-Pirscher, B., Steiner, A. K., Kirchengast, G., Schwärz, M., and Leroy, S. S.: The power of vertical geolocation of atmospheric profiles from GNSS radio occultation, J. Geophys. Res.-Atmos., 122, 1595–1616, https://doi.org/10.1002/2016JD025902, 2017.

Shaw, T. A., Perlwitz J., and Harnik, N.: Downward wave coupling between the stratosphere and troposphere: The importance of meridional wave guiding and comparison with zonal-mean coupling, J. Climate, 23, 6365–6381, https://doi.org/10.1175/2010JCLI3804.1, 2010.

Sjoberg, J. P. and Birner, T.: Transient Tropospheric Forcing of Sudden Stratospheric Warmings, J. Atmos. Sci., 69, 3420–3432, https://doi.org/10.1175/jas-d-11-0195.1, 2012.

Steiner, A. K., Lackner, B. C., Ladstädter, F., Scherllin-Pirscher, B., Foelsche, U., and Kirchengast, G.; GPS radio occultation for climate monitoring and change detection, Radio Sci., 46, RS0D24, https://doi.org/10.1029/2010RS004614, 2011.

Steiner, A. K., Ladstädter, F., Ao, C. O., Gleisner, H., Ho, S.-P., Hunt, D., Schmidt, T., Foelsche, U., Kirchengast, G., Kuo, Y.-H., Lauritsen, K. B., Mannucci, A. J., Nielsen, J. K., Schreiner, W., Schwärz, M., Sokolovskiy, S., Syndergaard, S., and Wickert, J.: Consistency and structural uncertainty of multi-mission GPS radio occultation records, Atmos. Meas. Tech., 13, 2547–2575, https://doi.org/10.5194/amt-13-2547-2020, 2020.

Verkhoglyadova, O. P., Leroy, S. S., and Ao, C.O.: Estimation of winds from GPS radio occultations, J. Atmos. Ocean. Technol., 31, 2451–2461, https://doi.org/10.1175/JTECH-D-14-00061.1, 2014.

Wang, R., Tomikawa, Y., Nakamura, T., Huang, K., Zhang, S., Zhang, Y., Yang, H., and Hu, H.: A mechanism to explain the variations of tropopause and tropopause inversion layer in the Arctic region during a sudden stratospheric warming in 2009, J. Geophys. Res.-Atmos., 121, 11932–11945, https://doi.org/10.1002/2016JD024958, 2016.

Wargan, K. and Coy, L.: Strengthening of the Tropopause Inversion Layer during the 2009 Sudden Stratospheric Warming: A MERRA-2 Study, J. Atmos. Sci., 73, 1871–1887, https://doi.org/10.1175/JAS-D-15-0333.1, 2016.

Wickert, J., Reigber, C., Beyerle, G., König, R., Marquardt, C., Schmidt, T., Grunwaldt, L., Galas, R., Meehan, T. K., Melbourne, W. G., and Hocke, K.: Atmosphere sounding by GPS radio occultation: First results from CHAMP, Geophys. Res. Lett., 28, 3263–3266, https://doi.org/10.1029/2001GL013117, 2001.

Wickert, J., Beyerle, G., König, R., Heise, S., Grunwaldt, L., Michalak, G., Reigber, Ch., and Schmidt, T.: GPS radio occultation with CHAMP and GRACE: A first look at a new and promising satellite configuration for global atmospheric sounding, Ann. Geophys., 23, 653–658, https://doi.org/10.5194/angeo-23-653-2005, 2005.

Yessimbet, K., Shepherd, T. G., Ossó, A. C., and Steiner, A. K.: Pathways of influence between Northern Hemisphere blocking and stratospheric polar vortex variability, Geophys. Res. Lett., 49, e2022GL100895, https://doi.org/10.1029/2022GL100895, 2022a.

Yessimbet, K., Ossó, A., Kaltenberger, R., Magnusson, L., and Steiner, A. K.: Heavy Alpine snowfall in January 2019 connected to atmospheric blocking, Weather, 77, 7–15, https://doi.org/10.1002/wea.4020, 2022b.

List of Acronyms

AO Arctic Oscillation

CDAAC COSMIC Data Analysis and Archive Center

CHAMP Challenging Minisatellite Payload

COSMIC Constellation Observing System for Meteorology, Ionosphere, and Climate

DJF December, January, February

ECMWF European Centre for Medium-Range Weather Forecasts

EP Eliassen Palm

ERA5 ECMWF Re-Analysis Version 5

FORMOSAT-3/COSMIC Formosa Satellite mission #3/Constellation Observing System for Meteorology, Ionosphere, and Climate

GCM General Circulation Model

GNSS Global Navigation Satellite System

GRACE Gravity Recovery and Climate Experiment

HRES high-resolution forecast

IB Instantaneous Blocking

IFS Integrated Forecasting System

INCA Integrated Nowcasting through Comprehensive Analysis

IPCC Intergovernmental Panel on Climate Change

JJA June, July, August

LEO Low Earth Orbit

MetOp Meteorological Operational Satellite

NAM Northern Annular Mode

NAO North Atlantic Oscillation

NOAA National Oceanic and Atmospheric Administration

NH Northern Hemisphere

OPSv5.6 Occultation Processing System version 5.6 (WEGC)

PV Potential Vorticity

QG Quasigeostrophic

RO radio occultation

SAC-C Scientific Application Satellite-C

SH Southern Hemisphere

SPV stratospheric polar vortex

SSW Sudden Stratospheric Warming

TIL Tropopause Inversion Layer

UCAR University Corporation for Atmospheric Research

WEGC Wegener Center for Climate and Global Change

WMO World Meteorological Organization

ZAMG Zentralanstalt für Meteorologie und Geodynamik

List of Figures

Figure 1. The 3D illustration of the jet stream and polar vortex structure in a simple climate model in the presence of wave-two topography. The three grey domes represent atmospheric height levels at 100 hPa, 10 hPa, and 1 hPa, respectively. Reprinted from https://www.martinjucker.com/viz/ (accessed on 20.10.2024).....10
Figure 2. North Atlantic blocking is shown as an anomaly in geopotential height at 500 hPa (shading) with the jet stream (wind at 250 hPa) represented by vectors for 2 January 2019, based on ERA5 reanalysis data. The omega symbol marks the position of the omega-shaped blocking pattern (see Yessimbet et al., 2022a; Fig. 4d).....11
Figure 3. Schematic illustration of the GNSS RO method. Reprinted from https://www.cosmic.ucar.edu/what-we-do/gnss-radio-occultation (accessed on 22.10.2024). 14
Figure 4. Daily number of RO profiles for different satellites (different colors) as a function of time from 2001 to 2017. Reprinted from Angerer et al. (2017). 15
Figure 5. Variety of circulation patterns associated with atmospheric blocking in the North Atlantic. Potential temperature θ (shading, in K) on the dynamical tropopause and 500-hPa geopotential height (black contours, every 60 m) for different dates indicated at the bottom of each panel. The abbreviations AC and C stand for anticyclonic and cyclonic, respectively. Figure reprinted from Woollings et al. (2018).....18
Figure 6. Climatological blocking frequency (shading) expressed as the percentage of blocked days per grid point for (a) the Northern Hemisphere for DJF (December, January, February) and (b) JJA (June, July, August) seasons, (c) the Southern Hemisphere for DJF and (d) JJA seasons based on the ERA5 reanalysis dataset for the period 1950 to 2010. Contours indicate the zonally asymmetric component of the 500-hPa geopotential height climatology. 20
Figure 7. The SPV configuration is shown for the two types of SSWs: (a) a displacement event in 2007 and (b) a split in 2009, highlighting the stages before and during the events (left and right columns). Based on GNSS RO, the shading indicates the wind speed at 50 hPa and the contours to the geopotential height at 50 hPa. 22
Figure 8. Composite mean of the evolution of SPV strength, indicated as zonal-mean zonal wind at 10 hPa and 60°N (dotted lines), and wave activity, indicated as vertical component of Eliassen Palm flux averaged over 45–75°N (solid lines), for absorbing SSWs (blue lines) and reflecting SSWs (red lines) based on GNSS RO observations. 23
Figure 9. 3D view of the SPV evolution during an SSW event shown as the zonal mean evolution of anomalous zonal wind (isosurfaces/contours) and anomalous Eliassen-Palm flux (arrows) as a function of latitude, time, and pressure. Reprinted from Jucker (2016). 24
Figure 10. Composites of time-height development of the northern annular mode for (a) 18 weak vortex events and (b) 30 strong vortex events. The events are determined by the dates on which the 10-hPa annular mode values cross –3.0 and +1.5, respectively. The indices are nondimensional; the contour interval for the color shading is 0.25, and 0.5 for the white contours. Values between -0.25 and 0.25 are unshaded. The horizontal lines near 10 km/300 hPa indicate the approximate boundary between the troposphere and the stratosphere. Reprinted from Baldwin and Dunkerton (2001).....26
Figure 11. Time-height development of the NAM during the winter of 1998 –1999. The indices have daily resolution and are nondimensional. Blue corresponds to positive values (strong polar vortex), and red corresponds to negative values (weak polar vortex). The contour interval is 0.5, with values between -0.5 and 0.5 unshaded. The thin horizontal line indicates the approximate boundary between the troposphere and the stratosphere. Reprinted from Baldwin and Dunkerton (2001). 27

Figure 12. Geopotential height anomalies at 500-hPa (shading) and 50-hPa (contours) depicting the negative NAO pattern during the SSW event in winter 2009-2010 (right) and the solid box corresponding to the Euro-Atlantic blocking; and a positive NAO pattern during the displacement SSW event in winter 2007-2008 (left). 28
Figure 13. Brunt-Väisälä frequency computed from GNSS RO averaged over 75-90° N within a time frame of +/- 30 days relative to the onset of the SSW events from 2007 to 2019. The upper panel shows the absolute values and the lower panel shows the anomalies. Hatched regions indicate dates when the zonal-mean zonal wind at 60° N and 10 hPa is negative (Yessimbet et al., 2024). 29
Figure 14. Schematic illustration summarizing the interactions between the strength of the NAO, the height of the tropopause, and the strength of the SPV. Reprinted from Ambaum and Hoskins (2002). 30
Figure 15. Climatological QG Eliassen–Palm flux vectors and divergence (shading) for November to March from 2006 to 2019 based on GNNS RO data. 33
Figure 16. Schematic illustration of a blocking system (black line, indicating a geopotential height or PV contour) and associated surface extremes during the cold season (October–March). Blue stars show areas where snowstorms are observed (eastern flank of the block). Areas with heavy precipitation are marked in light blue (poleward edge of the ridge and at both flanks). Areas with high integrated water vapor transport are illustrated in orange. Areas with cold temperature extreme is marked with blue dashed line. Reprinted from Kautz et al. (2022). 35

Bibliography

Afargan-Gerstman, H., and D. I. Domeisen (2020): Pacific modulation of the North Atlantic storm track response to sudden stratospheric warming events. *Geophysical Research Letters*, 47(2), e2019GL085007. https://doi.org/10.1029/2019GL085007.

Albers, J. R., and T. Birner (2014): Vortex preconditioning due to planetary and gravity waves prior to sudden stratospheric warmings. *Journal of the Atmospheric Sciences*, 71, 4028–4054. https://doi.org/10.1175/JAS-D-14-0026.1.

Ambaum, M. H. P., and B. J. Hoskins (2002): The NAO troposphere–stratosphere connection. *Journal of Climate*, 15, 1969–1978. https://doi.org/10.1175/1520-0442(2002)015<1969:TNTSC>2.0.CO;2

Andrews, D., Holton, J., and C. Leovy (1987): *Middle atmosphere dynamics*. Academic Press, 489 pp.

Angerer, B., Ladstädter, F., Scherllin-Pirscher, B., Schwärz, M., Steiner, A. K., Foelsche, U., and Kirchengast, G. (2017): Quality aspects of the Wegener Center multi-satellite GPS radio occultation record OPSv5.6. *Atmospheric Measurement Techniques*, 10(12), 4845–4863. https://doi.org/10.5194/amt-10-4845-2017.

Anthes, R. A. (2011): Exploring Earth's atmosphere with radio occultation: Contributions to weather, climate, and space weather. *Atmospheric Measurement Techniques*, 4(6), 1077. https://doi.org/10.5194/amt-4-1077-2011.

Athanasiadis, P. J., Yeager, S., Kwon, Y. O., et al. (2020): Decadal predictability of North Atlantic blocking and the NAO. *npj Climate and Atmospheric Science*, 3, 20. https://doi.org/10.1038/s41612-020-0120-6.

Attard, H. E., and A. L. Lang (2019): Troposphere–stratosphere coupling following tropospheric blocking and extratropical cyclones. *Monthly Weather Review*, 147(5), 1781–1804. https://doi.org/10.1175/MWR-D-18-0335.1.

Baldwin, M. P., Ayarzagüena, B., Birner, T., Butchart, N., Butler, A. H., Charlton-Perez, A. J., Domeisen D., Garfinkel C.I., Garny H., Gerber E. P., Hegglin M.I., Langematz U., and N. M. Pedatella (2021): Sudden stratospheric warmings. *Reviews of Geophysics*, 59(1), e2020RG000708. https://doi.org/10.1029/2020RG000708.

Baldwin, M. P., and T. J. Dunkerton (2001): Stratospheric harbingers of anomalous weather regimes. *Science*, 294, 581–584. https://doi.org/10.1126/science.1063315.

Barnes, E.A., Slingo, J. and Woollings, T. (2012): A methodology for the comparison of blocking climatologies across indices, models and climate scenarios. *Climate Dynamics* 38, 2467–2481. https://doi.org/10.1007/s00382-011-1243-6.

Barriopedro, D., García-Herrera, R., and Trigo, R. M. (2010): Application of blocking diagnosis methods to general circulation models. Part I: A novel detection scheme. *Climate Dynamics*, 35, 1373–1391. https://doi.org/10.1007/s00382-010-0767-5.

Bell, B., Hersbach, H., Simmons, A., Berrisford, P., Dahlgren, P., Horányi, A., et al. (2021): The ERA5 global reanalysis: Preliminary extension to 1950. *Quarterly Journal of the Royal Meteorological Society*, 147(741), 4186–4227. https://doi.org/10.1002/qj.4174.

Beyerle, G., Schmidt, T., Michalak, G., Heise, S., Wickert, J., and Reigber, C. (2005): GPS radio occultation with GRACE: Atmospheric profiling utilizing the zero-difference technique. *Geophysical Research Letters*, 32, L13806. https://doi.org/10.1029/2005GL023109.

Birner, T., and J. R. Albers (2017): Sudden stratospheric warmings and anomalous upward wave activity flux. *SOLA*, 13A, 8–12. https://doi.org/10.2151/sola.13A-002.

Boljka, L., and T. Birner (2022): Potential impact of tropopause sharpness on the structure and strength of the general circulation. *npj Climate and Atmospheric Science*, 5, 98. https://doi.org/10.1038/s41612-022-00319-6.

Brunner, L. (2018): A new perspective on atmospheric blocking from observations—Detection, analysis, and impacts (PhD thesis). *Scientific Report No. 76-2018*. Wegener Center Verlag.

Brunner, L., Schaller, N., Anstey, J., Sillmann, J., and A. K. Steiner (2018): Dependence of present and future European temperature extremes on the location of atmospheric blocking. *Geophysical Research Letters*, 45, 6311–6320. https://doi.org/10.1029/2018GL077837.

Brunner, L., and A. K. Steiner (2017): A global perspective on atmospheric blocking using GPS radio occultation—One decade of observations. *Atmospheric Measurement Techniques*, 10(12), 4727–4745. https://doi.org/10.5194/amt-10-4727-2017.

Butler, A. H., Sjoberg, J. P., Seidel, D. J., and K. H. Rosenlof (2017): A sudden stratospheric warming compendium. *Earth System Science Data*, 9(1), 63–76. https://doi.org/10.5194/essd-9-63-2017.

Chen, P., and W. Robinson (1992): Propagation of planetary waves between the stratosphere and troposphere. *Journal of the Atmospheric Sciences*, 49(24), 2533–2545. https://doi.org/10.1175/1520-0469(1992)049<2533:POPWBT>2.0.CO;2.

Cohen, J., Agel L., Barlow, M., Garfinkel, C. I. , and I. White (2021): Linking Arctic variability and change with extreme winter weather in the United States. *Science* 373,1116-1121. https://doi.org/10.1126/science.abi9167.

Dong, S., Sun, Y., Aguilar, E., Zhang, X., Peterson, T.C., Song, L., and Zhang, Y. (2018): Observed changes in temperature extremes over Asia and their attribution. *Climate Dynamics* 51, 339–353. https://doi.org/10.1007/s00382-017-3927-z.

Dörnbrack, A., Pitts, M. C., Poole, L. R., Orsolini, Y. J., Nishii, K., and H. Nakamura (2012): The 2009–2010 Arctic stratospheric winter: General evolution, mountain waves, and predictability of an operational weather forecast model. *Atmospheric Chemistry and Physics*, 12, 3659–3675. https://doi.org/10.5194/acp-12-3659-2012.

ECMWF (2021): Operational configurations of the ECMWF Integrated Forecasting System (IFS). Retrieved from https://www.ecmwf.int/en/forecasts/documentation-and-support [Accessed 6 April 2021].

Edmon, H. J., Jr., Hoskins, B. J., and M. E. McIntyre (1980): Eliassen–Palm cross sections for the troposphere. *Journal of the Atmospheric Sciences*, 37(12), 2600–2616. https://doi.org/10.1175/1520-0469(1980)037<2600:EPCSFT>2.0.CO;2.

Eliassen, A. and T. Palm (1960): On the transfer of energy in stationary mountain waves. *Geofysiske publikasjoner*, 22, 1–23.

Engdaw, M. M., Steiner, A. K., Hegerl, G. C., and A. P. Ballinger (2023): Attribution of observed changes in extreme temperatures to anthropogenic forcing using CMIP6 models. *Weather and Climate Extremes*, 100548. https://doi.org/10.1016/j.wace.2023.100548.

Garcia-Herrera, R., and D. Barriopedro (2006): Northern Hemisphere snow cover and atmospheric blocking variability. *Journal of Geophysical Research: Atmospheres*, 111, D21104. https://doi.org/10.1029/2005JD006975.

Garfinkel, C. I., Schwartz, C., White, I. P., and J. Rao (2020): Predictability of the early winter Arctic oscillation from autumn Eurasian snowcover in subseasonal forecast models. *Climate Dynamics*, 55, 961–974. https://doi.org/10.1007/s00382-020-05305-3.

Geller, M. A., and J. C. Alpert (1980): Planetary wave coupling between the troposphere and the middle atmosphere as a possible sun-weather mechanism. *Journal of the Atmospheric Sciences*, 37, 1197–1215. https://doi.org/10.1175/1520-0469(1980)037<1197:PWCBTT>2.0.CO;2

Gerber, E. P., and E. Manzini (2016): The Dynamics and Variability Model Intercomparison Project (DynVarMIP) for CMIP6: Assessing the stratosphere–troposphere system. *Geoscientific Model Development*, 9, 3413–3425. https://doi.org/10.5194/gmd-9-3413-2016.

Gerber, E. P., and Polvani, L. M. (2009): Stratosphere-troposphere coupling in a relatively simple AGCM: The importance of stratospheric variability. *Journal of Climate*, 22, 1920–1933. https://doi.org/10.1175/2008JCLI2548.1.

Greening, K., and A. Hodgson (2019): Atmospheric analysis of the cold late February and early March 2018 over the UK. *Weather*, 74, 79–85. https://doi.org/10.1002/wea.3467.

Hajj, G. A., C. O. Ao, B. A. Iijima, D. Kuang, E. R. Kursinski, A. J. Mannucci, T. K. Meehan, L. J. Romans, M. de la Torre Juarez, and T. P. Yunck (2004): CHAMP and SAC-C atmospheric occultation results and intercomparisons. *Journla of Geophysical Research Atmosphere*, 109, D06109. https://doi.org/10.1029/2003JD003909.

Hersbach, H., Bell, B., Berrisford, P., Hirahara, S., Horányi, A., Muñoz-Sabater, J., Nicolas, J., Peubey, C., Radu, R., Schepers, D., Simmons, A., Soci, C., Abdalla, S., Abellan, X., Balsamo, G., Bechtold, P., Biavati, G., Bidlot, J., Bonavita, M., Chiara, G.D., Dahlgren, P., Dee, D., Diamantakis, M., Dragani, R., Flemming, J., Forbes, R., Fuentes, M., Geer, A., Haimberger, L., Healy, S., Hogan, R.J., Hólm, E., Janisková, M., Keeley, S., Laloyaux, P., Lopez, P., Lupu, C., Radnoti, G., de Rosnay, P., Rozum, I., Vamborg, F., Villaume, S. and Thépaut, J.-N. (2020) The ERA5 global reanalysis. *Quarterly Journal of the Royal Meteorological Society*, 146, 1999– 2049. https://doi.org/10.1002/qj.3803.

Hines, C. O. (1974): A Possible Mechanism for the Production of Sun-Weather Correlations. *Journal of Atmospheric Sciences*, 31, 589–591. https://doi.org/10.1175/1520-0469(1974)031<0589:APMFTP>2.0.CO;2

Holton, J., and G. J. Hakim (2012): An Introduction to Dynamic Meteorology, vol. 5, Acad. Press, New York.

Holton, J. R., and C. Mass (1976): Stratospheric vacillation cycles. *Journal of Atmospheric Sciences*, 33, 2218–2225. https://doi.org/10.1175/1520-0469(1976)033<2218:SVC> 2.0.CO;2.

Horton, D., Johnson, N., Singh, D., Swain, D.L., Rajaratnam, B., and Diffenbaugh, N.S. (2015): Contribution of changes in atmospheric circulation patterns to extreme temperature trends. *Nature* 522, 465–469. https://doi.org/10.1038/nature14550.

IPCC (2013): Climate Change 2013: The Physical Science Basis. Contribution of Working Group I to the Fifth Assessment Report of the Intergovernmental Panel on Climate Change [Stocker, T. F., D. Qin, G.-K. Plattner, M. Tignor, S. K. Allen, J. Boschung, A. Nauels, Y. Xia, V. Bex, and P. M. Midgley (eds.)]. Cambridge University Press, Cambridge, United Kingdom and New York, NY, USA 1535pp.

IPCC (2021): Climate Change 2021: The Physical Science Basis. Contribution of Working Group I to the Sixth Assessment Report of the Intergovernmental Panel on Climate Change [Masson-Delmotte, V., P. Zhai, A. Pirani, S. L. Connors, C. Péan, S. Berger, N. Caud, Y. Chen, L. Goldfarb, M. I. Gomis, M. Huang, K. Leitzell, E. Lonnoy, J. B. R. Matthews, T. K. Maycock, T. Waterfield, O. Yelekçi, R. Yu, and B. Zhou (eds.)]. Cambridge University Press, Cambridge, United Kingdom and New York, NY, USA, 2391 pp. https://doi.org/10.1017/9781009157896.

IPCC, (2022): Climate Change 2022: Impacts, Adaptation, and Vulnerability. Contribution of Working Group II to the Sixth Assessment Report of the Intergovernmental Panel on Climate Change [H.-O. Pörtner, D.C. Roberts, M. Tignor, E.S. Poloczanska, K. Mintenbeck, A. Alegría, M. Craig, S. Langsdorf, S. Löschke, V. Möller, A. Okem, B. Rama (eds.)]. Cambridge University Press. Cambridge University Press, Cambridge, UK and New York, NY, USA, 3056 pp., https://doi.org/10.1017/9781009325844.

Jucker, M. (2016). 3D Interactive Generic Sudden Stratospheric Warming composite. In Journal of the Atmospheric Sciences. Zenodo. https://doi.org/10.5281/zenodo.46174

Jucker, M., and Reichler, T. (2018): Dynamical precursors for statistical prediction of stratospheric sudden warming events. *Geophysical Research Letters*, 45, 13,124–13,132. https://doi.org/10.1029/2018GL080691.

Karpechko, A. Y., Hitchcock, P., Peters, D. H., and A. Schneidereit (2017): Predictability of downward propagation of major sudden stratospheric warmings. *Q. J. R. Meteorol. Soc.*, 143, 1459–1470. https://doi.org/10.1002/qj.3017.

Kautz, L.-A., Martius, O., Pfahl, S., Pinto, J. G., Ramos, A. M., Sousa, P. M., and T. Woollings (2022): Atmospheric blocking and weather extremes over the Euro-Atlantic sector – a review. *Weather Clim. Dynam.*, 3, 305–336. https://doi.org/10.5194/wcd-3-305-2022.

Kodera, K., Mukougawa, H., and S. Itoh (2008): Tropospheric impact of reflected planetary waves from the stratosphere. *Geophysical Research Letters*, 35, L16806. https://doi.org/10.1029/2008GL034575.

Kodera, K., Mukougawa, H., and A. Fujii (2013): Influence of the vertical and zonal propagation of stratospheric planetary waves on tropospheric blockings. *Journal of Geophysical Research: Atmospheres*, 118, 8333–8345. https://doi.org/10.1002/jgrd.50650.

Kodera, K., H. Mukougawa, P. Maury, M. Ueda, and C. Claud (2016): Absorbing and reflecting sudden stratospheric warming events and their relationship with tropospheric circulation. *Journal of Geophysical Research: Atmospheres*, 121, 80–94. https://doi.org/10.1002/2015JD023359.

Kretschmer, M., Coumou, D., Agel, L., Barlow, M., Tziperman, E., and J. Cohen (2018): More-persistent weak stratospheric polar vortex states linked to cold extremes. *Bull. Am. Meteorol. Soc.*, 99, 49–60. https://doi.org/10.1175/BAMS-D-16-0259.1.

Legras, B., and M. Ghil (1985): Persistent anomalies, blocking and variations in atmospheric predictability. *Journal of Atmospheric Sciences*, 42, 433–471. https://doi.org/10.1175/1520-0469(1985)042<0433:PABAVI>2.0.CO;2

Limpasuvan, V., D. W. J. Thompson, and D. L. Hartmann (2004): The life cycle of Northern Hemisphere sudden stratospheric warmings. *Journal of Climate*, 17, 2584–2596. https://doi.org/10.1175/1520-0442(2004)017<2584:TLCOTN>2.0.CO;2.

Luntama, J.-P., Kirchengast, G., Borsche, M., Foelsche, U., Steiner, A., Healy, S.B., von Engeln, A., O'Clerigh, E., and C. Marquardt (2008): Prospects of the EPS GRAS mission for operational atmospheric applications. *Bull. Am. Meteorol. Soc.*, 89, 1863–1875. https://doi.org/10.1175/2008BAMS2399.1.

Lupo, A.R. (2021): Atmospheric blocking events: a review. Ann. N.Y. Acad. Sci., 1504: 5-24. https://doi.org/10.1111/nyas.14557.

Martineau, P., Son, S.-W., Taguchi, M., and A. H. Butler (2018): A comparison of the momentum budget in reanalysis datasets during sudden stratospheric warming events. *Atmospheric Chemistry and Physics*, 18, 7169–7187. https://doi.org/10.5194/acp-18-7169-2018.

Martius, O., Polvani, L. M., and H. C. Davies (2009): Blocking precursors to stratospheric sudden warming events. *Geophysical Research Letters*, 36, L14806. https://doi.org/10.1029/2009GL038776.

Matsuno, T., (1970): Vertical Propagation of Stationary Planetary Waves in the Winter Northern Hemisphere. *Journal of Atmospheric Sciences*., 27, 871–883, https://doi.org/10.1175/1520-0469(1970)027<0871:VPOSPW>2.0.CO;2.

Matthewman, N. J., and J. G. Esler (2011): Stratospheric sudden warmings as self-tuning resonances. Part I: Vortex splitting events. *Journal of Atmospheric Sciences*, 68, 2481–2504. https://doi.org/10.1175/JAS-D-11-07.1.

Matthias, V., and M. Kretschmer (2020): The influence of stratospheric wave reflection on North American cold spells. *Monthly Weather Review*, 148, 1675–1690. https://doi.org/10.1175/MWR-D-19-0339.1.

Maycock, A. C., and P. Hitchcock (2015): Do split and displacement sudden stratospheric warmings have different annular mode signatures? *Geophysical Research Letters.*, 42, 10943–10951. https://doi.org/10.1002/2015GL066754.

Messori, G., M. Kretschmer, S. H. Lee, and V. Wendt (2022): Stratospheric downward wave reflection events modulate North American weather regimes and cold spells. *Weather Clim. Dynam.*, 3, 1215–1236. https://doi.org/10.5194/wcd-3-1215-2022.

Mitchell, D. M., L. J. Gray, J. Anstey, M. P. Baldwin, and A. J. Charlton-Perez (2013): The influence of stratospheric vortex displacements and splits on surface climate. *Journal of Climate*, 26, 2668–2682. https://doi.org/10.1175/JCLI-D-12-00030.1.

Nakamura N. and C. S. Y. Huang (2018): Atmospheric blocking as a traffic jam in the jet stream. *Science* 361,42-47. https://doi.org/10.1126/science.aat0721.

Nakamura, H., M. Nakamura, and J. L. Anderson (1997): The role of high- and low-frequency dynamics in blocking formation. *Monthly Weather Review*, 125, 2074–2093. https://doi.org/10.1175/1520-0493(1997)125<2074:TROHAL>2.0.CO;2

Nakamura, H., and J. M. Wallace (1990): Observed Changes in Baroclinic Wave Activity during the Life Cycles of Low-Frequency Circulation Anomalies. *Journal of Atmospheric Sciences*, 47, 1100–1116, https://doi.org/10.1175/1520-0469(1990)047<1100:OCIBWA>2.0.CO;2.

O'Gorman P. A. (2015): Precipitation extremes under climate change Curr. Clim. Change Rep. 1 49–59. https://doi.org/10.1007/s40641-015-0009-3.

Olefs, M., W. Schöner, M. Suklitsch, et al. (2013): SNOWGRID – A new operational snow cover model in Austria. *Proc. Int. Snow Sci. Workshop*, 1–5, Grenoble – Chamonix Mont Blanc, Grenoble, France.

Perlwitz, J., and N. Harnik (2004): Downward coupling between the stratosphere and troposphere: The relative roles of wave and zonal mean processes. *Journal of Climate*, 17, 4902–4909. https://doi.org/10.1175/JCLI-3247.1.

Pfahl, S. (2014).: Characterising the relationship between weather extremes in Europe and synoptic circulation features. Nat. Hazard. Earth Sys. 14.6, pp. 1461 1475. https://doi.org/10.5194/nhess-14-1461-2014.

Piaget, N., P. Froidevaux, P. Giannakaki, F. Gierth, O. Martius, M. Riemer, G. Wolf, and C. M. Grams (2015): Dynamics of a local Alpine flooding event in October 2011: Moisture source and large-scale circulation. *Quarterly Journal of the Royal Meteorological Society*, 141, 1922–1937. https://doi.org/10.1002/qj.2496.

Pinto, J. G., T. Brücher, A. H. Fink, and A. Krüger (2007): Extraordinary snow accumulations over parts of central Europe during the winter of 2005/06 and weather-related hazards. *Weather*, 62, 16–21. https://doi.org/10.1002/wea.19.

Plumb, R. A. (1985): On the three-dimensional propagation of stationary waves. *Journal of Atmospheric Sciences*, 42, 217−229. https://doi.org/10.1175/1520-0469(1985) 042<0217:OTTDPO>2.0.CO;2

Polvani, L. M., and D. W. Waugh, (2004): Upward wave activity flux as a precursor to extreme stratospheric events and subsequent anomalous surface weather regimes. *Journal of Climate*, 17 (18), 3548–3554, https://doi.org/10.1175/1520-0442(2004)017<3548: UWAFAA>2.0.CO;2.

Rex, D. F. (1950): Blocking action in the middle troposphere and its effect upon regional climate I: An aerological study of blocking action. *Tellus*, 2(3), 196–211. https://doi.org/10.1111/j.2153-3490.1950.tb00331.x.

Roscoe, H. K., J. D. Shanklin, and S. R. Colwell (2005): Has the Antarctic vortex split before 2002? *Journal of Atmospheric Sciences*, 62, 581–588. https://doi.org/10.1175/JAS-3331.1.

Saidaliyeva, Z., Shahgedanova, M., Yapiyev, V., Wade, A. J., Akbarov, F., Esenaman uulu, M., Kalashnikova, O., Kapitsa, V., Kasatkin, N., Rakhimov, I., Satylkanov, R., Sayakbaev, D., Semakova, E., Severskiy, I., Petrov, M., Umirzakov, G., and Usubaliev, R. (2024): Precipitation in the mountains of Central Asia: isotopic composition and source regions, *Atmospheric Chemistry and Physics*, 24, 12203–12224, https://doi.org/10.5194/acp-24-12203-2024.

Scherllin-Pirscher, B., Steiner, A. K., and G. Kirchengast (2014): Deriving dynamics from GPS radio occultation: Three-dimensional wind fields for monitoring the climate. *Geophysical Research Letters*, 41, 7367–7374. https://doi.org/10.1002/2014GL061524.

Scherllin-Pirscher, B., Steiner A. K., Kirchengast G., Schwärz M., and Leroy S.S. (2017): The power of vertical geolocation of atmospheric profiles from GNSS radio occultation. *Journal of Geophysical Research Atmosphere*, 122, 1595–1616. https://doi.org/10.1002/2016JD025902.

Scherllin-Pirscher, B., Steiner, A. K., Anthes, R., Alexander, M., Alexander, S., Biondi, R., Birner, T., Kim, J., Randel, W., Son, S., Tsuda, T. and Zeng, Z. (2021): Tropical Temperature Variability in the UTLS: New Insights from GPS Radio Occultation Observations. *Journal of Climate* 34(8) pp. 2813-2838. https://doi.org/10.1175/JCLI-D-20-0385.1.

Scherrer, S. C., and C. Appenzeller (2006): Swiss Alpine snow pack variability: Major patterns and links to local climate and large-scale flow. *Climate Research*, 32, 187–199. https://doi.org/10.3354/cr032187.

Schöner, W., R. Koch, C. Matulla, et al. (2019): Spatiotemporal patterns of snow depth within the Swiss-Austrian Alps for the past half century (1961 to 2012) and linkages to climate change. *International Journal of Climatology*, 39, 1589–1603. https://doi.org/10.1002/joc.5902.

Shepherd, T. G. (2014): Atmospheric circulation as a source of uncertainty in climate change projections. *Nature Geoscience*, 7(10), 703-708. https://doi.org/10.1038/ngeo2253.

Shepherd, T.G.(2016): A Common Framework for Approaches to Extreme Event Attribution. *Curr Clim Change Rep* 2, 28–38. https://doi.org/10.1007/s40641-016-0033-y.

Sillmann, J., M. Croci-Maspoli, M. Kallache, and R. W. Katz (2011): Extreme cold winter temperatures in Europe under the influence of North Atlantic atmospheric blocking. *J. Climate*, 24, 5899–5913. https://doi.org/10.1175/2011JCLI4075.1.

Sjoberg, J. P., and T. Birner (2012): Transient tropospheric forcing of sudden stratospheric warmings. *Journal of Atmospheric Sciences*, 69, 3420–3432. https://doi.org/10.1175/JAS-D-11-0195.1.

Small, D., E. Atallah, and J. R. Gyakum, (2013): An Objectively Determined Blocking Index and its Northern Hemisphere Climatology. *Journal of Climate*, 27, 2948–2970, https://doi.org/10.1175/JCLI-D-13-00374.1.

Steiner, A. K., B. C. Lackner, F. Ladstädter, B. Scherllin-Pirscher, U. Foelsche, and G. Kirchengast (2011): GPS radio occultation for climate monitoring and change detection. *Radio Science*, 46, RS0D24. https://doi.org/10.1029/2010RS004614.

Steiner, A. K., Ladstädter, F., Ao, C. O., Gleisner, H., Ho, S.-P., Hunt, D., Schmidt, T., Foelsche, U., Kirchengast, G., Kuo, Y.-H. , Lauritsen, K. B., Mannucci, A. J., Nielsen, J.

K., Schreiner, W., Schwärz, M., Sokolovskiy, S., Syndergaard, S., and J. Wickert (2020): Consistency and structural uncertainty of multi-mission GPS radio occultation records. *Atmospheric Measurement Techniques*, 13, 2547–2575. https://doi.org/10.5194/amt-13-2547-2020

Steinfeld, D., Pfahl, S. (2019): The role of latent heating in atmospheric blocking dynamics: a global climatology. *Climate Dynamics* 53, 6159–6180. https://doi.org/10.1007/s00382-019-04919-6

Stucki, P., R. Rickli, S. Bronnimann, O. Martius, H. Wanner, D. Grebner, and J. Luterbacher (2012): Weather patterns and hydro-climatological precursors of extreme floods in Switzerland since 1868. *Meteorologische Zeitschrift*, 21, 531–550. https://doi.org/10.1127/0941-2948/2012/368.

Suitters, C. C., O. Martínez-Alvarado, K. I. Hodges, R. K. H. Schiemann, and D. Ackerley (2023): Transient anticyclonic eddies and their relationship to atmospheric block persistence. *Weather and Climate Dynamics*, 4, 683–700. https://doi.org/10.5194/wcd-4-683-2023.

Taguchi, M., and S. Yoden (2002): Internal interannual variability of the troposphere-stratosphere coupled system in a simple general circulation model. Part I: Parameter sweep experiments *Journal of Atmospheric Sciences*, 59, 3021–3036. https://doi.org/10.1175/1520-0469(2002)059<3021:IIVOTT>2.0.CO;2.

Taleb, N. N. (2007): *The Black Swan: The Impact of the Highly Improbable*. London: Allen Lane, Penguin Books Ltd.

Tibaldi, S. and F. Molteni (1990). On the operational predictability of blocking. Tellus A 42.3, pp. 343–365. https://doi.org/10.3402/tellusa.v42i3.11882.

Wang, Y., Li, Y., Wang, G., Yuan, Y., and Geng, H. (2023): Influences of sudden stratospheric warming events on tropopause based on GNSS radio occultation data. *Atmosphere*, 14(10), 1553. https://doi.org/10.3390/atmos14101553.

Wargan, K., and Coy, L. (2016): Strengthening of the tropopause inversion layer during the 2009 sudden stratospheric warming: A MERRA-2 study. *Journal of Atmospheric Sciences*, 73, 1871–1887. https://doi.org/10.1175/JAS-D-15-0333.1.

Weinberger, I., Garfinkel, C. I., White, I. P., and Birner, T. (2021): The efficiency of upward wave propagation near the tropopause: Importance of the form of the refractive index. *Journal of Atmospheric Sciences*, 78(8), 2605–2617. https://doi.org/10.1175/JAS-D-20-0267.1.

Wickert, J., Beyerle, G., König, R., Heise, S., Grunwaldt, L., Michalak, G., Reigber, C., and Schmidt, T. (2005): GPS radio occultation with CHAMP and GRACE: A first look at a new and promising satellite configuration for global atmospheric sounding. *Annals of Geophysics*, 23, 653–658. https://doi.org/10.5194/angeo-23-653-2005.

Wickert, J., Reigber, C., Beyerle, G., König, R., Marquardt, C., Schmidt, T., Grunwaldt, L., Galas, R., Meehan, T. K., Melbourne, W. G., and Hocke, K. (2001): Atmosphere sounding by GPS radio occultation: First results from CHAMP. *Geophysical Research Letters*, 28(17), 3263–3266. https://doi.org/10.1029/2001GL013117.

WMO (1978): Abridged final report of the seventh session of the Commission for Atmospheric Sciences. WMO Rep. 509, 113 pp.

WMO (2024): Extreme weather. Available at: https://wmo.int/topics/extreme-weather. Last access: 10 September 2024.

Woollings, T., Barriopedro, D., Methven, J., Son, S.-W., Martius, O., Harvey, B., Sillmann, J., Lupo, A. R., and Seneviratne, S. (2018): Blocking and its response to climate change. *Curr. Clim. Change Rep.*, 4, 287–300. https://doi.org/10.1007/s40641-018-0108-z.

Woollings, T., Hannachi, A., Hoskins, B., and Turner, A. (2010): A regime view of the North Atlantic oscillation and its response to anthropogenic forcing. *Journal of Climate*, **23**(6), 1291–1307. https://doi.org/10.1175/2009JCLI3087.1.

Yamazaki, A., and Itoh H. (2009): Selective absorption mechanism for the maintenance of blocking, *Geophysical Research Letters*, 36, L05803, https://doi.org/10.1029/2008GL036770.

Yessimbet, K., Ossó, A., Kaltenberger, R., Magnusson, L., and Steiner, A. K. (2021): Heavy Alpine snowfall in January 2019 connected to atmospheric blocking. *Weather*. https://doi.org/10.1002/wea.4020.

Yessimbet, K., Shepherd, T. G., Ossó, A. C., and Steiner, A. K. (2022): Pathways of influence between Northern Hemisphere blocking and stratospheric polar vortex variability. *Geophysical Research Letters*, 49, e2022GL100895. https://doi.org/10.1029/2022 GL100895.

Yessimbet, K., Steiner, A. K., Ladstädter, F., and Ossó, A. (2024): Observational perspective on sudden stratospheric warmings and blocking from Eliassen–Palm fluxes. *Atmospheric Chemistry and Physics*, 24, 10893–10919. https://doi.org/10.5194/acp-24-10893-2024.

Atmospheric blocking is a persistent, large-scale, quasi-stationary anticyclone that disrupts the westerly flow at midlatitudes, often leading to extreme weather. In the cold season, blocking influences stratospheric variability by modulating the upward propagation of planetary waves from the troposphere. This influence can contribute to the disruption of the stratospheric polar vortex (SPV) and lead to sudden stratospheric warming (SSW). An SSW event, in turn, can affect tropospheric circulation and favor blocking conditions. Both phenomena are associated with the occurrence of extreme weather, such as cold spells or heavy precipitation events. However, the details of their mechanisms and pathways of influence are not yet fully understood. This thesis aims to contribute to a better understanding of these processes by exploring the role of atmospheric blocking in the stratosphere-troposphere coupling and its influence on extreme weather events.

The first insight is provided by a case study of a record-breaking snowfall event in the northern Alps in 2019, associated with North Atlantic blocking, which was crucial for the advection of cold and moist air from the North Atlantic toward the Alps. The analysis shows the connection between blocking and specific SPV configuration during a major SSW event that occurred simultaneously and discusses their role in shaping this extreme snowfall and the implications for its prediction.

In the second part, the strength of the pathways of influence between European and West Pacific blocking and SPV variability is quantified using a causal inference-based framework and reanalysis data. Results show that both types of blocking affect the SPV primarily through upward wave activity fluxes, though this influence is not straightforward. In particular, for European blocking, the influence on the lower stratospheric wave activity flux is fully mediated by its effect on the upper tropospheric wave activity flux, while this is only partially the case for West Pacific blocking, suggesting that the mechanisms of their vertical influence differ. In addition, only two-thirds of the effect of upper tropospheric wave activity flux on SPV variability is mediated by lower stratospheric wave activity flux, while one-third occurs via a direct pathway. These findings clarify the pathways of influence between blocking and SPV variability.

Finally, an observational-based study of stratosphere-troposphere coupling and the influence of SSWs on blocking formation was conducted using Global Navigation Satellite System (GNSS) radio occultation (RO) measurements. GNSS RO data provide insight into the vertical structure of wave activity flux and its impact on the polar tropopause for different types of SSWs. In particular, reflecting SSW events connected to vortex displacement are observed to trigger downward propagation of wave activity that induces blocking over the North Pacific, while absorbing events connected to vortex split result in blocking over the North Atlantic and exhibit prolonged upward propagation of wave activity. Both types of SSWs lead to the enhancement of the polar tropopause inversion layer, with a stronger effect observed for absorbing events. The results highlight the differences in the magnitudes of downward impact on the troposphere and the resulting regional variations in blocking responses for different SSW types.

SR 107 | 2024 Atmospheric blocking – exploring its role in stratosphere-troposphere coupling and its influence on extreme weather events
Wegener Center Verlag, University of Graz, Austria. ISBN 978-3-9505053-6-8